The University Of Sheffield.

Agency for Science, Technology and Research

SINGAPORE

CREATING GROWTH. ENHANCING LIVES.

# Crush injury in zebrafish tail as a model for human bone fracture repair.

PhD thesis by

Monika Jagoda Tomecka

University of Sheffield

Department of Biomedical Science

September 2016

# Abstract

Bone fracture injuries, as well as their consequences, are important clinical issues. Several questions raised about them cannot be answered from observations of patients, therefore animal models of human fractures are needed. Zebrafish crush injury was developed here as an accurate model for human bone fracture repair. Whilst studies of amputation of the zebrafish adult tail attracted much interest as a model for regeneration, there has been very limited analysis of the process of repair of bone fractures. To address this, I established a zebrafish crush model and characterized it in comparison to mammalian bone fracture models. I further evaluated its usage in the zebrafish bone mutant, *frf*, known model for Osteogenesis Imperfecta. I showed striking similarities in the way of fracture repair between *frf*, rodent OI models and humans. I tested common human bone disease drugs on the zebrafish crush healing, further showing the usefulness and relevance of the model. Upon treatment with Bisphosphonates, human OI drugs, I observed a significant reduction in the remodelling stage of fracture healing, as well as in spontaneous fracture formation in juvenile OI zebrafish. These results mimic human clinical data. Last, but not least, I introduced controlled *S. aureus* infections to the crush site in order to model human *S. aureus* fracture infections. In conclusion, I established zebrafish crush model relevant to human physiology and pathology. I proved its usefulness in bone fracture healing characterization studies, in determining bone pathogenicity as well as in bone related drug treatment efficiency, and infection disturbance in bone repair.

# Contents

# List of abbreviations

| | |
|---|---|
| µ | micro |
| µg | microgram |
| µl | microliter |
| µM | micromole |
| ˚C | degrees Centigrade |
| AB | Wild type fish |
| amp | amputation |
| ANOVA | one-way analysis of variance |
| ATP | adenosine triphosphate |
| *bglap* | *osteocalcin* |
| BMP | Bone Morphogenetic protein |
| BSA | Bovine serum albumin |
| *col* | *collagen* |
| *CtsK* | *cathepsin-K* |
| DIC | Differential interference contrast |
| dCAPS | Derived Cleaved Amplified Polymorphic Sequences |
| DIG | Digoxigenin |
| dpa | Days post amputation |
| dpc | Days post crush |
| dpf | Days post fertilisation |
| dpi | Days post injection |
| DsRed | Discosoma RED |
| fig | Figure |
| fmol | femtomole |
| *frf* | *frilly fin* |
| gDNA | genomic DNA |
| h | hours |
| hpa | hours post amputation |
| hpc | hours post crush |
| hpf | Hours post fertilisation |

| | |
|---|---|
| GFP | Green Fluorescent Protein |
| IDT | Integrated DNA Technologies |
| IL1 | Interleukin-1 |
| ISH | In situ hybridization |
| KOH | potassium hydroxide |
| LB | Luria broth |
| min | minute |
| mg | milligrams |
| ml | millilitre |
| mM | milimolar |
| *msxc* | *muscle segment homeobox c* |
| mpf | Month post fertilisation |
| *mpx* | *myeloid-specific peroxidase* |
| NBCS | New Born Calf Serum |
| NEB | New England Biolabs inc |
| ng | nanograms |
| nm | nanometers |
| o/n | Overnight |
| OI | Osteogenesis Imperfecta |
| *osx* | *osterix* |
| PBS | Phosphate buffered saline |
| PBST | Phosphate buffered saline plus 0.1% tween20 |
| PCR | Polymerase Chain Reaction |
| PFA | Paraformaldehyde |
| Pro-K | Proteinase-K |
| RNA | Ribonucleic Acid |
| RT | Room Temperature |
| sec | Second |
| SAP | Shrimp alkaline phosphatase |
| SDS | Sodium dodecyl sulphate |
| sibs | siblings |
| SNP | Single Nucleotide Polymorphism |
| SOC | Super Optimal Broth |

| | |
|---|---|
| *spp1* | *Osteopontin* |
| TRAcP | tartrate-resistant acid phosphatase |
| UV | Ultra Violet |
| wpc | Weeks post crush |
| wpf | Weeks post fertilisation |

**Table 1.1 List of abbreviations**

# General introduction

## 0.0. Regeneration

Regeneration is the process of regrowing lost tissues (Brockes et al., 2001). This phenomenon can be found across the whole animal kingdom, however the degree of regeneration ability varies between different animal groups. Cnidarians and planarians can regrowth each and every part of their body, urodele amphibians are able to restore lost parts of organs and limbs including all tissues within them (Fig 0.1), while human regeneration capability is highly restricted to only liver, blood and skin (Tanaka and Reddien, 2011). The term regeneration is also used to cover processes occurring inside the animal body which maintain tissue morphology and function (Carlson, 2005), including organ regeneration, cellular regeneration and tissue hypertrophy (Yoshinari and Kawakami, 2011).
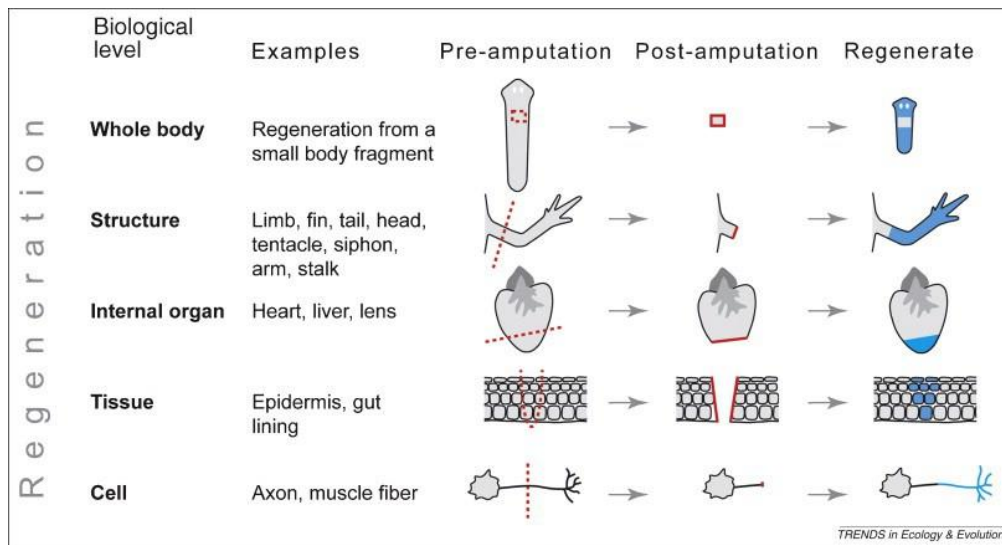


**Figure 0.1 Regeneration involves processes occurring on several biological levels.**

Distinct species might regenerate at none, all, or just a subset of these levels. Functional links between regenerative processes at successive levels are likely. It remains unclear which aspects of regeneration are homologous across different biological levels. Dotted red lines indicate amputation planes, continues red lines indicate wound surfaces; and blue fill indicates regenerated body parts (Bely and Nyberg, 2010)

Researchers study regeneration in order to fully understand the regenerative processes aiming to expand the regeneration potential of humans (Tanaka and Reddien, 2011). Urodele amphibians such as salamander and newts have been extensively examined for their ability to regrow amputated limbs, precisely restoring their form and cell types (McCusker et al., 2015). It has been shown that tissue regeneration is performed by sequential dedifferentiation, migration and redifferentiation of residual cells, however this process is lineage restricted, meaning that dedifferentiated cells can redifferentiate only into the same cell type (fig 0.2) (Tanaka and Reddien, 2011).
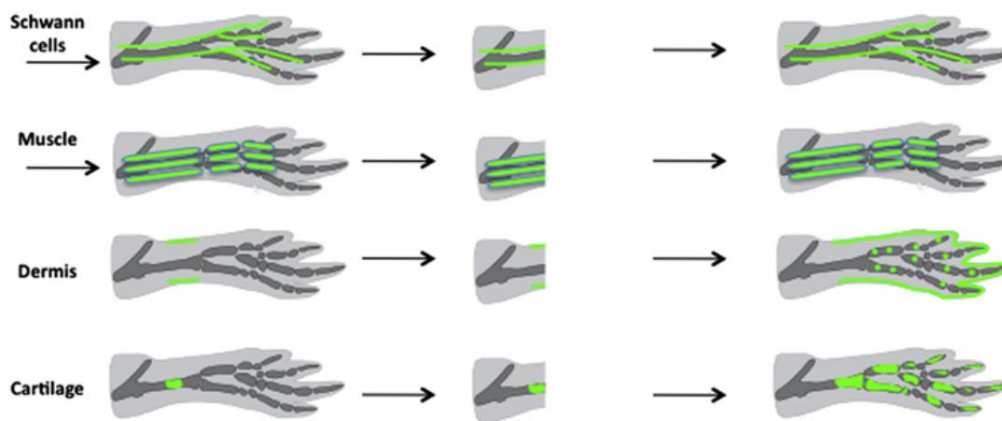


**Figure 0.2 Lineage-restricted tissue regeneration in transgenetically labelled Axolotl limb** GFP-labelled Schwann cells regenerated Schwann cells, muscle regenerated muscle, cartilage regenerated cartilage but interestingly dermis regenerated dermis, cartilage and connective tissues (Tanaka and Reddien, 2011)

### 0.0.1. Epimorphic regeneration

Axolotl restore their limbs through blastema formation in the process called epimorphic regeneration (fig 0.3). In this type of regeneration, the lost body part is fully restored, without scar formation, from dedifferentiating cells. The whole process can be divided into consecutive stages. Firstly, wound epithelium is formed in order to close the wound and cover tissues exposed to the external environment. This is followed by formation of an apical epithelial cap, formation of which triggers the dedifferentiation of residual stump cells, migration towards a forming blastema and proliferation. While the distal tip of the blastema proliferates, cells at the proximalblastma start redifferentiating back into cells lines they have arisen from, leading to full restoration of tissues and limb internal organisation.
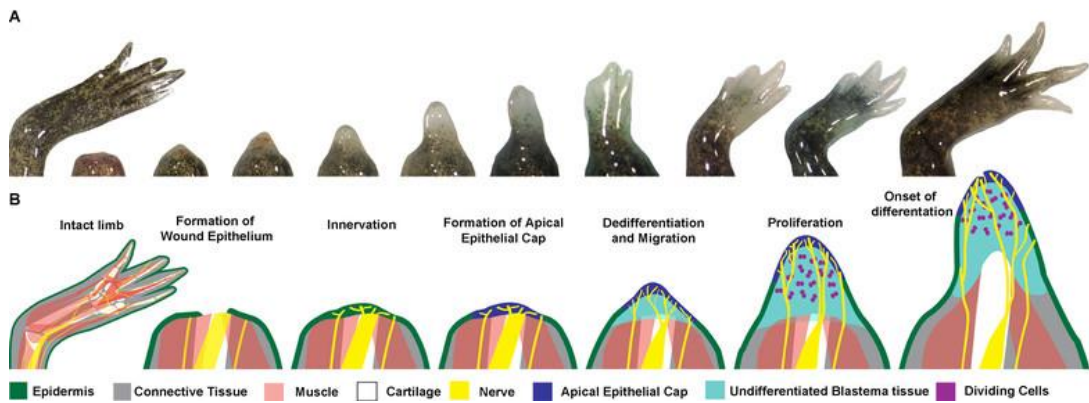
**Figure 0.3 Axolotl limb blastema development.**

**A)** Live images of the time course of limb blastema development showing an intact limb (first on the left) and 1, 7, 9, 11, 13, 15, 17, 21, 25, and 31dpa (consecutively to the right).

**B)** Schematic representation of the key steps in the regenerative process highlighted during blastema development. The tissue components are indicated by the coloured legend. The intact limb is composed of multiple tissues including epidermis, connective tissue, muscle, cartilage, and nerves, which are organized in a specific way to generate functional structures (left). Within hours following an amputation, a wound epithelium covers the edge of the severed limb. Within days, this wound epithelium becomes innervated, and becomes a specialized signalling centre called the apical epithelial cap. It induces cell dedifferentiation in the underlying stump and attracts cells, which accumulate below it. At later stages of development, the cells in the basal region of the blastema start to differentiate, while the cells at the distal tip of the blastema remain in an undifferentiated and proliferative state. Eventually, all the blastema cells differentiate into fully structured limb. (McCusker et al., 2015)

Epimorphic regeneration can also be observed in zebrafish upon tail amputation (fig 0.4) (Nechiporuk and Keating, 2002). Blastema formation in zebrafish follows the same steps of wound closure, blastema formation and regenerational outgrowth as described previously for axolotl, giving rise to the full range of differentiated tissues like blood vessels, muscles, skin and bone.
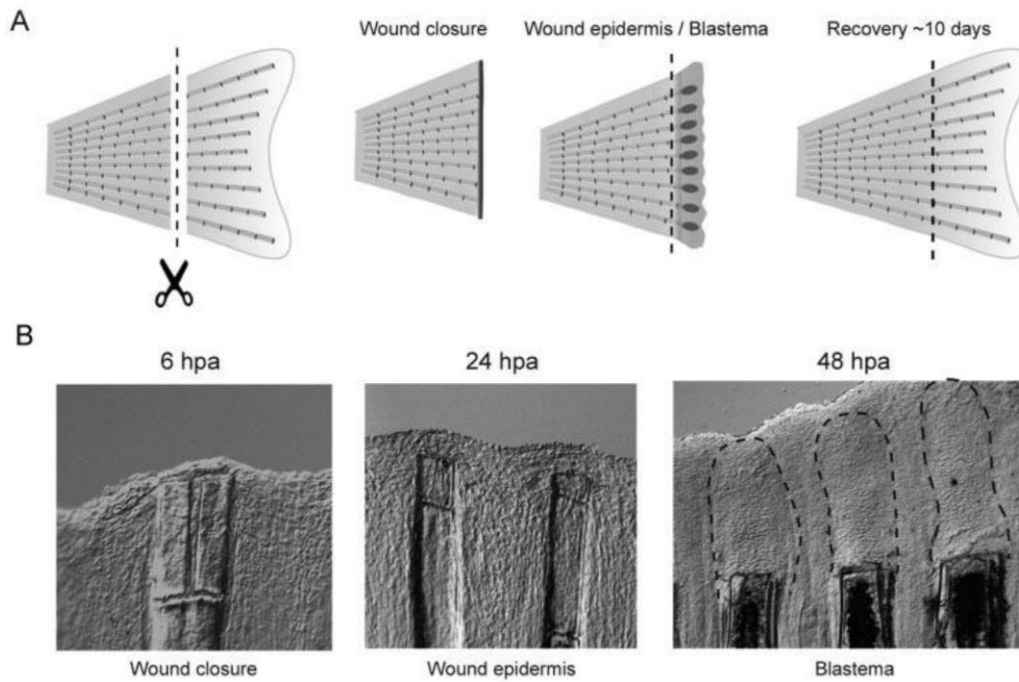
**Figure 0.4 Adult fin regeneration through blastema formation upon amputation of zebrafish tail**

**A)** Key steps in regeneration following amputation: wound closure, wound closure by epidermis and blastemal formation, tail regrowth/ recovery.

**B)** Appearance of tissues at key regeneration steps. Dotted lines in B indicate the blastema regions.

(Yoshinari and Kawakami, 2011)

Blastemal formation, growth and differentiation is a highly controlled process. Many research groups work towards understanding cellular pathways driving this phenomenon. The full signalling network is yet to be determined but over last two decades many signalling pathways and cross-talk between them, leading to organised regenerational regrowth have been revealed (Fig 0.5) (Wehner and Weidinger, 2015). It is known that FGF signalling is needed for blastemal proliferation as it has been shown that in the absence of fibroblast growth factors (Fgfs) or their receptors, blastemal outgrowth is arrested (Poss et al., 2000, Whitehead et al., 2005). Interestingly, Hh signalling is tightly connected to FGF in blastemal outgrowth process. Activation of Hh signalling promotes blastema proliferation even in FGF inhibited fins leading to partial rescue of regeneration (Lee et al., 2009). Retinoic acid (RA) has also been shown as a crucial regulator of blastemal proliferation showing an ability to enhance blastemal growth (Blum and Begemann, 2012). Bone morphogenetic protein (BMP) signalling has been shown to play a role in

differentiation of osteoblasts and blastemal patterning leading to bony rays formation (Stewart et al., 2014). IGF signalling was reported as present during blastemal growth, however its inhibition was not powerful enough to supress blastemal proliferation suggesting that it plays an indirect role in epimorphic regeneration through cellular communication, not in controlling blastemal proliferation (Stewart et al., 2014).
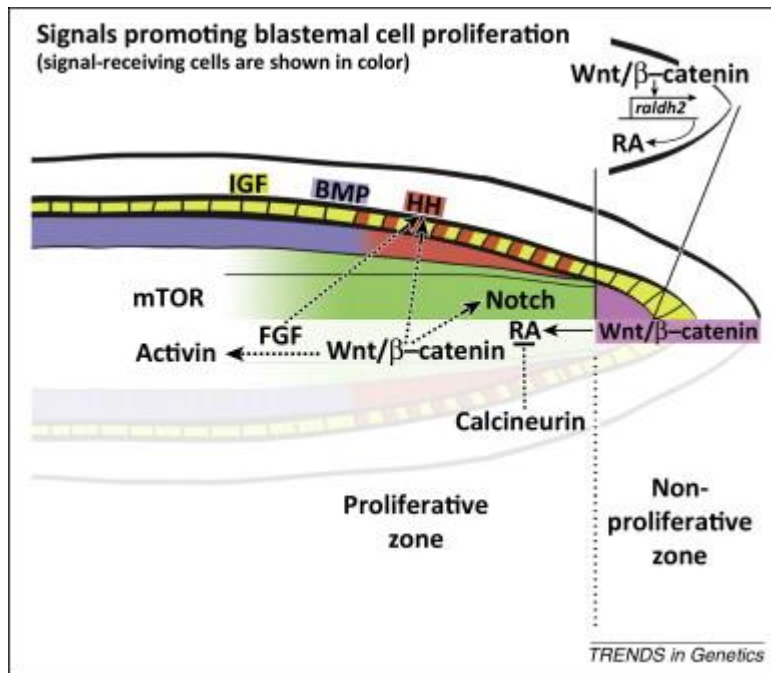


**Figure 0.5 Schematic representation of regulation of blastemal proliferation.**

Proliferative and non-proliferative zones are shown. Colours indicate regions where pathways are active. Arrows with dotted line indicate predicted interactions (Wehner and Weidinger, 2015)

## 0.1.     Fin ray as a human bone model

The mechanism of bone restoration through blastemal formation is intriguing. Bone regeneration is a unique type of regeneration and up to date only amphibians and teleost fish were found to be able to perform it (Tanaka and Reddien, 2011). Researchers hope that full understanding of the processes occurring throughout bone regeneration will help us to activate those mechanisms in humans. Zebrafish caudal fin is the most commonly used model in research studies due to its size and ease of access (Geraudie et al., 1995). Moreover, an injured caudal fin does not affect fish mobility, therefore, it does not perturb viability. The fin consists of bony rays called lepidotrichia (Fig 0.6 B). Each lepidotrichium is made of bone matrix and consist of two hemirays covered with osteoblasts (bone forming

cells). Each lepidotrichium is a separate, pipe like structure, filled with fibroblasts and other cells types such as pigment cells. Each lepidotrichium has an artery passing through the middle of it and two veins laying just along its sides (Fig 0.6 C). Due to their physical appearance, bony rays (lepidotrichium) can be used to model diaphysis of the long human bone. In both rays and diaphyses, a hard bony structure protects a delicate interior. Geometry and transparency of zebrafish tail allow observation of the movement of cells in the tail in homeostasis stage as well as during the regeneration process.
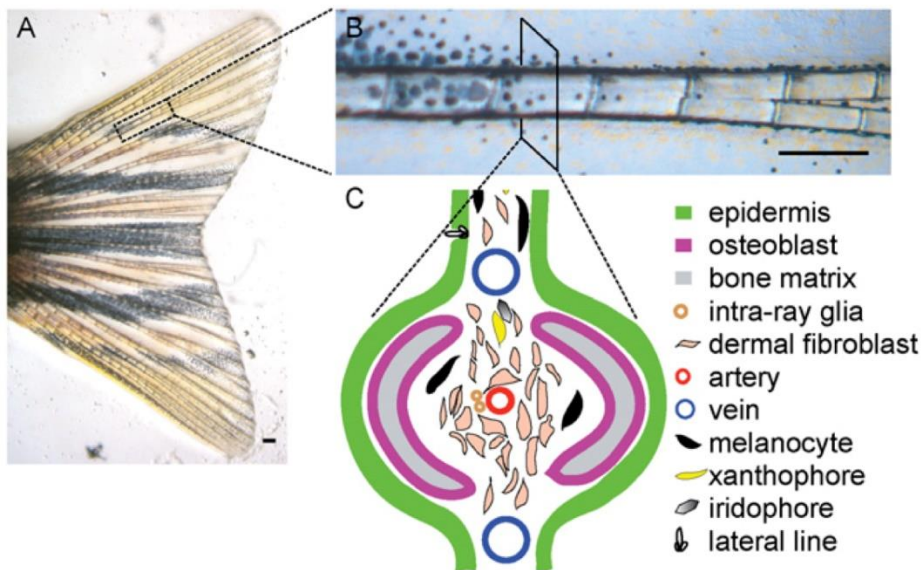


**Figure 0.6 Adult caudal fin structure**

**A)** The caudal fin contains of 18 lepidotrichia (bony rays)

**B)** Each one is segmented and has ability to bifurcate (split and give rise to two separately elongated rays)

**C)** Schematic representation of the ray cross section identifying distribution of different types of cells

(Tu and Johnson, 2011)

## 0.2. Zebrafish tail bone formation

Lepidotrichia are formed in the dermis in the process called intramembranous ossification (decribed in details below in section 0.6). Morphogenesis of zebrafish tail skeleton can be divided into distinct steps. Starting just after somitogenesis, caudal skeleton forming mesenchyme (CSM) arises from the caudal somites (Fig 0.7 A). At the same time, zic1/zc4 are expressed, blocking further cell proliferation and expression of *Twist* (Fig 0.7 A). End of the body gets dorsally bended at the ural region, while hypurals form ventrally from CSM

(Fig 0.7 B). Lepidotrichia are formed as an extension from hypurals following their symmetry (Fig 0.7 C). As the fin is growing the symmetrical plane of hypurals and lepidotrichia rotates dorsally up to the point where it alines with the midline of the fish body axis (Fig 0.7 D). While the tail straightens, it keeps growing in size along with growth of fish body.
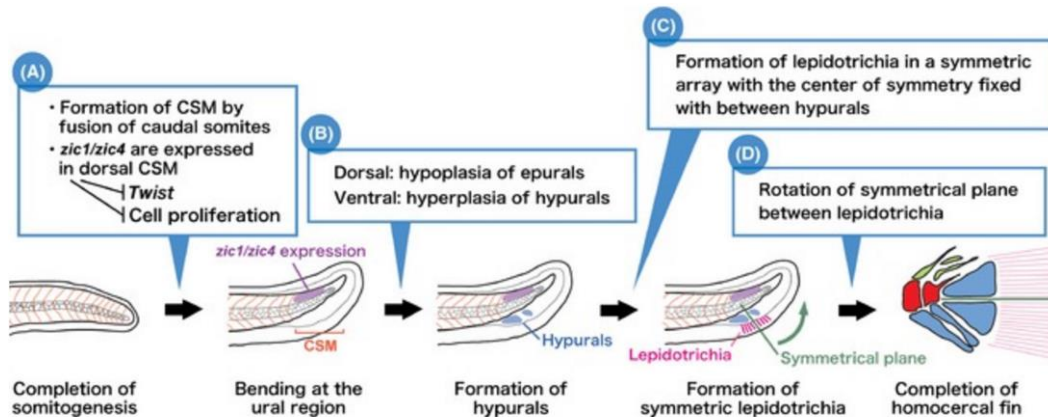


**Figure 0.7 Schematic representation of morphogenesis of zebrafish tail skeleton.**

**A)** After completion of somitogenesis, caudal skeleton forming mesenchyme (CSM) is formed by fusion of caudal somites. Simultaneously, dorsal CSM begun to express zic1/zic4, what blocks cell proliferation and twist expression.

**B)** Terminal axis bending of the ural region. After terminal axis bending, caudal skeletal components form; hypoplasia of epurals is observed in dorsal side and hyperplasia of hypurals in ventral side.

**C)** Lepidotrichia are formed in a symmetric array with the center of symmetry fixed with between hypurals.

**D)** Symmetrical plane between hypurals and lepidotrichia rotates as upward bending of the urostyle proceeds so that it finally fits in the midline of the body axis. Red lines indicate lepidotrichia (fin rays) and green line indicates symmetrical plane (Moriyama and Takeda, 2013)

## 0.3.    Zebrafish in research

Zebrafish was established as a laboratory animal model a few decades ago and has grown in popularity (Mariotti et al., 2015). This 3cm teleost fish holds huge research potential given its transparency in the embryonal stages, short generation time, and a high fecundity. The ability to inject nucleic acid into one cell stage embryos allows a wide range of genome modifications leading to gene mutations as well as the creation of transgenic lines (Mariotti

et al., 2015). Optical translucence allows for optical screening for fluorescent markers and in vivo tracking of cell migration. Moreover, fluorescently labelled cell lines are able to be tracked in vivo in larvae as well as in adults without the need for surgical intervention (Hammond and Moro, 2012). In just over 20 years, zebrafish research transformed from lineage tracing of dye injected cells in developing zebrafish embryos (Schilling and Kimmel, 1994) and big scale chemical zebrafish mutagenic screens (Driever et al., 1996), to creating transgenetically labeled, lineage-specific single cells through the Zebrabow approach (Pan et al., 2013) and indels production or single nucleotides exchanges using CRISPR/Cas9 technique (Irion et al., 2014). Nowadays, researchers employ zebrafish not only for basic research to understand fundamental molecular genetic pathways, mechanisms of development and organogenesis, but also for disease modelling and regeneration studies, including epimorphic regeneration of amputated tails and cardiac regeneration studies.

## 0.4.     Zebrafish in bone research

Zebrafish importance in bone research has experienced an exponential growth in the last 2 decades (Hammond and Moro, 2012, Mackay et al., 2013, Watson and Kwon, 2015, Mariotti et al., 2015). Numerous bone mutants were discovered in large-scale genetic screens (Driever et al., 1996). Mutants were named based on their phenotypicappearance (van Eeden et al., 1996). With help of genetic mapping and genome sequencing, several bone related genes were identified as causative of diseases (Howe et al., 2013). Many of them were progressively linked to human genetic diseases and now serve researchers as zebrafish models of human bone diseases. In addition, they helped to understand disease progressions and molecular pathways. Zebrafish models for Osteogenesis Imperfecta (OI) is a good example of this process. The first identified OI zebrafish model was the *chihuahua* mutant*,* and originated from a forward-genetic screen using X-irradiation (Fisher et al., 2003). Mapping identified a mutation of *col1a1a* which corresponds to the mutation in the human COL1A1 gene, which causes the majority of OI cases (Fisher et al., 2003). Some OI patients do not possess mutations in COL1, rather in collagen processing genes (Valadares et al., 2014). Identified in another mutagenic screen *frilly fins* (*frf)* fish (van Eeden et al., 1996) displayed an OI phenotype and was identified as an accurate model for human OI type XII. *frf* corresponds to mutations in zebrafish *bmp1a* gene, which was shown to be causative in a number of OI cases (Asharani et al., 2012). This finding helped in define the role of Bmp1 in collagen formation in bone (described in greater detail in chapter 2). Several other human bone diseases, such as Fibrodysplasia Ossificans Progressiva (Shen et

al., 2009), Raine Syndrome (Eames et al., 2011), osteoporosis (Yu et al., 2016, Barrett et al., 2006) and others were similarly modelled in zebrafish (Mackay et al., 2013). With the advantage of CRISPR/Cas9 to induce specific genetic modifications, zebrafish is poised to contribute further to modelling human bone diseases.

## 0.5.    Human skeleton

### 0.5.1.    Bone types

The human skeleton is a dynamic and complicated structure. Bones comes in several shapes including long bones eg. femur, flat bones eg. sternum, short bones eg. wrist bones and irregular bones eg. vertebra (Fig 0.8) (Clarke, 2008).
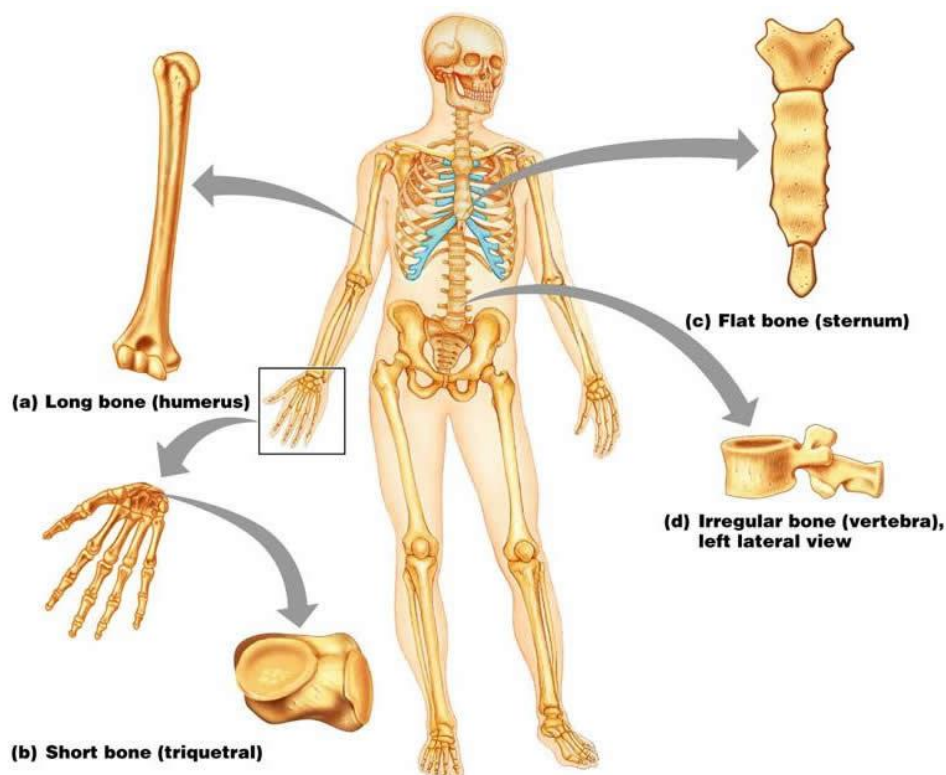


**Figure 0.8 Types of bones in human body**

Examples of different bone types based on bone geometry

http://classes.midlandstech.edu/carterp/Courses/bio210/chap06/lecture1.html

### 0.5.2.    Types of bone cells

In order to understand how bones are formed, we have to be familiar with bone related cells types. There are three main types of bone related cells: bone resorbing cells called osteoclasts which are derived from hematopoetic stem cells , origin bone forming cells

called osteoblasts derived from mesenchymal stem cells and osteocytes which are osteoblasts that have become embedded in the bone matrix (Fig 0.9). There are also mature quiescent osteoblasts called lining cells, which can be found on bone surfaces (fig 0.9) (Imai et al., 2013). Balanced activity of these cell types is necessary for bone homeostasis and healthy natural bone turn over.
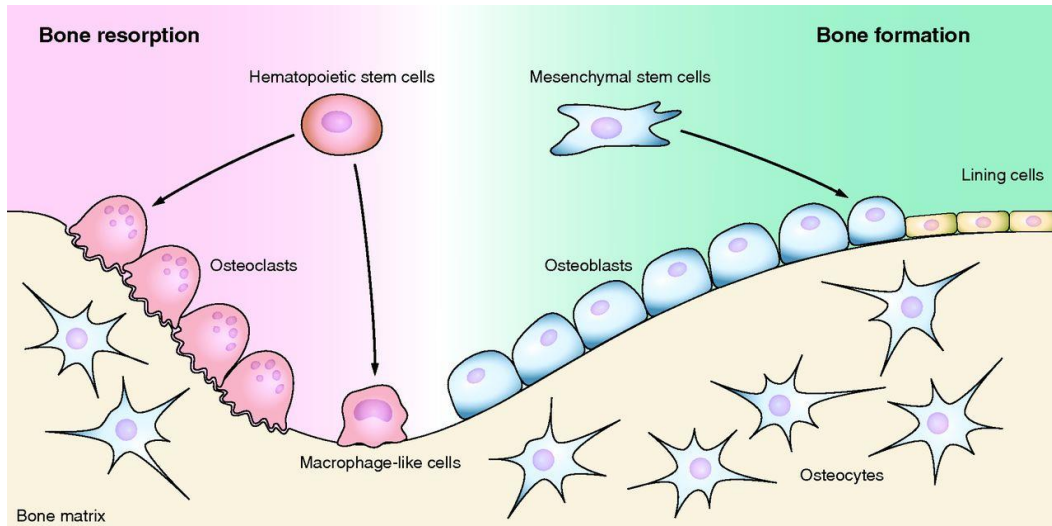


**Figure 0.9 Human bone cellular structure**

There are three main types of bone related cells: hematopoetic stem cells origin bone resorbing cells called osteoclasts, mesenchymal stem cell origin bone forming cells called osteoblasts and originated from them osteocytes which are embedded in the bone matrix. There are also mature quiescent osteoblasts called lining cells, which can be found on bone surfaces (Imai et al., 2013)

## 0.6.    Bone forming mechanisms

Bones are formed through two distinct mechanisms: intramembranous ossification, where bone is laid directly into intramesenchymal space by bone forming osteoblasts, or by endochondral ossification where bone matrix is deposited over a cartilage scaffold.

In intramembranous ossification, bone is formed from an ossification centre which forms in the fibrous connective tissue membrane from mesenchymal cells clustering together and differentiating into osteoblasts (fig 0.10 A1). Newly differentiated osteoblasts secrete osteoid (proteinaceous bone matrix), which is slowly mineralised, trapping some osteoblasts inside it. Trapped osteoblasts become osteocytes (fig 0.10 A2). Osteoid accumulates between embryonic blood vessels and forms random nets of connections. This

forms the forming sponge like woven bone on the outside of which, periosteum is formed by condensation of vascularized mesenchyme cells (fig 0.10 A3). As the bone grow it become more compact, trabeculae thicken and with time, peripheral woven bone is replaced with mature lamellar bone, leaving spongy bone in the centre where vascular tissue becomes red marrow (fig 0.10 A4).

In endochondral ossification, bone matrix is laid over the cartilage scaffold. Osteoblasts secrete osteoid firstly around the diaphysis (middle part of the bone) of the hyaline cartilage model, forming a bone collar (fig 0.10 B1). Concomitantly a primary ossification centre is formed in the middle of hyaline cartilage model (fig 0.10 B1) leading to cavities formation by calcifying and deteriorating of the centre of the diaphysis (fig 0.10 B2). Spongy bone forms around these cavities, which are invaded by the periosteal bud blood vessels (fig 0.10 B3). While ossification continues and the diaphysis elongates, osteoclasts form a medullary cavity in the centre of the diaphysis by removing residual bone matrix (fig 0.10 B4). At the same time, secondary ossification centres are formed at both ends in remaining cartilage model (fig 0.10 B4). Expansion of all ossification centres lead to ossification of the epiphyses and to reduction of initial hyaline cartilage to only epiphyseal plates and articular cartilages (fig 0.10 B5).
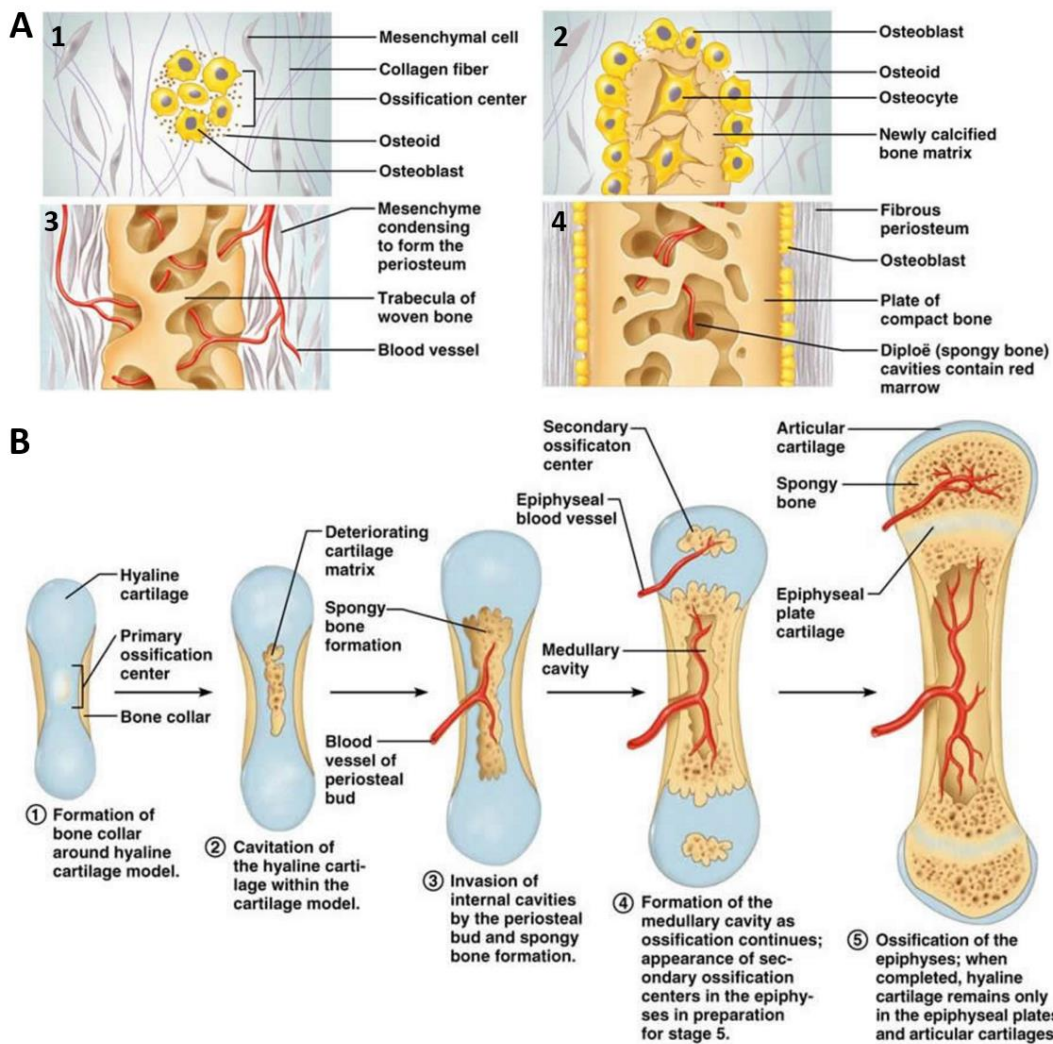
**Figure 0.10 Types of bone formation**

**A)** Intramembranous ossification

1 an ossification centre appearance in the fibrous connective tissue membrane

2 bone matrix secretion within the fibrous membrane

3 woven bone and periosteum formation

4 bone collar of compact bone formation and red marrow appearance

**B)** Endochondral ossification

1 bone collar formation

2 cavitation

3 spongy bone formation

4 modularly cavity formation and secondary ossification

5 ossification of the epophyses

http://classes.midlandstech.edu/carterp/Courses/bio210/chap06/lecture1.html

## 0.7. Comparison between bones of humans and teleost fish

### 0.7.1. Similarities

There are many similarities between the bones of human and the bones of fish. Understanding them can serve to our advantage in using zebrafish as a model organism for human bone disorders (Apschner et al., 2011). Important examples of shared features include: the presence of two types of ossification (membranous and endochondral) in human as well as in zebrafish (Weigele and Franz-Odendaal, 2016), in both organisms bone mineral is composed of hydroxyapatite-like calcium-phosphate crystals (Laize et al., 2014), bone matrix deposition is done by alkaline phosphatase positive osteoblasts of mesenchymal origin while bone resorption by tartrate-resistance acid phosphatase expressing osteoclasts of hematopoietic origin (Witten and Huysseune, 2009).

### 0.7.2. Differences

There are also some differences which are important to remember when examining results obtained from zebrafish bone research. Skeletogenicity of zebrafish appears to be more complex as compared to the human. Zebrafish bones consist of osteocytic (osteocyte containing) bone as well as anosteocytic (osteocyte lacking), while all human bones are purely osteocytic (Shahar and Dean, 2013). Mechanosensing in human bones is performed by osteocytes, while in zebrafish it is performed by osteoblasts lining the bone. Zebrafish bone contains collagen I and II while human bones contain only collagen type I (Laize et al., 2014). Osteoclasts of zebrafish can be mono- or multinucleated, while human possess only multinucleated osteoclasts (Witten and Huysseune, 2009).

## 0.8. Genetic markers for bone related cell types

It is important to mention that genetic markers for the majority of bone formation related cell types are shared across the two species. Established markers for different stages of cellular maturation of bone cells are expressed. For example, different stages of osteoblast maturation can be marked by the range of genetic markers: *runx2* for preosteoblast, *osterix* for intermediate osteoblasts and *osteocalcin* for differentiated osteoblasts (Knopf et al., 2011). Secreted phosphoprotein 1/Osteopontin (spp1) is another non-collagenous extracellular matrix (ECM) protein present in active osteoblasts, which can serve as another useful marker (Dedeoglu, 2014). *Collagen I (col1)* is an important building element of bone matrix and its deposition can act as an indicator for osteoblastic activity (Neff et al., 1998).

Interestingly, *collagen X* (*col10*), which in mammals is used as exclusively cartilage marker, in zebrafish has been shown as a bone marker (Fang et al., 2016) as well as cartilage marker (Casar-Borota et al., 2016). *Sox9* is used as a chondrocyte marker in zebrafish and upregulates *collagen II* (*col2*) (Yue et al., 2016), the main building element of cartilage. Osteoclasts, on another hand, are bone resorbing cells of hematopoietic origin which also possess a distinct set of genetic markers. Osteoclast precursors express receptor activator of nuclear factor κ-β *(rank),* while preosteoclasts and mature osteoclasts express *cathepsin-K* (*CtsK)* and tartrate-resistant acid phosphatase (TRAcP) (Sharif et al., 2014). Accurate usage and understanding of genetic markers help in revealing molecular events underlying phenotypic changes.

# 1. Chapter 1 – Development of a crush injury model in zebrafish tail to model human bone fracture

## 1.1. Introduction

### 1.1.1. Bone fracture

A bone fracture is a medical condition characterised by loss of bone integrity. It can be caused by an accident through mechanical stress on the bone, as well as by genetic conditions like Osteogenesis Imperfecta or diseases developed with age like osteoporosis (Donaldson et al., 2008). There are several types of fractures, therefore clinicians follow complicated classifications to describe particular cases. These include open versus closed where skin and muscle penetrance is observed; simple versus comminute, which takes under consideration amount of fracture lines and bone fragments created; complete versus incomplete where fracture injury spatially separates parts of broken bone or the bone stays intact despite the fracture occurrence. In addition, the division can be made based on fracture plane (transverse, longitudinal, diagonal, spiral or complex) as well as by broken bone dislocation (displacement/shortage, angulation or rotation) (Fig 1.1). Bone fracture is a highly complex injury involving the bone and adjacent tissues, therefore detailed understating from mechanical, biological and histological aspects is needed (Schneidmuller et al., 2011).
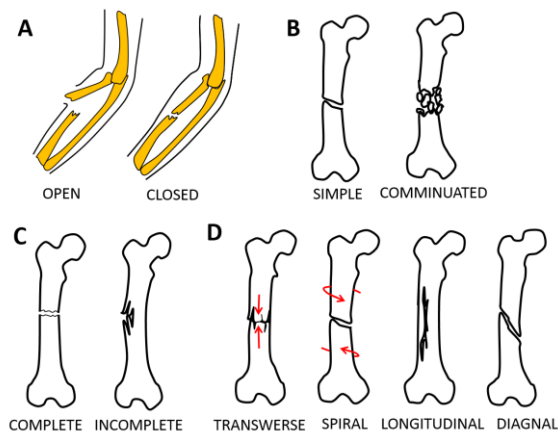


**Figure 1.1 Types of bone fractures**
**A)** open versus closed
**B)** simple versus comminute
**C)** complete versus incomplete
**D)** divided based on fracture plane

### 1.1.2. Epidemiology of fracture

Bone fracture is described as an underestimated medical problem (Donaldson et al., 2008). Epidemiological studies showed that annual fracture incident in UK involved 3.6% of the population, including patients of all ages (Donaldson et al., 2008). It was rated in the top three most common injuries of childhood and adolescence (Baker et al., 2016). The vast majority of bone fractures result from complex, multi-tissue injuries and their incidence is significantly higher in men than women. The possibility of fracture occurrence is the highest in young and middle-aged males and elderly females. Long bone fractures, which are the main focus of this study, are the second most common fracture type, just after fractures in hands and feet (Donaldson et al., 2008), out of which femoral fractures are the most common (Bridgman and Wilson, 2004). However, fractures heal, so do they really pose a serious concern to population health?

### 1.1.3. Fracture healing research

According to the literature, there are 5.6 million fracture cases annually happening in USA and around 5 to 10% of them do not heal properly (Einhorn, 1995). Predicted causes of healing failure include smoking, diabetes, infection and genetics. Previous and current smokers were 32% ($P = 0.04$) and 37% ($P = 0.01$) respectively less likely to achieve fracture union that non-smokers (Castillo et al., 2005), whilst retrospective case studies indicate diabetics have a significantly prolonged fracture healing time (Loder, 1988). Infections are known to cause delayed consolidation, failed osteosynthesis and fracture non-union (Baruah, 2007). Finally genetic predisposition such as genetic diseases like Osteogenisis Imperfecta (OI) are well documented to lead to non-union fracture formation in 23% of Osteogenisis Imperfecta patients (Gamble et al., 1988). Thus, in order to understand why those factors lead to healing problems, the process of fracture healing must be fully understood (Morshed, 2014). Last few decades showed increased interest in the processes of fracture healing. Several case studies (Schilcher et al., 2013) and research articles were published which emphasised the need for understanding mechanical, physiological and biological aspects of this process in humans.

### 1.1.4. Human fracture healing

The fracture healing process was divided into four healing stages (Fig 1.2) (Bostrom et al., 1995): inflammation, soft callus formation, hard callus formation and remodelling. Despite being well defined by their own characteristics, stages can overlap each other and

transitions between them are smooth, no hard defined temporal borders between stages can be observed.
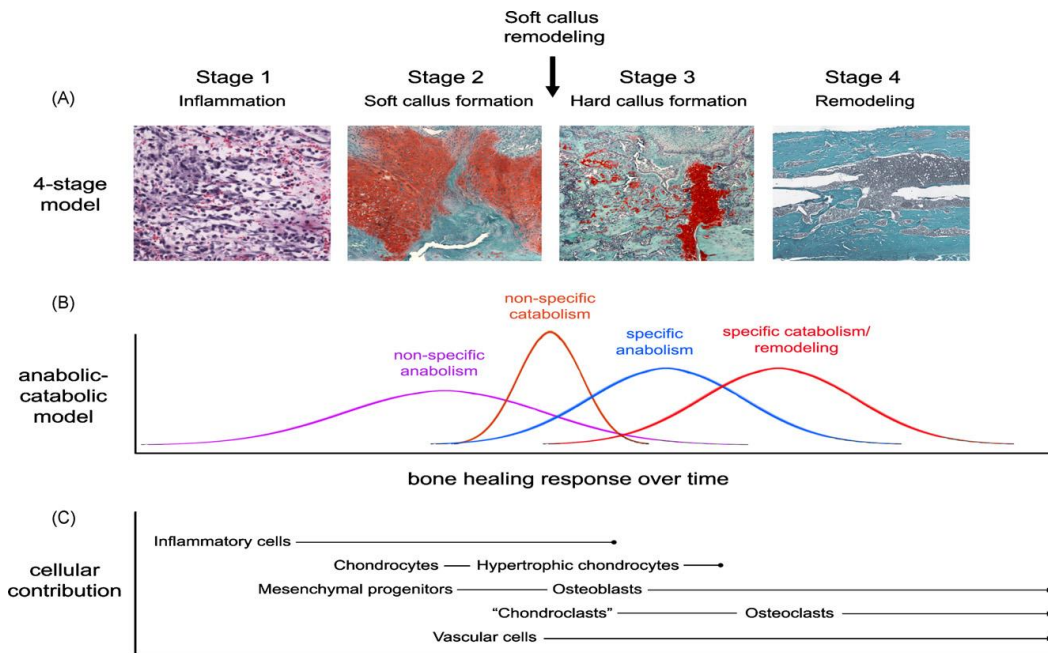


**Figure 1.2 Models of fracture repair and the cellular participants.**

**A)** Representative series of images of the four-stage model of fracture healing. Between the classical stages 2 and 3, the soft callus is systematically remodeled.

**B)** The anabolic/catabolic model of fracture repair that incorporates the concepts of non-specific anabolism (the early wound repair processes) and non-specific catabolism (soft callus remodeling)

**C)** Cellular contributors to the fracture repair processes. The source(s) of mesenchymal progenitors that are able to differentiate into osteoblasts remain ambiguous.

(Schindeler et al., 2008)


### 1.1.4.1. Inflammation (Stage 1)

Inflammation stage occurs almost immediately after fracture occurrence. Tissue trauma leads to activation of wound healing response, inflammatory cells are recruited while broken blood vessels create hematoma. Vascularisation and blood supply to the fracture site are critical for correct fracture healing, therefore angiogenesis guidance is an important role of the inflammation stage. All cellular interactions at this stage are highly regulated at the molecular level by cytokines and growth factors, including IL-1, IL-6 and TNFs, PDGFs and VEGFs, which possess chemotactic effect on surrounding cells and tissues (fig 1.3) (Pape et al., 2010). Inflammatory cells are recruited into crush site and persist there for the

first few days to clear foreign bodies, microbes and cellular debris. Phagocytic cells are recruited to the injury site to clear it from unwanted particles, created throughout homeostasis disturbance.
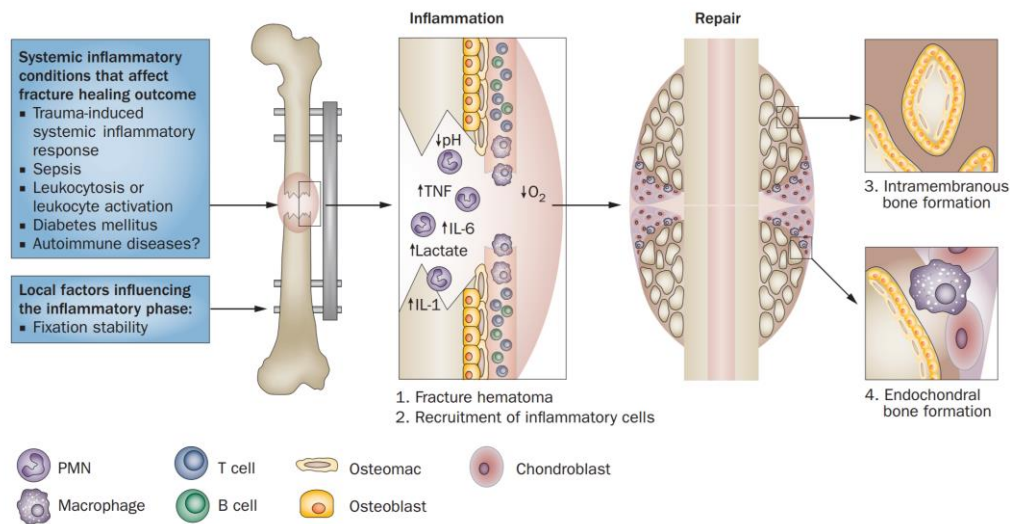


**Figure 1.3 Schematic representation of inflammation stage of fracture healing.**

**1)** The hematoma formation as a result of blood clotting. The hematoma is characterized by low pH and hypoxia, and contains anti-inflammatory and pro-inflammatory cytokines together with inflammatory cells from the peripheral blood

**2)** Rapid recruitment of immune cells into the site of injury. neutrophils being the first cells, followed by macrophages and lymphocytes.

**3)** Osteomacs (osteoclasts precursors) are crucial for osteoblast-driven mineralization in zones of intramembranous ossification

**4)** Inflammatory macrophages mainly contribute to endochondral bone formation

PMN, polymorphnuclear neutrophils.

(Claes et al., 2012)

### 1.1.4.2.    Soft callus formation (Stage 2)

Soft callus formation is characterised by cartilage deposition around the fracture site. A ball of cartilage is formed by resident chondrocytes or recruited mesenchymal stem cells to encapsulate the breakage, stabilizing it and holding broken bone ends in place (fig 1.4. 2). This stage is crucial in mechanically unstable fractures. In case of stable fracture occurrence, where broken bone parts stay intact and no deviation from the original location is observed, stage 2 is sometimes omitted and intramembranous bone formation can be observed. Cartilage callus formation stage is characterised by chondrocyte

recruitment to the fracture site, collagen type II deposition and expression of growth factors such as TGF –β2 and –β3, PDGF , IGF and FGF-1 (Bianco and Robey, 2000, Bhakta et al., 2006).

### 1.1.4.1. Hard callus formation (Stage 3)

Hard callus formation is performed by osteoblasts, which can either already reside near the fracture site or arise from osteoprogenitors activated by osteogenic factors. During this stage, the soft callus is vascularised and gradually replaced by hard callus through the mineralized material deposition, which is laid onto cartilage scaffold leading to the woven bone formation (fig 1.4. 3). Cartilage scaffold usage in mineralization support indicates endochondral ossification. Intramembranous ossification occurs when cartilage formation is omitted and mineralized tissue is laid directly onto fractured bone (Bielby et al., 2007). Hard callus ensures rigidity, eliminates the movement and reduce flexibility at the fracture site.

### 1.1.4.2. Remodelling (Stage 4)

Remodelling is characterised by replacing of woven bone by cortical and trabecular bone and trimming bony callus away (fig 1.4. 4). Progressive reduction in the callus width is a result of osteoclasts work and is used as an indicator for correctly progressing remodelling stage. In humans, it can last up to a few years to observe full callus remodelling. However, the fracture site might be recognised even years later.
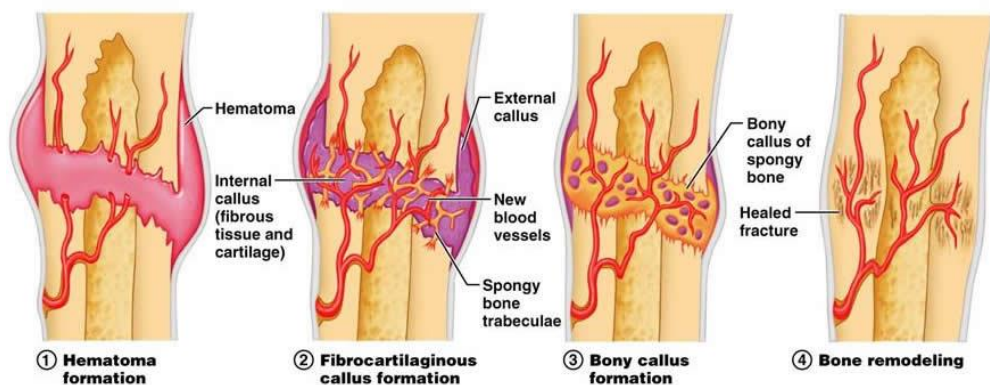


**Figure 1.4 Four stages of human bone fracture healing**

**1)** inflamation and hematoma formation

**2)** Fibrocartilsginous callus formation

**3)** Bony callus formation

**4)** bone remodeling

http://classes.midlandstech.edu/carterp/Courses/bio210/chap06/lecture1.html

Since the four stages recovery model had been first established, the vast amount of research has been done to reveal molecular pathways underlying fracture healing process (Slowik and Bermingham-McDonogh, 2013). Each of stages is related to the specific cell types, driven by certain molecules e.g. cytokines and growth factors (Bolander, 1992). However, only partial understanding can be obtained from human fractures as they do not permit experimental intervention. In order to elucidate the process of fracture healing, animal models have been employed (Hammond and Moro, 2012).

## 1.1.5. Animal fracture models

Several species were used as models to mimic human bone fracture conditions. This includes big mammals such as sheep, whose bone size and structure was shown to be very similar to human and used for mechanobiological studies of fractures (Egermann et al., 2008). Unfortunately, studies using sheep are very costly due to size and lifespan of those animals, which lead to limited repeat numbers of experiments. Similar limitations were reported in research on pigs and goats which have been widely used to model fracture infection (Reizner et al., 2014). Other big animals used for bone fracture studies were dogs (Lenehan et al., 1985), which have been used for decades for testing mechanical and radiological fracture treatments. However, due to ethical issues and several public protests experiments performed on dogs were limited in recent years.

With recent developments in genome manipulation and transgenesis, the last two decades brought a deeper understanding of cellular movements through cell lineage tracing techniques. This has contributed to a shift towards small animal usage for bone research. The tissue-specific cellular contribution is easier to test on small rodents like rats, rabbits or genetically modified mice. These were widely used for bone fracture modelling (Reizner et al., 2014, Garcia et al., 2013). However, bone examination in small rodents can be performed only by surgical intervention by opening the flesh in order to reach to the bone. There was a real need for a model organism in which bone could be examined noninvasively. It has been previously shown than certain bones of teleost fish can be examined noninvasively (Hammond and Moro, 2012), therefore progression of bone healing could be tracked in those. Following this trend, teleost fish were recently used in bone fracture research (Sousa et al., 2012, Geurtzen et al., 2014, Takeyama et al., 2014). This was first explored by Sousa et al. (2012) and compared fracture repair to epimorphic regeneration of zebrafish tail after amputation (Sousa et al., 2012). The ray fracture model

was expanded by Geurtzen et al. (2014), comparing ray fractures to skull injuries, and demonstrated osteoblast dedifferentiation, migration, and re-differentiation at both injury types. Osteoblast and osteoclast recruitment to the crush site was also assessed in medaka, another small teleost fish, presenting recruitment of osteoblasts and two types of osteoclasts to the fracture site (Takeyama et al., 2014).

## 1.1.6. A new zebrafish bone crush injury model

Sousa et al. (2012) proposed that partial amputation of zebrafish tail was not an ideal approach to model human bone fractures. They decided to compare zebrafish responses to the amputation and to the ray fracture. Firstly, they examined both regenerative processes side by side through amputating one lobe of the tail and crushing rays in the other lobe (fig 1.5 A). They reported strong changes in tissue architecture at the crush side comparing to hardly distinguishable amputation plane at 10dpc/a (fig 1.5 B, C). They showed that crush injury destroys only bone elements and epidermis (fig 1.5 D) and reported uncalcified callus formation around the crush site and suggested similarities to human bone fracture healing (fig 1.5 E, F).
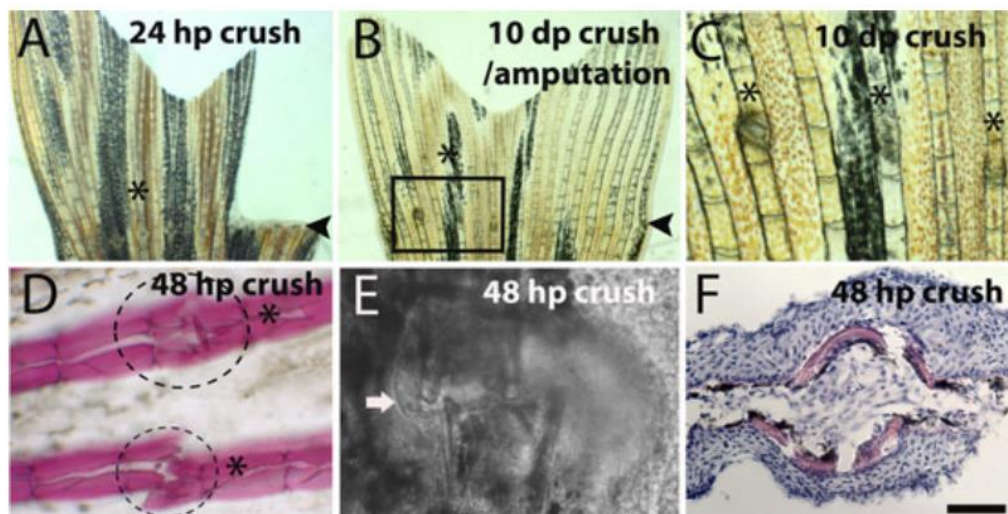


**Figure 1.5 Differences in tissue architecture after crush and amputation induced regeneration in the same caudal fin.**

**A–C)** Bright filed image of a caudal fin after crush and cut at (A) 24hpc/a and (B) 10dpc/a. (C) Magnification of the inset in picture B.

**D)** Alizarin Red staining for bone matrix at 48 hpc; dashed lines indicates the region of callus formation that is not stained with Alizarin Red.

**E)** Bright field confocal image of 48hpc injury site, the arrow highlights the callus structure.

**F)** Hematoxilin/Eosin staining in a transversal section of a 48hpc ray.

Arrowheads indicate the amputation plane and asterisks indicate crush injury area in A and B, and crush injury sites in C and D. Scale bar corresponds to 500 μm in A and B, 200 μm in C, 100 μm in D and 50 μm in E and F (Sousa et al., 2012)

Sousa et al. (2012) proceeded to conduct comparative molecular characterisation. Firstly blastema formation was assessed using the blastema marker *muscle segment homeobox B* (msxb) (Nechiporuk and Keating, 2002). They reported that blastema formation was delayed in the crush injury as compared to amputation (fig 1.6 A-D). In addition, they examined proliferation around the injury side using the proliferation marker PCNA (fig 1.6 E, F) and concluded that initiation of proliferation was also delayed after crush injury, when compared with epimorphic regeneration after amputation.
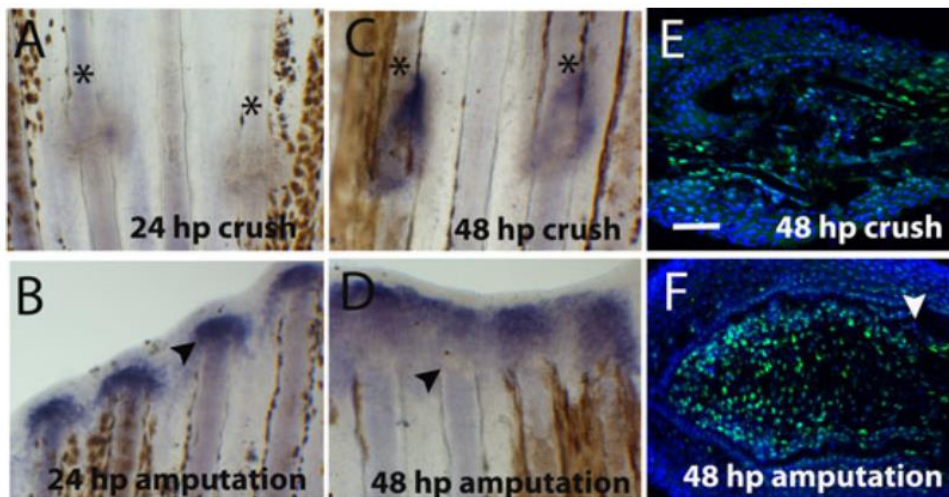


**Figure 1.6 Blastema marker, *msxb*, and proliferation after crush injury.**

**A–D)** Whole mount in situ hybridization for msxb mRNA at (A) 24hpc (B) 24hpa (C) 48hpc (D) 48hpa.

**E-F)** Immunohistochemistry for the proliferation marker PCNA (green) at (E) 48hpc around the crush injury site and (F) 48hpa blastema (distal region is to the left and proximal to the right). DAPI (blue) is staining the nuclei.

Arrowheads indicate the amputation plane and asterisks indicate crush injury sites. Scale bar corresponds to 100 μm. (Sousa et al., 2012)

They went on to molecular examination of bone formation. They decided to use early skeletogenesis marker *osterix (osx)*, a marker of the intermediate stages of skeletogenesis *collagen 1 (colI)*, and also a late differentiation marker involved in mineralisation, *osteonectin (osn)* (Sousa et al., 2012). Based on results of the In Situ Hybridization they concluded delayed skeletogenic gene expression in crush as compared to amputation (fig 1.7) (Sousa et al., 2012).
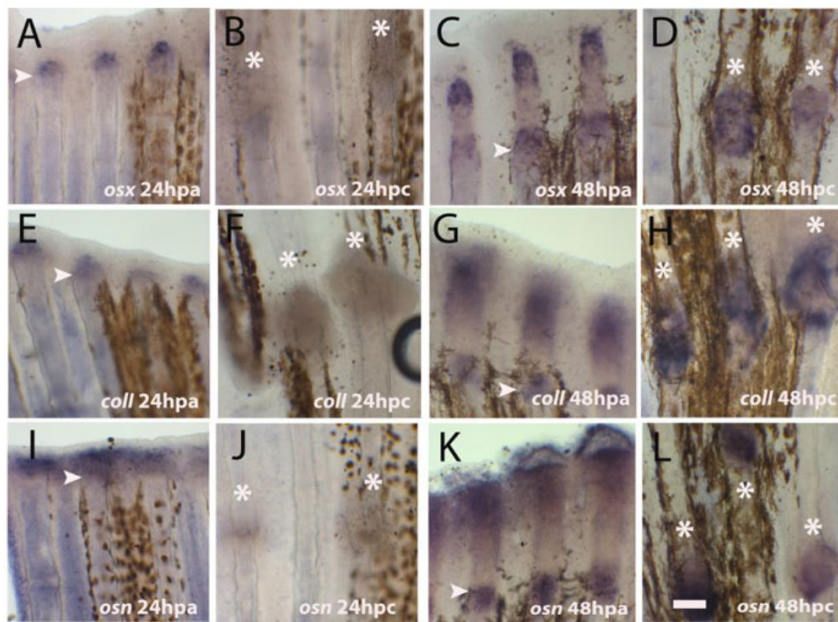


**Figure 1.7 Expression of skeletogenesis genes after crush injury.**

**A–L)** Whole mount in situ hybridization for mRNA detection

**A–D)** *osterix* at (A) 24hpa; (B) 24hpc (C) 48hpa (D) 48hpc

**E–H)** *collagen I* at (E) 24hpa (F) 24dpc (G) 48hpa (H) 48hpc

**I–L)** *osteonectin* at (I) 24hpa (J) 24hpc (K) 48hpa (L) 48hpc

Arrowheads indicate the amputation plane and asterisks indicate crush injury sites. Scale bar corresponds to 100 μm in all panels. (Sousa et al., 2012)

In order to assess whether the delayed osteogenic gene expression delayed the deposition of the new bone tissue, they used Anti-Zns5 antibody which labels osteoblast at any stage of their differentiation. The results reassure researchers that osteogenesis is delayed based on the lack of Anti-Zns5 antibody expression in the crush site at 24hpc in contrast to 24dpa (fig 1.8 A, B).
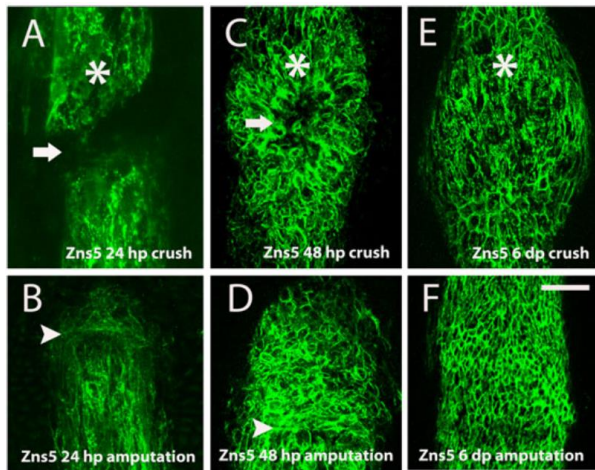
**Figure 1.8 Skeletal cell deposition was delayed and patterning was affected after crush injury.**

**A–F)** Immunohistochemistry with the antibody anti-Zns5 to detect skeletal cells. (A) 24hpc, the arrow highlights the lack of bone cells deposition (B) 24hpa (C) 48dpc (D) 48hpa (E) 6dpc (F) 6dpa, near the amputation plane.

Arrowheads indicate the amputation plane and asterisks indicate crush injury sites. Scale bar corresponds to 50 μm in all panels. (Sousa et al., 2012)

Interestingly, experiment using Anti-Zns5 antibody also showed structures of newly formed bone and differences in the new bone geometry between crush and amputation injuries (fig 1.8 C-F). Bone formed around the crush had a spherical shape and seem to be deposited from proximal as well as distal sides of the injury, in contrast to amputation where bone is structured in more organised way, formed in the straight proximal to distal line. Differences in new bone patterning led authors to conclude that crush injury leads to prolonged bone repair as compared to amputation (Sousa et al., 2012).

Overall, Sousa et al. (2012) concluded that regeneration after crush injury is delayed when compared with amputation, however both of them share similar molecular mechanisms. Authors suggested that crush injury leads to prolonged bone repair as compared to amputation and that it may impair bone re-patterning (Sousa et al., 2012).

## 1.1.7. Aim of experiments shown in this chapter

Inspired by those findings I have decided to look more closely into similarities and differences between crushing and amputating bones in zebrafish tail as well as trying to identify similarities and differences between human bone fracture and crush injury in zebrafish tail.

## 1.2.    Materials and methods

### 1.2.1.    Animal licence

All experiments performed in UK were approved by Ethical Review Committee under Project Licence no 40/3459 and Principal Personal Licence no 40/10722. Experiments performed in Singapore were under The Institutional Animal Care and Use Committee (IACUC) number 140924.

### 1.2.2.    Zebrafish husbandry

Zebrafish lines used for experiments performed in UK were bred and housed in the Bateson Centre aquaria in The University of Sheffield, under strictly regulated conditions controlled by UK Home Office. Fish used for experiments in Singapore were bred and housed in the aquaria of Institute of Molecular and Cell Biology in Biopolis, Singapore and were controlled by the Agency for Science, Technology and Research and The Institutional Animal Care and Use Committee. All were kept in a regulated 14:10 hour light-dark cycle.

### 1.2.3.    Zebrafish nucleic acid collection

#### 1.2.3.1.    Extraction of zebrafish genomic DNA

Whole zebrafish embryos, the tip of adult zebrafish tail or scales were used as a source for genomic DNA. Adult tissue was collected from live, anesthetised individuals. Zebrafish were fin clipped or scaled by gentle body stroking with forceps along the body axis from anterior to posterior. Collected tissues were digested for 4h in 55˚C in lysis buffer with 1% Proteinase K (Boehringer 1000144, 10mg/ml in PBST stock). The enzymatic reaction was stopped by 15min enzyme inactivation at 98˚C. Ready to use genomic DNA was stored at -20˚C until required.

#### 1.2.3.2.    Embryos RNA Extraction

Pools of embryos of the same developmental stage were homogenized in 200µl of Trizol (Sigma-Aldrich, T9424), another 300µl of Trizol was added, mixed and incubated at room temperature (RT) for 5min. 100µl of chloroform was added, the mixture was shaken for 15sec and incubated for 3min at RT. Each tube was centrifuged at 12000G for 10min at 4˚C. The supernatant was removed, the pellet was washed with cold 70% ethanol and spun at 7500G for 5min. Ethanol was removed and the pellet was left to air-dry, then dissolved in 30µl water. Concentration was checked on nano-drop spectrophotometer, and size was checked by electrophoresis 1% agarose gel. RNA was kept at -80˚C until needed for cDNA preparation.

### 1.2.3.3. cDNA Synthesis

Pre-reaction mix was prepared from 1µl Oligo(dT) Primer (Invitrogen, 18418012), 11µl of 1µg of extracted RNA dissolved in water and 1µl of 10mM dNTP Mix. Components were mixed together, incubated for 5min at 65˚C and cooled down on ice for 2min. Remaining reaction components were added: 4µl of 5x First-strand buffer, 1µl of 0.1M DTT, 1µl of RNAse inhibitor and 1µl of Superscript III RT. All 20µl were mixed and incubated for 1 hour (1h) in 50˚C for cDNA synthesis followed by 15min in 70˚C for polymerase inactivation. The reaction's products were stored at -20˚C until needed.

## 1.2.4. In situ Hybridization

### 1.2.4.1. Probe design

Sequences used for probe design were downloaded from Ensembl database (www.ensembl.org). Primer sequences were designed using the online primer designing website, Primer3 (www.Primer3.com). Probe length was kept between 600 and 1100bp ensuring 3'UTR incorporation. Primers used for probe templates preparation are listed in Table 1.2.

| Name of the primer | Sequence of the primer in 5' to 3' direction 5' -> 3' |
|---|---|
| bglap f | ACAGAAGCGAACATGAAGAGTC |
| bglap r T3 | **GGATCCATTAACCCTCACTAAAGG**GAACCCATAGTAGGTTTTATAGGCGG |
| Sox9a f | GCACAAGAAAGATCACCCCG |
| Sox9a r T3 | **GGATCCATTAACCCTCACTAAAGG**GACGACTCATATGGGCATGCA |
| sox9b f | CCGTACCCCACATTCAGCTA |
| sox9b r T3 | **GGATCCATTAACCCTCACTAAAGG**GACCCTTCCCTCATAGCAGG |
| col2a1a f | AGAAGACATCCAGACTGCCC |
| col2a1a r T3 | **GGATCCATTAACCCTCACTAAAGG**GGGAGTGGGATGGATTGGGAA |
| col2a1b f | AACAGAAGTGCTTCCGAACG |
| col2a1b r T3 | **GGATCCATTAACCCTCACTAAAGG**TTGTCCTGATTCGAGGCTCT |
| Fbl1f | CAGCCTTCAAAGGGTGATGC |
| Fbl1r T3 | **GGATCCATTAACCCTCACTAAAGG**TGTGTCCACCAGTGGGCAGCGCA |
| hmcn2 f | CAGCCCTCAGCTCACATACA |
| hmcn2 r T3 | **GGATCCATTAACCCTCACTAAAGG**CACTGGAGGAACCAACACCT |
| il1f | ATGGCATGCGGGCAATATGA |
| il1r T3 | **GGATCCATTAACCCTCACTAAAGG**CTAGATGCGCACTTTATCCT |
| ctsK f | CCTTAGTCCTCAGAACCTGGTG |

| | |
|---|---|
| ctsKr T3 | **GGATCCATTAACCCTCACTAAAGG**ATCCAGTACTTCTTGCCTCTCG |
| Col10f | CCCATGCTTGTTTTCCTGTT |
| Col10r T3 | **GGATCCATTAACCCTCACTAAAGG**TCCAAACAGATCTGACCTTGC |
| spp1 f | GGACCAGGCAGCTACAGAAG |
| spp1r T3 | **GGATCCATTAACCCTCACTAAAGG**CACTGCCGTCTGTCGTCTAA |
| Col1 f | GCCAGCAGATTGAGAGCATC |
| Col1 r T3 | **GGATCCATTAACCCTCACTAAAGG**TGAGCAAAAGCGACGAACAA |

**Table 1.2 List of primers used for probes templates preparations. Sequence in bold indicate T3 polymerase binding site.**

### 1.2.4.2. Template preparation

RNA probes were synthetized from genomic DNA, cDNA or premade plasmids. PCR reaction used appropriate primers. 100µl PCR reaction consisted of 20ng of plasmid (or 1µl of 1:10 dilution of cDNA or genomic DNA) and 1µl of each primer (from 25µM stock). Primers were designed with T3 sequence attached to 5' end of the reverse primer to allow RNA synthesis directs from PCR product (highlighted in red, Table 1.2). Each PCR reaction consisted of initial denaturation 3min step at 95˚C followed by 35 cycles consisting of 45sec denaturation at 95˚C, 30sec annealing at the annealing temperature ranging from 50 to 61˚C and elongation at 72˚C, with timing depending on the length of expected PCR product. After 35 cycles, the reaction was incubated for additional 10min at 72˚C. As the final step, the reaction was cooled down to 4˚C and product was run on a 1% agarose gel to clean it up and to check product size by comparison to 2-Log DNA Ladder (New England BioLabs N3200L) run along the side. Upon correct result DNA band was gel extracted using QIAquick Gel Extraction Kit (QIAGEN ID28706) following kit protocol and kept at -20˚C until required as the template for RNA probe synthesis.

### 1.2.4.3. RNA probe synthesis

Probe RNA was transcribed from DNA templates. Transcription mix was prepared including 1µg DNA dissolved in nuclease free water to a volume of 13µl, 2µl of DIG RNA Labelling mix (Roche 11277073910), 1µl of Protector RNase Inhibitor (Roche 03335399001), 2µl of 10x Transcription buffer and 2µl of T3 RNA polymerase (both from Roche 11031163001), mixed well and incubated for 2h at 37˚C. 1µl of TURBO™ DNase (ThermoFisher AM1348) was added and incubated for 15min at 37˚C. 30µl of nuclease free water and 30µl of Lithium chloride were added (ThermoFisher AM1348), mixed thoroughly and placed for 30min at -20˚C. Tubes were centrifuged at 4˚C and 12000G for 15min to precipitate the RNA. The supernatant was removed, the pellet was washed with 1ml of 70% ethanol, centrifuged again and after removing all alcohol, re-suspended in nuclease free water.

### 1.2.4.4. In situ hybridization reaction

In situ hybridization of selected genes were performed using the standardized protocol for whole mount samples adapted from Thisse and Thisse (2008) . Probes were designed and synthesized as described above. Fish tails collected after amputation and after crushes were arranged based on time of recovery after injury. Amputated tails of the same recovery times as crushed tails were pooled in one Eppendorf tube, e.g., 3 days post crush (3dpc) with 3 days post amputation (3dpa). 1.5ml tubes were used throughout the experiment. Tails were washed gradually with 100% methanol for and moved to -20˚C for storage.

Solutions used (50ml):

| | |
|---|---|
| HYB- | 25ml formamide |
| | 12.5ml 20X SSC |
| | 250µl 20% Tween-20 |
| | 460µl 1M Citric acid |
| | fill with $H_2O$ up to 50ml |
| HYB+ | 25mg tRNA |
| | 50µl heparin stock |
| | Topped up to 50ml with HYB- |
| Blocking Buffer | 1ml sheep serum |
| | 100mg BSA |
| | Topped up to 50ml with PBST |
| Staining buffer | 5ml tris pH9.5 1M |
| | 2.5ml MgCl2 1M |
| | 1.66ml NaCl 4M |
| | 250µl 20% Tween-20 |
| | Topped up to 50ml with PBST |
| Bleaching solution | 10% H2O2 |
| | 0.5 XSSC |
| | 5% Formamide |

**Table 1.3 List of solutions used for ISH**

On day 1, tails stored in 100% methanol at -20˚C were rehydrated through methanol series 10min in 60% Methanol in PBST, 10 min in 30% Methanol in PBST, then washed in PBST 2 x 5min. Tissues were digested 10 min with Proteinase K (10

µg/ml) in PBST and re-fixed in 4% PFA-PBS for 20min in room temperature (RT). After four sets of 5min PBST washes samples were placed in HYB+ (Table 1.3) in 70˚C for 2h then HYB+ was replaced by HYB+ containing 1 in 200 dilutions of antisense RNA probe and hybridized at 70˚C, overnight.

Day 2 consisted of series of 10min washes in 70ᵒC: 25% 2X SSCT/75% Hyb- (Table 1.3), 50% 2X SSCT/50% Hyb-, 75% 2X SSCT/25% Hyb-, 2X SSCT. Then 30min 0.2X SSCT wash in 70ᵒC. Followed by series of 10min washes in Room Temperature (RT): 25% PBST/75% 0.2X SSCT, 50% PBST/50% 0.2X SSCT, 75% PBST/25% 0.2X SSCT and PBST. After washes samples were placed in blocking buffer (Table 1.3) for 3-4h at RT and incubate in antibody solution overnight with agitation (anti-DIG 1:10000) at +4˚C.

Day 3 consisted of six sets of 15min washes in PBST and two sets of 5min washes in freshly prepared staining buffer (Table 1.3). Afterward, samples were moved to staining solution prepared with staining buffer, 4.5µl of 50mg/ml NBT and 3.5ul 50 mg/ml BCIP per each 1 ml of solution. Reaction run at RT until staining development then it was stopped by 15min wash in PBST 1mM EDTA. Samples were re-fixed in 4% PFA 30' and put through MeOH series. They were kept in 100% methanol for 2h and gradually rehydrated (60%, 30% MeOH in PBST). After two sets of 5min washes in PBST, specimens were bleached in bleaching solution (Table 1.3) for 10min in 37 °C, wash three times in PBST and put through glycerol series (50%, 100%). They were kept in RT in 100% glycerol until imaging.

### 1.2.5. Imaging

Stained samples were imaged on Axio Imager Z2 (Zeiss).

### 1.2.6. DNA constructs/plasmids synthesis for transgenic line creation

#### 1.2.6.1. Multi Gateway

Multi Gateway cloning system (Invitrogen) was used to create transgene contains plasmids. Multi Gateway system allows for simultaneous cloning of 3 DNA fragments: p5e landing on 5'end of the construct, pMe in the middle and p3e on the 3' end, into a backbone called destination vector (fig 1.9). Method was published by Karimi at al. (2007).
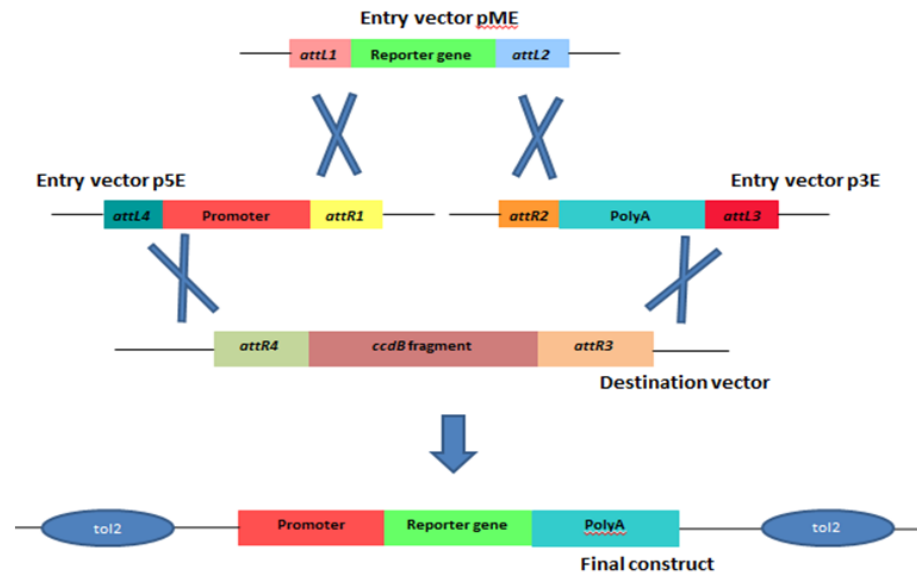
**Figure 1.9 Graphical representation of Gateway reaction**

Gateway enzymatic reaction allows for simultaneous insertion of 3 entry vectors into destination vector in pre-determined order. Content of p5e entry vector will always be instrted at 5' end, pMe in the middle and p3e at 3' end. Backbone of destination vectoe can be modified for specific use e.g. to carry tol2 sides allowing further construct incorporation into zebrafish genome.

For zebrafish research, the destination vector was previously modified to carry Tol2 sites as well as marker gene CryA-Venus. Tol2 sites allow incorporation of the construct into zebrafish genome after microinjecting it into one cell stage zebrafish embryo together with Tol2 transposase mRNA. CryA promoter drives Venus expression in the lens as a reporter gene. Upon successful insertion of the construct into the fish genome, Venus fluorescence protein was expressed in CryA expressing cells – in the eyes. This allowed fast screening of embryos for construct incorporation. In my constructs, p5e was carrying promoters of interest, either *osteocalcin (bglap), osterix* or *twist*, which were supplied from HR lab resources. pMe carried Kaede coding gene, a photosensitive protein whose conformation can be changed by exposure to UV light (Li et al., 2010), resulting in a shift of absorbance and emission of the light spectrum, visually changing fluorescent protein from green to red. Such a photosensitive protein permits lineage tracing of specific cell types. P3e contained sequences encoding a polyA tail signal used to stabilize mRNA after transcription.

### 1.2.6.2. Cloning promoters into p5e

Promoters were cut from preexisting plasmids, appropriate restriction enzymes were chosen, compatible with existing p5e, in order to create desired p5e plasmid. Osx was cut out from osterix:mCherry plasmid from lab resources by BamHI and KpnI enzymes and ligated into previously digested with the same unicutters p5e MSCII plasmid, creating osterix p5e (fig 1.10).
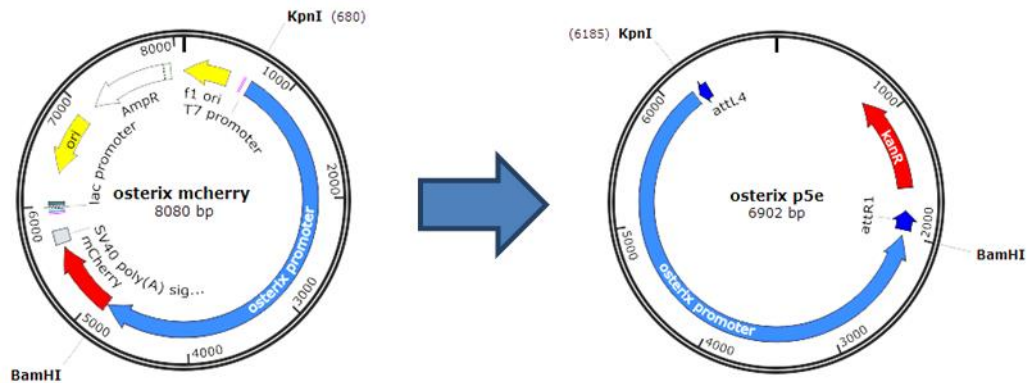


**Figure 1.10 graphical representation of restriction digest cloning**

This example shows cloning of osx promoter into p5e entry vector, which can be further used in Gateway cloning reaction in order to create constructs driving other genes under control of osx promoter.

### 1.2.6.3. Restriction digests cloning

Components of restriction digest (Table 1.4) were mixed well and incubated at 37˚C for 2h allowing full digestion of DNA. Digested plasmids were run on 1% agarose gel along with 3µl of loading buffer allowing DNA visualization. DNA band sizes were checked under the UV light. Bands of expected sizes were excised and extracted using QIAquick Gel Extraction Kit (QIAGEN Cat No/ID28706) following kit protocol. Gel extracted DNA was used for ligation reaction (Table 1.4) run for 10min at 25˚C, followed by transformation.

| Restriction digest (20 µl) | 0.5µl of each enzyme |
| --- | --- |
| | 2µl of adequate to this enzymes buffer |
| | 2µg of plasmid DNA |
| | water topped up to 20µl |

| 1% agarose gel | 0.6g agarose |
|---|---|
| | 60ml TBA (electrophoresis buffer) |
| | 2µl ethidium bromide |
| Ligation reaction | 8µl of gel extracted DNA |
| | 1µl of Quick Ligation Reaction Buffer |
| | 1µl of Quick T4 DNA Ligase |

**Table 1.4 Reagents needed for Restriction digest cloning**

### 1.2.6.4. Transformation

TOP10 competent cells (ThermoFisher C404006) were used for transformation. 5µl of ligation reaction were added to 45µl of thawed on ice cells. 30s heat shock at 55˚C was performed to force plasmid uptake by hollowed bacteria. Recovery phase of 1h at 37˚C in SOC medium was followed by overnight incubation on LB agar with appropriate antibiotic selection.

### 1.2.6.5. Plasmid DNA isolation

Ten colonies were picked from each LB plate using sterile pipette tips and transferred to 2ml of LB with appropriate antibiotic for 16-18h incubation on 37˚C shaker. Next day bacteria were harvested by centrifugation and plasmid was extracted with QIAprep Spin Miniprep Kit (QIAGEN Cat No/ID: 27106), used following manufacturer protocol.

### 1.2.6.6. Cloning confirmation

Isolated plasmid was subjected to restriction digest with a dual cutter digesting plasmid into two uneven parts which allow determination of successful cloning.

### 1.2.6.7. Gateway Cloning - LR reaction

Accurate amounts of reaction components (Gateway® LR Clonase® II Enzyme mix, Invitrogen, Catalog number**:** 11791100) were added to ensure high cloning efficiency. The protocol was adapted from original stated in manual provided by LR clonase manufacturer, Invitrogen. 10 µl reaction consisted of 10fmol of each entry vector, 20fmol of destination vector, 1µl of TE buffer and 1µl of LR clonase. The Reaction was mixed well and incubated for 16h at 25˚C, followed by reaction termination by addition of 1µl ProK provided in the kit and 10min incubation at 37˚C, then stored at -20˚C until transformation.

## 1.2.7. Microinjections into zebrafish embryo

Pairs of adult zebrafish were kept overnight separated from each other by the transparent divider. Just before the start of injections, the divider was removed. After 5min eggs were collected and kept in embryo water with 0.1% of methylene blue ready for injections. Glass

needles used for injections were pulled with Sutter Instruments P-97 Flaming/Brown Micropipette Puller using Standard Wall Borosilicate Tubing without Filament (Sutter Instruments B100-50-10). Narishige IM-300 Microinjector was used. The nucleic acid in the concentration of 20ng/µl was injected into 1cell stage eggs lined up against microscope slide placed in the petri dish. For plasmid DNA injections 40ng/µl of plasmid was mixed 1:1 with Tol2 RNA prior to injections.

Despite successful transgene incorporation and transgenic lines creation, lines were not used in experiments presented in this thesis due to weak fluorescence signal.

### 1.2.8. Zebrafish transgenic lines

The followed transgenic lines were used: *myeloid-specific peroxidase (mpx)* transgenic line *Tg(mpx:GFP)*, previously known as Tg(*mpo*:GFP) (Renshaw et al., 2006) marking neutrophils - used for assessing inflammation in injured zebrafish; *osterix (osx)* transgenic line *Tg(osx:mCherry)* (Spoorendonk et al., 2008) marking osteoblasts - used for ossification tracing; and *ETS transcription factor a (fli1)* transgenic line Tg(*fli1*:EGFP) marking blood vessels (Lawson and Weinstein, 2002) - used in assessing changes in blood vessel sizes over time.

All of the above-mentioned transgenic lines were used to analyse temporal progression of crush healing and stages of recovery.

### 1.2.9. Tail amputation and crush injury

Adult zebrafish, 1 year old (1ypf – year post fertilization) +/- 2 months, were anaesthetized in 0.013% tricaine in fish water and placed on a petri dish. Excess water was removed by paper tissue and the fish was positioned on its side, anterior to the left, dorsal to the top. The tail was spread out evenly on the surface of the petri dish. Dish with anesthetized fish was placed under the dissecting stereomicroscope. A scalpel blade was used to amputate end of the tail at the position of most proximal ray bifurcation. Alternatively, forceps number 5 were used to perform a bone crush. Four crushes per tail were introduced, on the 2$^{nd}$ and 4$^{th}$ ray from both dorsal and ventral sides of the tail at the second segment anterior to the first level of bifurcation (Fig 1.11 A). Bone crush was performed in the middle of the segment with the minimal strength needed to crush through both of the hemirays without impacting for adjacent tissues (Fig 1.11 B). After surgery, fish were returned to the tank with fish water for recovery.
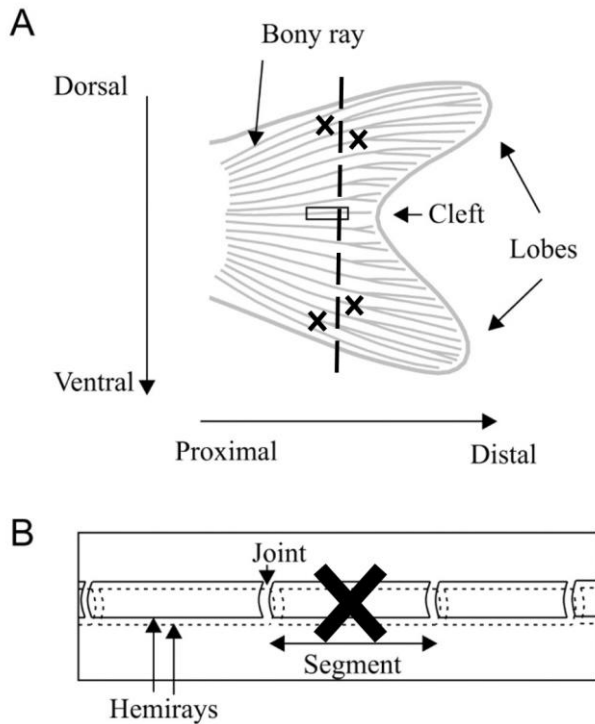
**Figure 1.11 Crush injury location on the zebrafish tail**

**A** schematic representation of zebrafish tail with amputation plane indicated by dashed line and crush sites indicated by crosses

**B** schematic representation of one bony ray with a crush site indicated by the cross

Image adapted from Rolland-Lagan et al. (2012)

## 1.2.10. Tail collection and storage

Subsequent tail collection was planned based on the required stage of regeneration/repair. Anesthetized fish were culled through instant brain disruption by needle poke, following Schedule1 rules and regulations for animal husbandry and humane culling. Fish was instantly moved to petri dish and a scalpel blade was used to dissect the tail off. Collected tails were placed in 4% Paraformaldehyde (PFA) solution and kept at 4˚C, shaking, overnight (o/n). The following day, specimens were washed in PBST briefly, then moved through methanol series consisting of 30%, 60%, and 100% methanol. Specimens were kept 10 min in each solution and then stored in 100% methanol at -20˚C.

## 1.2.11. Cartilage and bone staining – fixed tissues

Alizarin red and alcian blue are well-known dyes used for skeletal staining. Many protocols were established to ensure the best possible performance. I adjusted these standard protocols to produce best results in available conditions.

### 1.2.11.1. Two colour cartilage and bone staining

Specimens stored in 100% methanol in -20°C were moved to Alcian blue solution (consisting of 0.1% Alcian Blue (Sigma-Aldrich, A5268), 20% 0.1M Acetic Acid (Fluka, 38050) and 80% methanol) for overnight staining at room temperature. This was followed by a methanol/PBS wash series consisting of 10min washes in 100%, 60%, 30% methanol, and two 10min PBST washes. Subsequently, samples were pre-incubated in 0.5% KOH for 15min and moved to 0.2% Alizarin Red solution in 0.5% KOH for overnight staining at room temperature. Next day, three sets of 5min washes with 0.5% KOH were performed followed by 1h hydrogen peroxide bleaching (3% $H_2O_2$ in 1% KOH). Upon completion, three sets of 10min PBST washed were performed and samples were moved to glycerol for storage (UltraPure™ Glycerol, Invitrogen, Catalog number: 15514011).

### 1.2.11.2. Separate colour staining

When separate staining of cartilage and bone was required, the above protocol was divided for two separate staining protocols, either for Alizarin Red or Alcian Blue, to give better staining resolution.

### 1.2.11.3. HCl Alcian Blue staining

Rehydrated tissues kept in 100% methanol at -20°C were rehydrated through methanol series (100%, 60%, 30%) and washed twice with PBST for 10min then moved to Alcian Blue stain solution (1% HCl, 0.1% Alcian Blue in H2O) for overnight staining. Next day, the samples were washed 15min in PBST and bleached in the bleach solution (0.3% $H_2O_2$, 1% KOH in water) for 30min at 37°C, then washed in PBST and stored in glycerol.

### 1.2.11.4. A two-colour acid-free cartilage and bone stain

Stored tissues were re-hydrated from methanol as above and moved to acid-free double stain solution contain 1ml of Part A solution and 10µl of Part B solution. Part A consist of 0.02% Alcian Blue, 0-200mM $MgCl_2$ and 70% ethanol while Part B is a 0.5% Alizarin Red in water. After staining, tissues were bleached in 1.5% $H_2O_2$ and 1% KOH for 20min in room temperature, then moved to 20% glycerol with 0.25% KOH for 30min, 50% glycerol with 0.25% KOH for 2h and finally to 50% glycerol with 0.1% KOH for storage, kept in 4°C until imaging.

Protocol was adapted from Walker and Kimmel (2007)

## 1.2.12. Fluorescent bone staining in vivo

Alizarin Red S (Sigma-Aldrich, A5533) and Calcein (Sigma-Aldrich, 17783) were used for fluorescent in vivo bone staining. 0.001% Alizarin Red or 0.0005% calcein in fish tank water

was used for overnight staining. Fish were immersed in small tanks in 200ml of staining solution the night before imaging. Following day, they were moved to clean water for a quick wash, anesthetized and imaged under a Zeiss fluorescent microscope.

### 1.2.13.    Callus size measurements

Callus sizes were measured in AxioVision software. The width of the callus was measured in µm and normalized against the width of an unbroken part of proximal, segment, in order to omit ray size differences between individuals and obtain actual callus sizes. Therefore, data about callus size was presented and plotted on the chart as a proportion of unbroken bone.

## 1.3.    Results

### 1.3.1.    Fracture healing is considered a distinct type of regeneration

Fracture healing leads to restoration of the original bone from prior to the injury, without fibrous scar formation (Marsell and Einhorn, 2011). Fracture healing can be considered as a distinct type of regeneration, as it leads to restoration of lost tissue in almost exact form (Epari et al., 2010). In zebrafish, regeneration usually refers to their ability to regrow lost tail through the blastema formation and epimorphic regeneration. Therefore, the starting point for this project was to compare a crush in zebrafish caudal fin to the process of amputated tail regeneration, widely explained in the literature (Akimenko et al., 1995, Ng et al., 2014).

### 1.3.2.    Experimental setup

For 7 consecutive days, tail amputations or crush injuries were performed on 10 adult fish each. Both techniques were performed as described in Materials and Methods, at the level of the most proximal bifurcations in the tail. Crush injury was performed at 4 rays in each tail, 2nd and 4th from dorsal and ventral sides of the tail. On the 8th day, fish were humanely culled following the Schedule 1, Act 1986 Code of practice regulations. Their tails were collected, halved (separating two tail lobes from each other), fixed in 4% PFA and stored in 100% methanol at -20˚C. Specimens were grouped according to the amount of days of post-injury recovery, e.g. 1 day post crush (1dpc) or 1day post amputation (1dpa). For each ISH experiment, four tail lobes of amputated tails were put together with four of the ones holding crushed rays at each collected time points of post-injury recovery 1-7days post (1-7dp). Representative images of results can be seen in fig1.12 A.

### 1.3.3.    Osteogenic markers are expressed during bone crush repair as well as in blastemal outgrowth

Sousa et al. (2012) developed a zebrafish fracture model performed on rays of the caudal fin. They showed that several skeletogenic markers are expressed after crush injury and have summarized that skeletogenic response was delayed in the crush as compared with amputation. I decided to check this more extensively, investigating not only 1 and 2 day post amputation/crush (dpa/c) as Sousa et al. (2012) did, but every day up to 7dpa/c (fig1.12). I used skeletogenic markers stated in the publication as my starting point, including *collagen 1a1a (col1a1a), collagen10a (col10a), osteocalcin (bglap)* and *osteopontin (spp1).*

**Figure 1.12 Temporal progression of osteogenic genes expression in injured zebrafish tails**

**A)** Whole mount in situ hybridization results showing osteogenic genes expression throughout 7days time course of zebrafish tail recovery after crush or amputation (amp). Scale bar corresponds to 100 µm in all panels, n=8

**B)** Graphic representation of time point of certain markers appearance, identified by colours of names allocated in panel **A**

### 1.3.4.      Skeletogenic genes expression patterns

*Collagen type 1 alpha 1a* (*Col1a1a*) presence was detected in the crush site as early as 1dpc (Fig 1.12A, *Col1* crush) while following amputation, detection was possible only at 2dpa (Fig 1.12A, *Col1* amp 2dp*). Col1a1a* expression in the crush site on 1dpc was loosely scattered around the crush area covering mainly ray parts adjacent to the crush. By 4dpc, temporal progression showed directed staining condensation towards crush plane, a transverse axis through the crush. 5dpc showed clearance of expression from the centre of the crush. On 6dpc expression was detected particularly in the periphery of the crush area, forming an oval shape around the crush site, whilst by 7dpc staining was almost gone. In the amputation case, light staining came on 2dpa at the amputation plane. 3dpa showed strong staining of the tissue expanding distally from the amputation plane. On 4dpa, staining was seen on the distal ridge of newly formed outgrowth and this pattern continued to be detected till 7dpa with additional inter-segmental staining on 7dpa.

*Collagen type 10 (Col10)* was upregulated as soon as 3dpa/c (Fig 1.12). The difference in its expression between crush and amputation lay not in the timing of the appearance but in the pattern of expression. In the fin outgrowth after amputation, *col10* seemed to reside in the nascent bony rays formed in the blastema. Expression increased towards the distal end of the nascent bone, marking mainly the tip of newly formed rays (fig 1.12A, *col10* amp). In the crush, it appeared from the proximal side of the crush on 3dpc and moved towards the centre of the callus by 5dpc, where it was detected until 7dpc (fig 1.12A, *col10* crush). It should be noted that in zebrafish *col10* is marking both, cartilage (Casar-Borota et al., 2016) and bone (Fang et al., 2016).

*Osteocalcin (bglap)* expression was detected from 4dpa/c onwards. Osteocalcin expression appeared at the base of the outgrowth of the amputation and on the proximal bone adjacent to the crush, which might indicate directions from which osteoblasts were recruited to the site of injury. Staining progressively expanded distally during outgrowth after amputation (fig 1.12A, *bglap* amp). In the crush, injury staining appeared broadly spread on the crushed rays but not in the crush site at 4dpc. Over time spatial distribution changed from broadly spread across a few segments around the crush site to tightly encapsulating the crush itself (fig 1.12A, *bglap* crush).

*Osteopontin (spp1)* expression upon the crush injury was observed as soon as 1dpc as scattered single cells around the crush site, both on the rays and also in the area surrounding them. By 2dpc staining appeared strong and crush localized, however, some

cells were stained also adjacent to the crush segment joints. 3, 4 and 5dpc staining appear much weaker with the second wave of strong upregulation by 6dpc appearing directly at the crush plane (fig 1.12A, *spp1* crush). In the blastemal outgrowth after amputation staining appeared in the rays at the amputation plane and in loosely scattered cells in the blastema at 2dpa. Expression persisted until 3pda, but from 4dpa onwards its appearance became localized to the inter-segmental junctions in regenerated rays. From 5dpa onwards additional staining was detected at the tip of forming rays (fig 1.12A, *spp1* amp).

Based on these early stage experiments, similar trends in the bone markers in response to bone injury in the crush as well as in amputation were observed. However, ranges of differences, spatial as well as temporal (fig 1.12B) were noted. Encouraged by these results, further amputations to crush healing comparisons were performed, focusing on cellular contribution to those healing processes.

### 1.3.5. Fibroblasts do not contribute to crush healing

As Homeobox *msx* genes were previously proposed as markers of the blastema (Akimenko et al., 1995), I decided to use them to check if crush injury activates blastema marker expressions. I decided to use *msxC,* as its expression in blastema was already established (Ng et al., 2014). Moreover, In larval zebrafish fins, msxC marks fibroblasts, which later contribute to adult lepidotrichia (Lee et al., 2013) in chick developmental studies *msx* genes also were suggested as fibroblasts markers (Akiba et al., 2001). Therefore, I was interested to find out if fibroblasts take part in crush regeneration. Another two genes, *hmcn2* and *fbln1* known to mark fibroblasts (Lee et al., 2013) were tested along with msxC (fig 1.4).

Surprisingly, none of the three genes show expression in the crush regeneration while all of them are expressed in the blastema outgrowth (fig 1.4). *msxC* showed similar expression pattern to *hmcn2*. Expression appeared as soon as 2dpa at the amputation plane. On 3 and 4dpa it becomes broader along the proximo-distal axis, yet moved together with blastema outgrowth to the distal tip of developing rays. By 5 and 6dpa staining moved to the distal ridge of blastema, yet still appeared very strong. Staining of *fbl1* was weaker and more localized although the pattern remains very similar to the other two genes. It appears on 2dpa, becoming stronger, localized at the tip of newly formed rays at 3dpa, and moving to the blastema ridge by 4 and 5dpa. By day 6, the expression had eased.
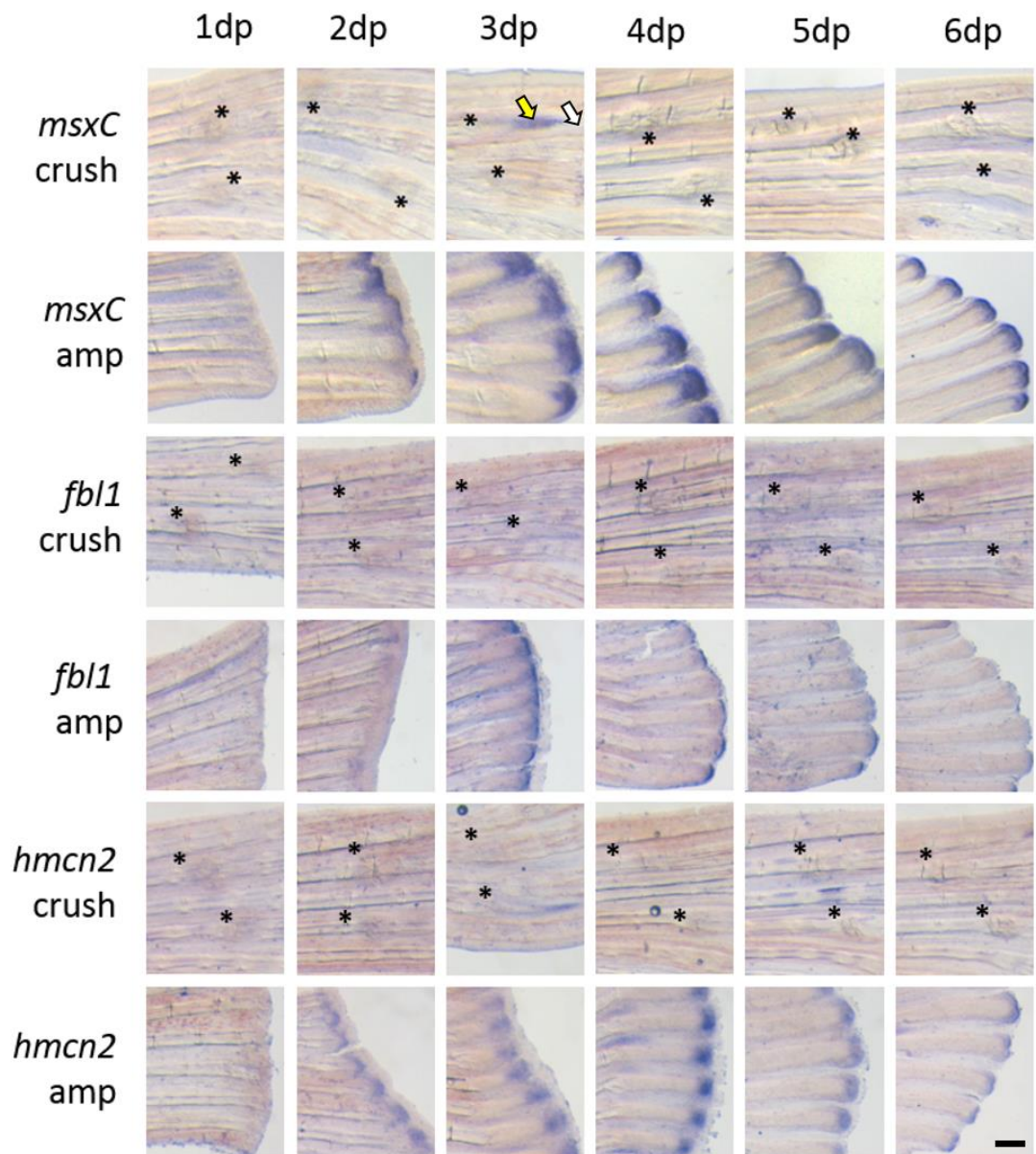
**Figure 1.13 Fibroblast do not take part in crush recovery**

Whole mount in situ hybridization results showing fibroblast markers expression throughout 7days time course of zebrafish tail recovery after crush and amputation (amp). Yellow arrow shows blastemal outgrowth at the incident of ray loss, white arrow indicates lack of distal part of broken ray.

Scale bar corresponds to 100 μm in all panels, asterisks indicate crush injury sites, n=8

It is important to mention that small blastema formation was observed after loss of distal part of ray following some of the crush injuries (fig 1.13, msxC crush 3dp). Blastema is known to be formed after fin amputation (Adamski et al., 2014) as well as individual rays loss (Abel et al., 2014). Studies showed blastema formation after surgical removal of a few

segments of the ray (Abel et al., 2014). Data showed that small blastema can also be formed as a result of bone fracture (yellow arrow in fig 1.13, *mscC* crush), where lepidotrichia distal to the crush are lost (white arrow in fig 1.13, msxC crush 3dp). Recovery undergoes through blastema driven regeneration. The reason for the loss of ray in a number of circumstances is unclear. More information about ray loss after the crush is provided in chapter 4.

## 1.3.6. Zebrafish crush repair phases mirror those of mammalian fracture repair

As I determined that crush injury does not form a blastema nor repair via epimorphic regeneration, unless the broken ray get lost. I asked what might be the mechanism underlying bony ray healing after the crush. I decided to look for stages of mammalian bone fracture recovery in our crush model.

Mammalian fracture repair follows 4 stages of recovery: inflammation, soft callus formation, hard callus formation and remodelling (Schindeler et al., 2008). I decided to check if those four stages can be detected throughout zebrafish ray crush healing.

### 1.3.6.1. Stage 1 – inflammation

I checked two types of inflammatory cells: macrophages and neutrophils. I used whole mount in situ hybridization (ISH) of Interleukin1 (*il1*) to a mark inflammatory cells. Probe of *il1* was previously described as marker for inflammatory cells (Ogryzko et al., 2014) and it was shown to mark cells in first 24h post injury. I performed ISH for *il1* on tails which were collected 1, 2, 4, 8, 12, 16, 20 and 24hours post crush (hpc) with 4 lobes per time point. Results of ISH were confirmed with neutrophil-specific Tg(*mpx:GFP)* transgenic zebrafish line, which was imaged at 5min post crush (5mpc) and 3, 7.5, 10.5, 15.5, 25.5, 72hpc. Fig 1.14 B shows changes in cellular movement around the same crush in described range of time points.

Inflammatory cells were recruited to crush site as soon as 2 hours after injury and the peak of *il1* was detected 8hpc and remains very strong until 12hpc (fig 1.14A). Results from Tg(*mpx:GFP)* signal display a similar time points for neutrophils recruitment, however, fluorescent cells are detected in the crush for longer, up to 15.5hpc, suggesting that recruited leukocytes persist in the crush but do not activate interleukin gene expression anymore or that GFP perdured in cells longer that *il1* mRNA. Both of the markers were cleared from the crush site by 24hpc, with the interesting phenomenon of explicit exclusion of neutrophils from the crush by 72hpc (fig 1.14B, 72hpc).
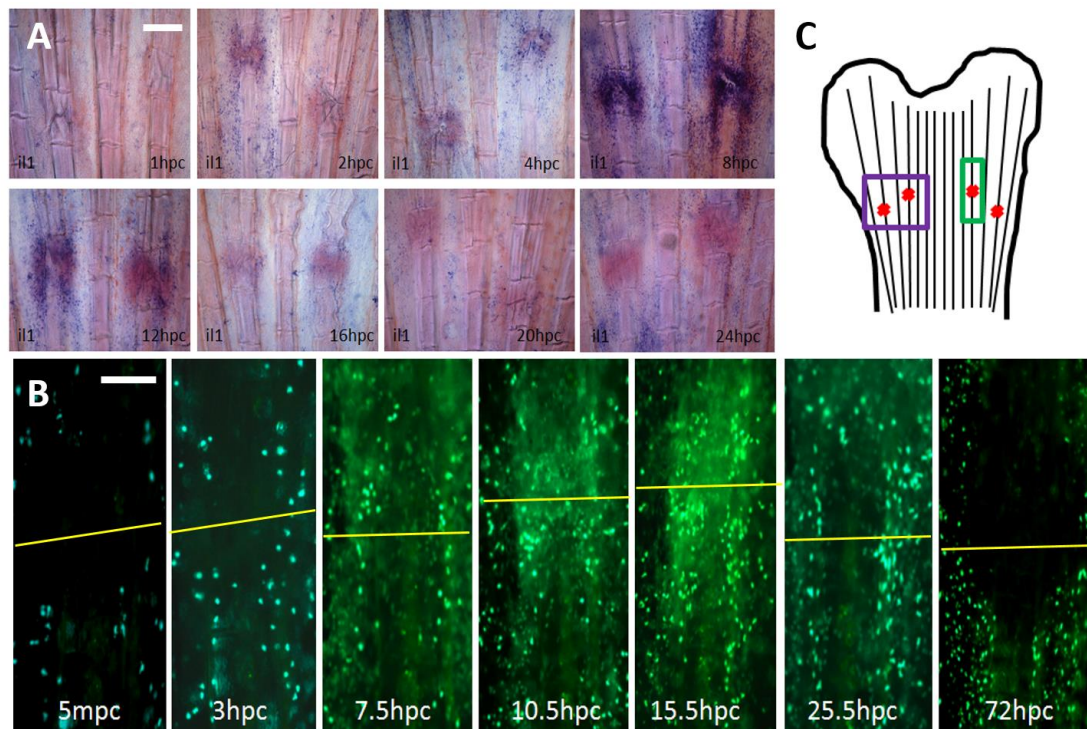
**Figure 1.14 Inflammation stage in crush injury appears almost immediately after the crush**

**A)** *il1* whole mount in situ hybridization marking inflammatory cells within the crush sites throughout the first 24hpc, timing first cells appearance for 2hpc and peak of inflammatory response for 8-12hpc, n=8

**B)** Tg(*mpx:GFP*) crush time course showing neutrophils recruitment to the crush site and very strong clearance from the crush site by 72hpc, n=8

**C)** graphical representation of zebrafish tail with introduced crush injuries marked as red crosses. Purple rectangular represent area which was imaged in panel **A** and green rectangular represent area which was imaged in panel **B**

Yellow lines indicate crush plane. Scale bar corresponds to 100 μm in all panels in **A**, and 50μm in all panels **B**

### 1.3.6.2. Stage 2 – cartilage callus formation

Cartilage callus formation is an important element stabilizing the fracture site. It is more flexible than bone, allowing alignment of two parts of the broken bone. However, it is rigid enough to keep broken parts in one place, preventing further disruptions of neighbouring tissues. Cartilage callus formation was tracked here by Alician Blue staining. Alcian Blue stains acidic polysaccharides such as glycosaminoglycans in cartilage, allowing temporal analysis of cartilage formation (Walker and Kimmel, 2007). Several protocols for Alcian Blue combined with Alizarin Red were tried (fig 1.15) but double staining made it difficult to distinguish between stainings and to determine staining intensity. Therefore, Alcian Blue single staining was performed for optimal effect. Staining shows clearly marked callus at 4dpc. Blue stain becomes incorporated into the ball of tissue encapsulating the crush. The process of callus formation seems to start at 3dpc and persist until at least 5dpc.

Cartilage formation might seem slightly controversial to be observed in dermal bone repair as dermal bone is believed to be produced through intramembranous ossification (Santamaria et al., 1992), which does not contain cartilage formation step (fig 0.10). Therefore, I went to the literature to find a possible explanation for this phenomenon. Upregulation of chondrogenic markers in blastema was previously reported by Smith et al. (2006). Encouraged by those findings, I decided to check chondrogenic markers in the crush as well as after the amputation. It was shown that paralogs of chondrogenic genes might play an important role (Duran et al., 2015), therefore I checked both, a and b versions of sox9 and col2a1 genes (fig 1.16).

Expression of paralogs of *sox9* as well as *col2a1* can be found in the crush as well as amputation cases (fig 1.16). Staining appeared weak, despite the prolonged time of stain development indicating either: low amounts of mRNA present in the specimen or just a weak and ineffective probe. However, I rejected the second possibility by testing probes in developing zebrafish embryos as a control while staining tails. Embryo stain was strong and cartilage specific and compared to previously published patterns (Thisse, 2005). Both paralogs of *sox9* were noticed in the blastema at 3dpa, however, the only *sox9a* appeared in the crush on 3dpc. *Sox9* staining was very faint and inconsistent across the samples, therefore it was hard to determine chondrocyte presence based on it alone. *Col2a1* staining, despite also being faint, was more noticeable in the crush and amputation. Interestingly, the spatial distribution of the stain differentiates both the paralogs from each other. *Col2a1a* appeared distally to the crush, while *col2a1b* was present directly at the

crush site, where cartilage callus was getting formed. *Col2a1b* was stronger than *col2a1a* in the distal amputated fin (fig 1.16).
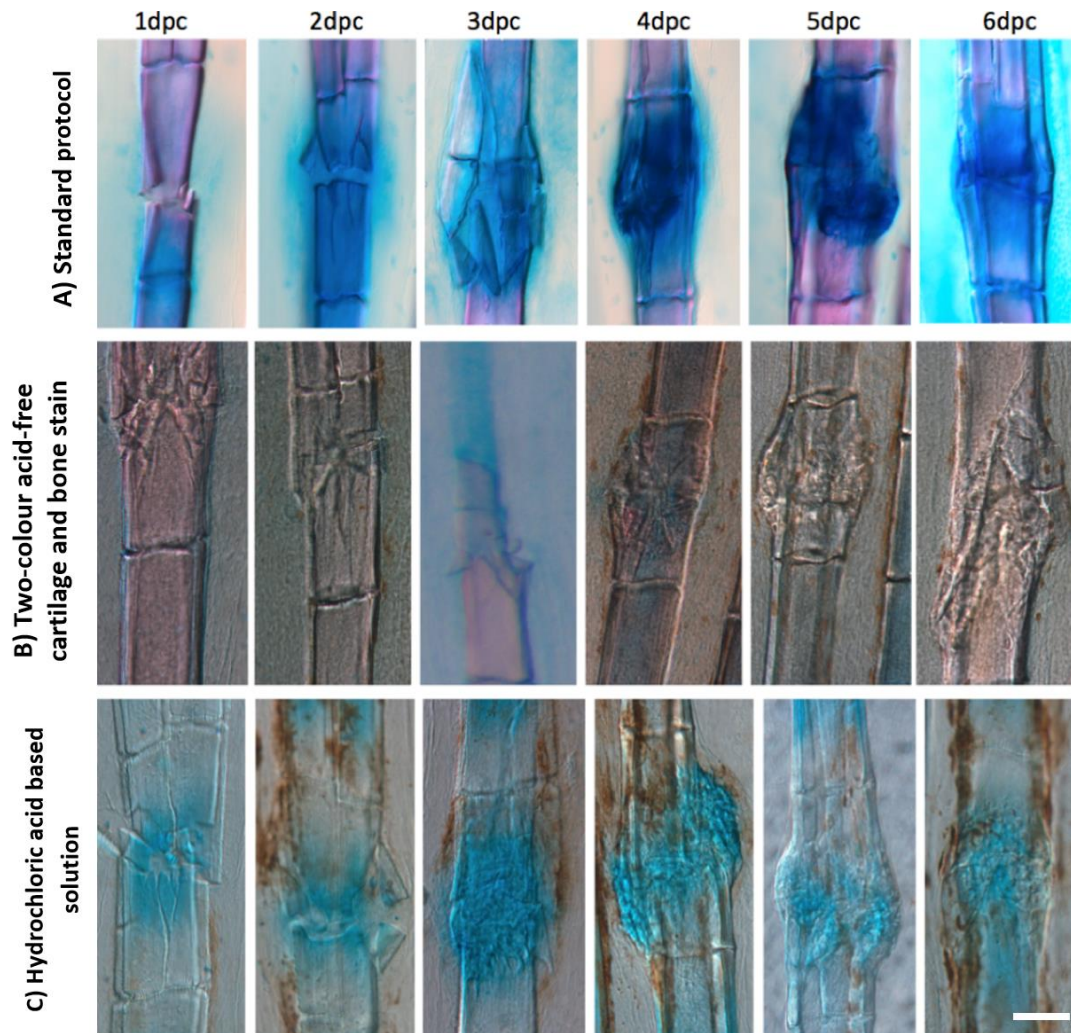


**Figure 1.15 Differences between 3 cartilage staining protocols**

**A)** Standard combined Alizarin Red and Alcian Blue protocol showed very strong overlapping staining of tissues, which made it impossible to distinguish between cartilage and bone calluses formation stages

**B)** Two-colour acid-free cartilage and bone stain, initially developed for zebrafish larva staining (Walker and Kimmel, 2007) appeared extremely week for adult bone, therefore distinguishing between bone and cartilage was not possible. Interestingly, we observed ray loss in 3dpc sample, where two tissues were clearly distinguishable from each other

**C)** Hydrochloric acid based solution stain appeared to be the most accurate for this experiment clearly reviling cartilage callus formation starting at 3dpc and forming rounded callus ball at 4dpc around the crush site

Scale bar corresponds to 50 µm in all panels.
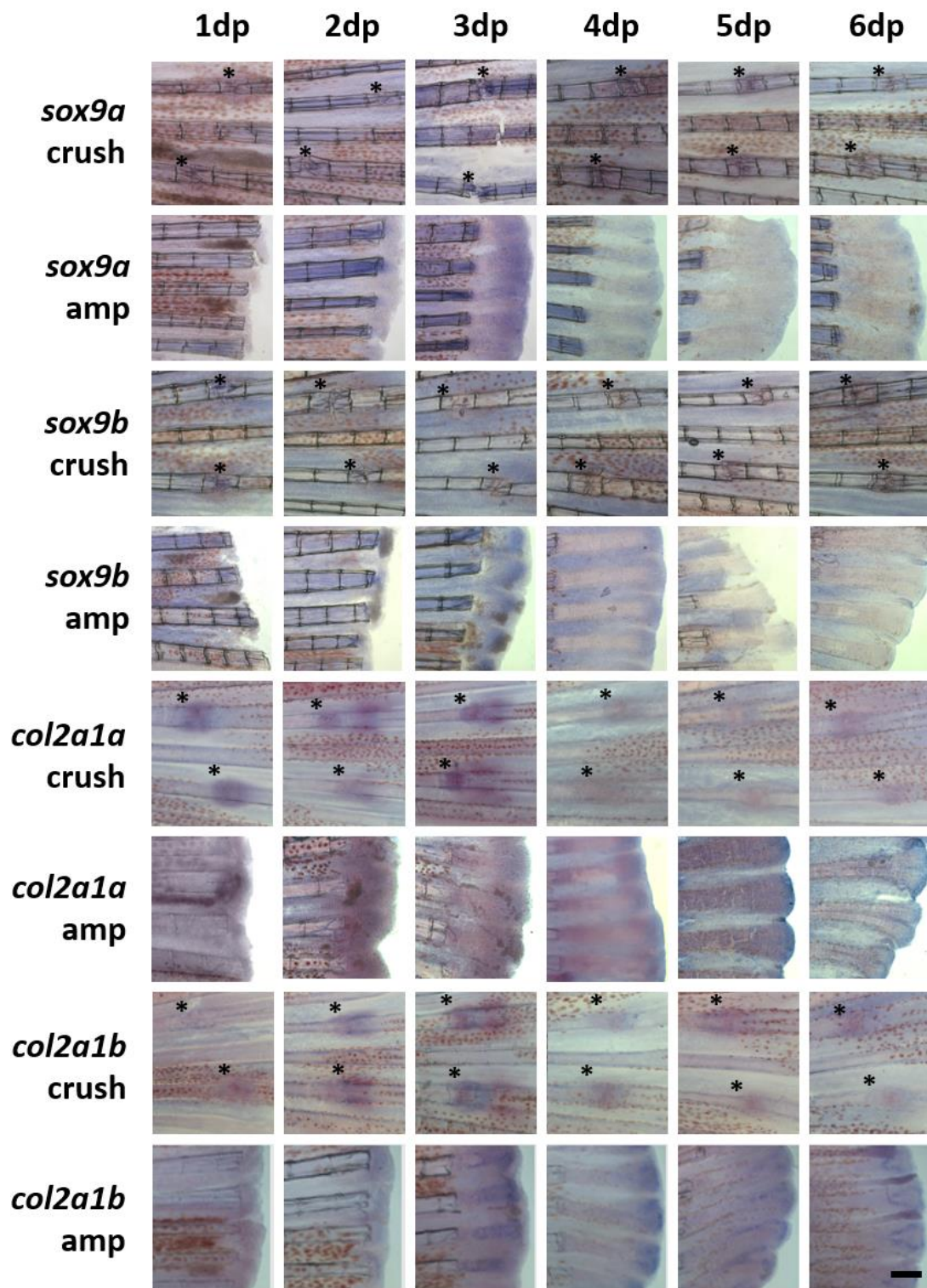
**Figure 1.16 Temporal progression of chondrogenic genes expression**

Whole mount in situ hybridization results showing cartilage formation markers expression throughout an 8days time course of zebrafish tail recovery after crush and amputation (amp). Scale bar corresponds to 100 µm in all panels. Asterisks indicate crush injury sites.

### 1.3.6.3. Stage 3 – hard callus formation

Hard callus (bony callus) was formed by ossification of the cartilage callus. At that stage, cartilage callus seems to work as a scaffold for osteoblasts to deposit mineralised tissue on (Slowik and Bermingham-McDonogh, 2013). I performed Alizarin Red staining (separate from Alician Blue) (fig 1.17A). Alizarin red stains mineralized tissues, therefore all bony elements are stained red from 1dpc, however, strongly stained new bone deposition is clearly distinguishable from old bone, starting from 4dpc, when mineralized tissue starts to be laid around the crush and fracture edges. Ossification of the callus became obvious from 5dpc onwards (fig 1.17A).
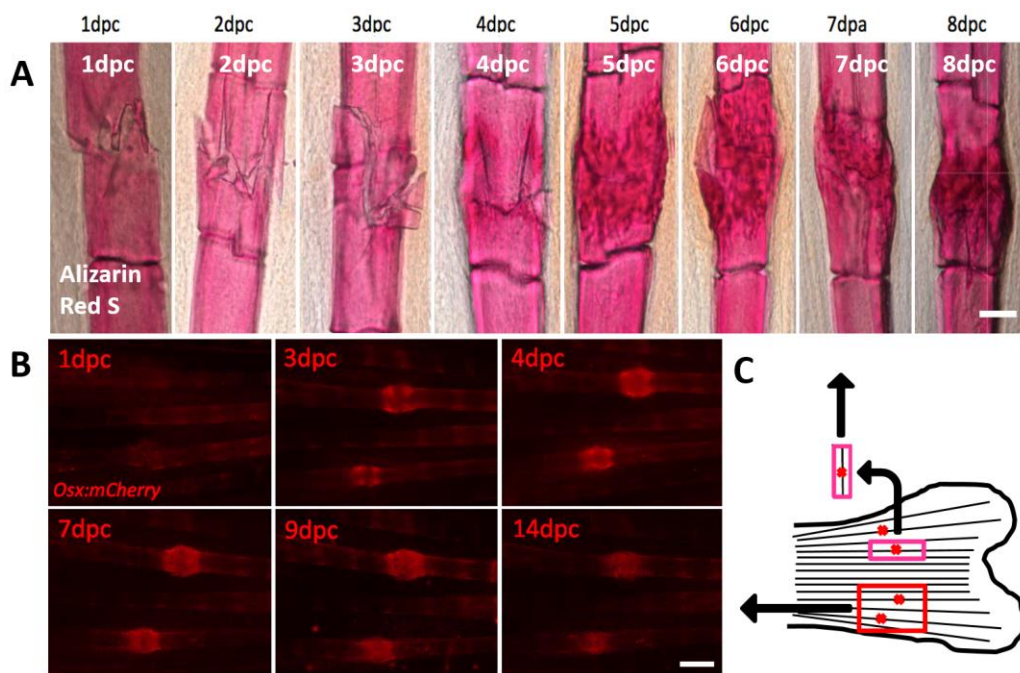


**Figure 1.17 Stage 3 – hard callus formation clearly noticeable from 5dpc**

**A)** Alizarin Red stain on fixed crush tissue from 1dpc to 8dpc

**B)** *Tg(osx:mCherry)* transgenic line marking *osterix* in bone laying osteoblast accumulated around forming callus

**C)** graphical representation of zebrafish tail with introduced crush injuries marked as red crosses. Pink rectangular represent area which was imaged in panel **A** and red rectangular represent area which was imaged in panel **B**

Scale bar corresponds to 50 µm in all panels in **A**, and 100µm in all panels **B**

Together with chemical bone stains, I observed osteoblast recruitment to crushes by use of transgenic lines. I attempted to create two transgenic lines, Tg(*osx:Kaede)* and Tg(*osc:Kaede*) to mark respectively early and late osteoblasts in vivo. Unfortunately, I did not succeed to obtain founders with good expression level. Therefore, I used

*Tg(osx:mCherry)* (Renn and Winkler, 2009) which showed good fluorescence in the crush. By using this line, promoter induction in osteoblast recruitment to the crush site was observed as early as 3dpc, forming strongly fluorescent bulky callus by 7dpc, and which faded away by 14dpc (fig 1.17B).

These results, together with skeletogenic markers, marked by ISH shown in Figure 1.12, allowed us to time stage 3 occurrence for approximately 4dpc to 8dpc. However, mineralised matrix continued to be deposited beyond this point and osteoblasts were still active, as they play an active role in the remodelling stage.

### 1.3.6.4.    Stage 4 – remodelling

In order to evaluate remodeling of bony callus, crushes were stained with Alizarin Red S, allowing tracking callus formation and re-formation (fig 1.18A). Callus sizes were measured in AxioVision software. The width of the callus was measured in µm and normalized against the width of an unbroken part of ray, of a segment proximal to the crush, to control for ray width differences between individuals and to obtain actual callus sizes. The region of measurement was indicated by white brackets in fig 1.18A, where 1 indicated width of unbroken bone in adjacent segment. Therefore, callus size was presented and plotted on the chart as a fold of unbroken bone (fig 1.18C). According to these data, width of mineralized callus at 5dpc is approximately 1.4 proportion of unbroken bone and it was progressively reduced over time. By 14dpc callus size was significantly reduced as compared to 5dpc and continued to be reduced with the time (fig 1.18A, C). Significance was checked by one-ways ANOVA using GraphPad Prism 7.01 program.

Osteoclasts, bone resorbing cells play the main role in bone remodelling. They bring back the original bone shape through trimming away bony callus. I used *cathepsin K* (*ctsK*) as an osteoclast marker and through ISH I was able to determine when the expression of *ctsK* is enhanced, showing us osteoclast recruitment to the crush site (fig 1.18B). *CtsK* stain appeared as soon as 1dpc and was highly localised to the crush site. 2dpc staining remains strong, however, its localisation changed to the crush peripheries. By 3dpc staining intensity decreased, however, it risen again in the second wave of upregulation at 10dpc. It appeared crush localized and remained in this position through 13, 16, and 19dpc. By 22dpc staining intensity was decreased again.

*CtsK* upregulation in the 1st and 2nd day post crush suggests high bone resorption on those two time points. Due to my observations osteoclasts worked then to clear the crush site of

bone debris scattered around the crush, formed in the process of bone crushing. Osteoclast active between 13 and 19dpc was presumably trimming bony callus away.

These data were consistent with the TRAcP staining on those time points performed by my colleague from Roehl lab, Luis Medina Sanches.



**Figure 1.18 Remodelling takes place from 9dpc onwards**

**A)** Alizarin Red S in vivo staining marking newly formed bone, white brackets show the way how callus was measured

**B)** ISH results showing cartilage formation markers expression throughout 7days time course of zebrafish tail recovery after crush

**C)** callus size shown as a fold of unbroken bone * p<0.05 ** p<0.01, ANOVA, n=8

Scale bar corresponds to 50 μm in all panels in **A**, and 100μm in all panels **B**

## 1.4. Discussion

### 1.4.1. Unlike amputation, crush injury in zebrafish tail does not heal through epimorphic regeneration

Based on the results presented in this chapter I state that process of healing after crush and after amputation significantly differ from each other. Unlike amputation, crush healing did not undergo epimorphic regeneration through blastema formation. I was not able to detect blastemal markers through 7 days post crush recovery, whilst blastema markers were strongly expressed after amputation (fig 1.13). Additionally, mini blastema formation after loss of distal part of the broken ray (fig 1.13, yellow arrow) supported my interpretation that two mechanisms of healing can work interchangeably depending on the severity of the injury. In support of this, Abel et al. (2014) showed that not only amputation can cause blastema formation, but also the removal of a few segments of an individual ray. I propose the presence of a mechanism detecting the severity of an injury, which directs and triggers adequate type of healing. Inflammatory cells have been previously shown to be able to sense tissue damage (Chen and Nunez, 2010) and activate and recruit different cell types to the injury site such as osteoblasts or osteoclasts, through cytokines such as il1 and il6, as well as growth factors, such as TNFs, PDGFs and VEGFs (Pape et al., 2010), therefore I propose that they are responsible for this mechanism.

### 1.4.2. Crush injury in zebrafish tail heals through 4 stages of fracture healing

I focused on understanding the process of crush healing in the rays of the fish tail. I aimed to reveal organised, step by step mechanism which follows crush injury. I found, that it precisely followed previously described four stages of mammalian fracture healing model (Slowik and Bermingham-McDonogh, 2013).

#### 1.4.2.1. Stage 1 - inflammation

Inflammation was reported by *il1* ISH staining marking neutrophils and macrophages (Ogryzko et al., 2014). In addition, I used in vivo time series of Tg(*mpx:GFP)* possessing fluorescently labelled neutrophils. Results of both assays overlap, giving a strong indication of the inflammatory response in the first 2dpc. Inflammatory cells were clearly excluded from the crush site by 3dpc. It is interesting to compare it with previously published amputation data, where inflammatory cells were reported to reside at blastema for up to 7dpa (Petrie et al., 2014). Possible explanations for faster inflammatory cells clearance in the fracture site might be correlated to the size of the wound, indicating area exposed for external factors which could determine the time needed for total clearance of pathogens

and debris form the injury site. Another explanation for fast inflammatory cells removal from fracture site might be physical exclusion of inflammatory cells by forming callus. This poses an interesting research question if prolonged inflammation, for example through an infection, can delay or block callus formation and the repair process (more information in Chapter 4).

### 1.4.2.2.    Stage 2 – cartilage callus formation

Firstly, I presented cartilage callus formation by Alcian Blue staining, which marks cartilage glycosaminoglycans. Cartilage formation in the dermal bone of zebrafish tail is a controversial topic, previously mentioned in several publications (Smith et al., 2006). This problem was addressed in Smith et al. (2006) research on regeneration outgrowth after tail amputation, where chondrogenic markers, like *sox9* and *col2*, were present in blastema. Those findings were evaluated in Duran et al. (2015) where evidence of chondrogenic markers presence was shown by ISH on sections of developing blastema. I used these markers to evaluate cartilage callus formation following crush injury in the zebrafish tail. I performed ISH on a time course of amputation recovery and also crushed specimens to give a full picture of cartilage forming potential. My results supported previously published findings of chondrogenecity in recovering injury in zebrafish tail. Staining for *col2* and *sox9* in blastema formed after amputation was noticeable, however, weak staining and background reduced the clarity of the results. ISH repetitions with different experimental conditions did not improve results, indicating that the amount of cartilage formation is probably low, as found previously (Smith et al., 2006, Duran et al., 2015). Cartilage marker staining after crush injury was much more defined and localised to the injury. I conclude that cartilage callus formation in the zebrafish tail crush healing can be considered a distinct and independent stage of recovery. In order to improve the quality of results, future ISH could be performed on criosections as demonstrated in literature (Duran et al., 2015, Smith et al., 2008).

### 1.4.2.3.    Stage 3– hard callus formation

Hard callus formation was initially examined by ISH stainings of known osteogenic markers, such as *bglap, spp1* and *osx*. All of them mark stages of osteoblast development and their successive appearance allowed understanding of recruitment and maturation of osteoblast throughout hard callus formation. I evaluated changes in spatial distribution of staining throughout the temporal progression of the healing process. Osteogenic markers were strongly upregulated throughout recovery after crush. *Col1* and *spp1* staining appear as soon as 1dpc followed by the appearance of *col10* and *osx* on 3dpc and *bglap* on 4dpc. This

indicated that osteogenic processes are triggered as soon as 1dpc injury, probably by residing osteoblasts. By 3dpc *osx* and *col10* markers were visible at the crush site, indicating recruitment and differentiation of new osteoblasts. Their maturation activated *bglap,* which I noticed at the crush site 4dpc. All osteogenic markers remained expressed till 7dpc, indicating that bone deposition takes place continuously. It is important to mention that osteoblasts are required at callus mineralization stage as well as in remodelling (Slowik and Bermingham-McDonogh, 2013). Therefore, we were not able to determine the time point of the finish of stage 3, yet know start time point and time point of stage 3 peak performance. Moreover, Alizarin Red, Alizarin Red S, and Calcein stainings indicated mineralized tissue deposition around the fracture site forming a hard callus. Callus growth indicated hard callus formation stage and narrowing of the callus indicated initiation of the remodelling stage.

### 1.4.2.4. Stage 4 - remodelling

Remodelling is the 4th and the last stage of fracture healing. Osteoclasts, working antagonistically to osteoblasts, are the main cell type involved in this step. Remodelling is based on bony callus resorption. The importance of osteoblasts should not be underrated as the remodelled bone has to be laid down after osteoclastic resorption. The ratio between anabolism and catabolism of bone in this recovery stage is shifted towards catabolism, since the overall outcome is a reduction of bone callus mass. I examined osteoclast presence by *cstK* ISH, known as an osteoclast marker. Osteoclasts recruitment to the crush site was seen as early as 1dpc. This can be explained by the presence of bone debris scattered around the crush site. Debris form due to crush injury, therefore, osteoclasts are recruited early in the healing process to remove debris and to smoothen rough edges of the broken bone, preparing the broken bone fragment for re-joining. From a cellular point of view, it was shown that osteoclast possess *il1* receptors on their surface (Boyle et al., 2003).Therefore they are sensitive to the activation of inflammatory response by inflammatory cells, which I observed in stage 1. After initial upregulation of *ctsK*, staining signal reduces until 10dpc when it re-appears. I predicted that this is the time when callus remodelling takes place. Staining persists in place until 19dpc and is much reduced by 22dpc. I observed the reduction in bony callus size until at least 38dpc, suggesting remodelling occurs continuously until at least this time point, and probably beyond as the total callus resolution at this time point was not present.
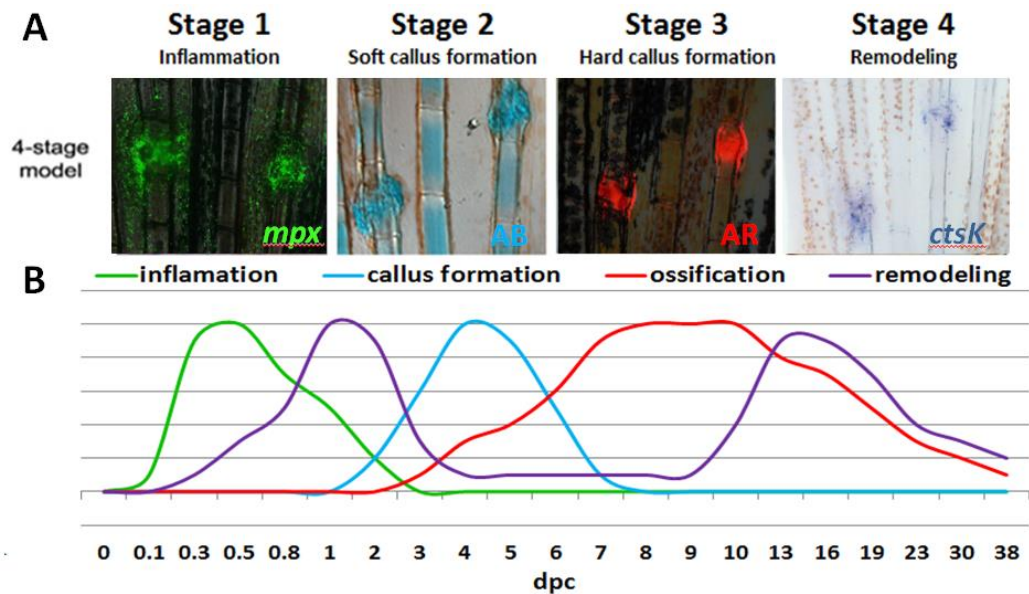
**Figure 1.19 Graphical representation summarising 4 stages of crush healing in zebrafish ray**

**A)** Example of techniques used to indicate each stage

**B)** Qualitative readout of markers expression

### 1.4.3. Four stages are easily distinguishable yet highly overlapping in temporal progression

Based on my results I was able to show a temporal distribution of all stages (fig 1.19). All stages overlapped, probably due to high molecular cross-talk between tissues and cells. Markers of all stages appear gradually. This phased response mimics results seen in mammalian models (Slowik and Bermingham-McDonogh, 2013). Zebrafish recovery time was twice as fast as the time reported in rodent animals. In rodent models, such as mice, the inflammatory stage can take up to 7 days, peak of cartilage callus formation was timed at 7-9days post trauma, peak of hard callus formation set as 14dpc and recovery usually starts not earlier than 3-4week post crush and take years to be fully finished (Einhorn, 1998, Marsell and Einhorn, 2011). The zebrafish crush model presented here cuts the required research time in half. Inflammation completely cleared from crush site by 3dpc, cartilage callus stage was timed for 3 to 5dpc and peak of hard callus formation lies around 7dpc.

### 1.4.4. Crush injury is a reliable and adequate model for human bone fracture

According to the results presented in this chapter, I showed that the crush model in the tail of zebrafish undergoes the same stages of regeneration as previously described in the healing of breakages in mammalian bones (Bostrom et al., 1995, Slowik and Bermingham-

McDonogh, 2013). With all the advantages of using zebrafish in biomedical research, this field could be easily expanded. I believe that presented here crush model can serve as fast and accurate fracture model allowing understanding of fracture healing at cellular and molecular level.

In addition, the crush model is able to help in understanding the impact of drugs or genetic diseases on fracture healing. By simply measuring differences between treated, untreated or disease affected individuals, we can determine which step of healing is perturbed.

In the following chapters, I am presenting the full range of examples showcasing the importance of zebrafish crush model in biomedical research. These range from experiments on bone mutants and drug treated animals to bacterial infection in crushed rays.

# 2. Chapter 2 – Fracture healing in an Osteogenesis Imperfecta Model

## 2.1. Introduction

### 2.1.1. Osteogenesis imperfecta

Osteogenesis imperfecta (OI), also called brittle bone disease, is a genetic disease mainly characterized by high bone fragility. Other phenotypic traits include blue sclera, impaired hearing, skeleton deformity, and dentinogenesis imperfecta (Forlino et al., 2011). OI is a highly diverse disease in term of genotype and phenotype. Currently, 15 different types of OI can be distinguished (Valadares et al., 2014), out of which the first four are caused by mutations in collagen I genes and differ from each other by the strength of symptoms. Type I is very mild with rare spontaneous fractures and mild skeleton deformations, whilst type II is the most lethal one. Children with type IV OI are born with many deformations of skeleton, numerous fractures of long bones, and a narrow chest with broken ribs, leading to premature death, usually due to inability to breathe. Based on malformations severity, types III and IV lay in between types I and II, with moderate strength of phenotype. An OI classification scale was made over 3 decades ago by Sillence (Sillence et al., 1979) and has been kept up to date as a guideline for assignment of OI types. Types V to XV are caused by mutations in non-collagen genes and usually are phenotypically compared to one or two phenotypic profiles out of four described by Sillence's division (Galicka, 2012). Genes mutated in types V to XV codes collagen-related proteins and correspond to either collagen chaperones or foldases encoded by *SERPINH1* and *FKBP10* (OI type XI)*;* collagen modifiers, e.g. components of 3-Hydroxylation Complex encoded by *CRTAP*, *LEPRE1*, *PPIB* (OI types VII, VIII and IX); collagen mineralization proteins encoded by *SERPINF1* and *IFITM5* (OI type V and VI); and collagen structural processing protein encoded by *BMP1* (OI type XII) (Marini et al., 2014). The focus of this thesis is type XII with mutations in *BMP1* gene.

### 2.1.2. Role of BMP1 in bone formation context

Bone morphogenetic protein-1 (BMP-1) is a tolloid-like metalloproteinase that plays a crucial role in osteogenesis (Asharani et al., 2012). In addition, it processes non-osteogenic related extracellular proteins like probiglycan, prolysyl oxidase, the γ2 chain of laminin-5 and chordin as well as in‑activating other bmp family proteins like BMP2 and BMP4 (Perren

et al., 1975). For the purpose of this study, my focus was shifted towards its importance in bone as well as cartilage formation by cleavage of C-terminus from procollagen precursors. C-terminus cleavage is crucial for precise collagen fibril formation (McKibbin, 1978), in particular, Col1, which is the main building element of osteoid and col2 of cartilage. Bmp1 was shown to cleave procollagens precursors for both of these proteins, as well as other collagen types (Perren et al., 1975).

### 2.1.3.  Spontaneous fractures and bone healing problems in OI patients

OI patients are well known for being prone to spontaneous bone fractures (Forlino et al., 2011). OI fractures display healing problems, delaying recovery or unabling fracture joining, creating non-union fractures (Gamble et al., 1988). OI fractures often lead to severe bone deformations, which express the need for surgical corrections (Anam et al., 2015). However, osteotomy performed on malformed OI patient bones, often also fall into slow- or non-healing category (Munns et al., 2004), the explanation for this are not known. Clinicians wish to understand details of OI fracture healing, therefore need for the animal model of OI fracture creation was expressed (Anam et al., 2015).

### 2.1.4.  Animal OI models

Previously reported spontaneous animal OI cases, including dogs (Campbell et al., 2001), cats (Evason et al., 2007) and recreated mutogenetically mice (Chipman et al., 1993) proved that this human disease can be easily modelled in animals. OI mouse models have been researched for over 2 decades, with most of them arising from mutagenic screens and exhibit mutations in collagen 1 genes, leading to mimicking OI types I to IV (Khillan et al., 1991, Pereira et al., 1993). A recent boom of genome modification tools, allowed researchers to create mouse mutants with desired mutations in col1, e.g. Brtl/+ murine model for OI type IV (Forlino et al., 1999) as well as other genes like IFITM5, mimicking OI type V (Lietman et al., 2015) . Unfortunately, the Bmp1 mouse mutant was perinatal lethal, therefore creating mouse model of OI type XII became a challenge (Suzuki et al., 1996). In order to create $Bmp1^{-/-}$ murine mutant, $Bmp1$ was conditionally targeted in order to induce postnatal ablation and avoid the prenatal lethality of $Bmp1^{-/-}$ (Muir et al., 2014). Null mice presented typical for OI phenotype including weak and brittle bones, spontaneous fracture formation and other skeletal features such as porous cortical bone (Muir et al., 2014).

### 2.1.5. Zebrafish OI mutants

Mutagenesis screens in zebrafish revealed several bone mutants, which have been shown to constitute OI model. These include severe and mild col1a1a mutants *Chihuahua (chi)* (Fisher et al., 2003) and *microwaved (med)* as well as *frilly fins (frf)* (van Eeden et al., 1996). The latter was identified as a *bmp1a* mutant and modelled a form of OI due to mutations in BMP1. Fish characterization was performed and compared with human BMP1 deficient patients showing striking similarities (Asharani et al., 2012). *frf* possessed fragile bones prone to spontaneous fractures, with elevated mineral density.

### 2.1.6. Aims of experiments shown in this chapter

Fractures of *frf* mutants were not assessed previously for healing ability and were not compared to human fracture healing ability, and this is the aim of experiments in this chapter.

## 2.2. Materials and methods

### 2.2.1. *frf* fish alleles used

4 different alleles of *frf* mutant fish were used. They were previously mapped and described by Asharani et al. (2012). *frf*$^{ty69}$ possessed missense mutation within the protease domain affecting conserved amino acids, *frf*$^{tp34}$ possessed nonsense mutation that truncated the protein at the end of the proteolytic domain, *frf*$^{tm317}$ and *frf*$^{tf5}$ possessed splice-site mutations, where *frf*$^{tm317}$ led to 21 amino acid long deletion from proteolytic domain and *frf*$^{tf5}$ created several erroneous splice products (fig 2.1) (Asharani et al., 2012). The range of mutant alleles provided range of phenotypical severity from *frf*$^{tp34}$ being the strongest allele, followed by *frf*$^{tm317}$, *frf*$^{ty69}$, *a*nd *frf*$^{tf5}$.
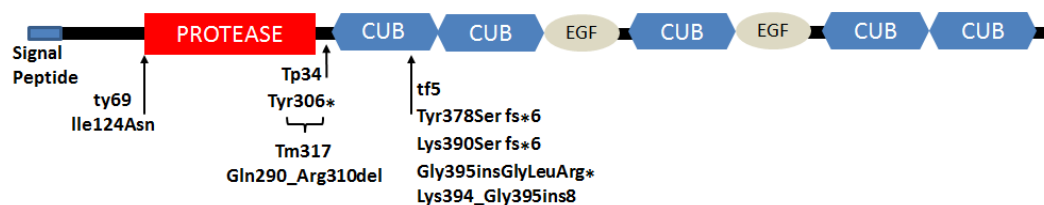


**Figure 2.1 Graphical representation of BMP1 domain structure. The locations of zebrafish mutations in *frf* were identified under the structure.**

Schematic view of BMP1 domain structure with indicated locations of identified zebrafish mutations. Note that the *frf*$^{tf5}$ mutation generates multiple splice isoforms.

Image adapted from (Asharani et al., 2012)

## 2.2.2. dCAPS screens for mutants

Genomic DNA was extracted from scales of individual adult zebrafish as described in chapter 1, then diluted 1:1 with water and used for PCR reaction with tm317_dcaps primers (Table 2.1). Standard 10µl PCR reaction was performed with 1µl of diluted gDNA, 1µl of each primer (from 10µM stock), 5µl of 2X GoTaq Green Master Mix (Promega M7122) and 2µl of Nuclease-Free Water. The reaction consisted of 35 cycles with 53°C annealing temperature.

| Name of the primer | Sequence of the primer in 5' to 3' direction 5' -> 3' |
|---|---|
| tm317_dcapsf | TTG TGT TTG TTT CTT GAC AGA GG T |
| tm317_dcapsr | GTT TTA AAG TCA ACA TAT GCG TAA TTC TCT CA |

**Table 2.1** $frf^{tm317}$ **dCAPS primers sequences**

After PCR reaction was completed, 2µl NEB4 buffer, 1µl MfeI enzyme (or 0,5 µl MfeI-HF) and 7µl H$_2$O were added to each tube. The total 20µl reaction was mixed and incubated for 2h at 37°C to allow complete PCR product digestion. To examine digest results, the reaction was run on a 4% gel to allow accurate separation of DNA fragments. Wild type fish showed a 178 bp band, $frf^{tm317}$ mutants 146 bp and 33 bp fragments and $frf^{tm317/+}$ showed all three bands.

## 2.2.3. Corrected total crush fluorescence measurements

Corrected total crush fluorescence was used to measure fluorescent signal emitted by neutrophils in the crush area of Tg(*mpx*:GFP) fish. The protocol for corrected total cell fluorescence was adapted from (McCloy et al., 2014) where single cell fluorescence is measured in cell culture and normalized against the fluorescence of the background. I used the same methodology, however, I submitted cells with crushes. Fluorescent channels were separated using ImageJ and the crush area was defined using green channel (fig 2.2A). The same crush area was used for all time points, assuring consistency in measurements. All measurements were normalised against initial fluorescence detected at the crush site just before an injury (mean fluorescence at 0 hpc) (fig 2.2B).
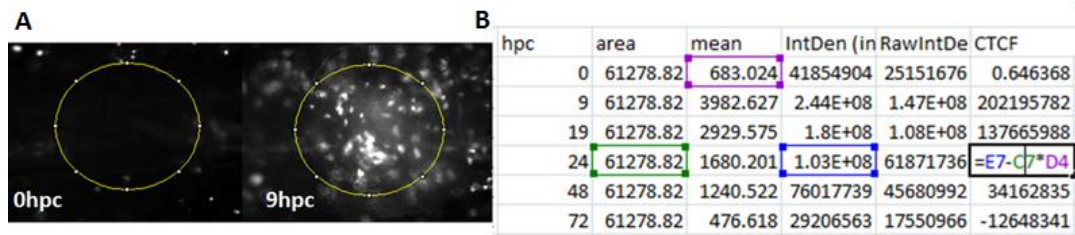
**Figure 2.2 Obtaining corrected total crush fluorescence**

**A)** defining measurement area indicating crush on 32bit images at different time points post crush

**B)** CTCF calculated as a difference between measured fluorescence intensity and base fluorescence from the same place before the crush

The original Corrected total cell fluorescence (CTCF) was calculated according to the formula: **CTCF = Integrated Density – (Area of selected cell X Mean fluorescence of background readings)** (McCloy et al., 2014). In here, CTCF (corrected total crush fluorescence) was calculated according to crush adjusted formula: **CTCF = Integrated Density – (Area of selected crush X Mean fluorescence of 0hpc readings)**. Microsoft Excel was used for calculations (fig 2.2B)., results were transferred to Graphpad Prism 7 in order to create charts.

## 2.3.    Results

I decided to check bone regeneration ability of OI zebrafish mutants. Asharani et al. (2012) describe that *frf* fish bone density is abnormal in both vertebral centra and fin rays, leading to bone fragility. It was shown that *frf* mutants, similarly to human OI patients, suffer from bone malformations and spontaneous bone fractures (Asharani et al., 2012). However, there was no data available on the healing of those fractures. Moreover, an ability of bone regeneration after amputation in *frf* fish mutants was not assessed.

### 2.3.1.    OI zebrafish maintain tail regeneration ability

I decided to assess regeneration ability of *frf* mutants on the example of *frf*$^{ty69}$, one of the stronger mutant alleles. I assessed if the process of regeneration after tail amputation was normal in those fish despite bone related gene mutations. Tails of *frf* mutants were misshaped, often shorter and lacking normal fin shape. I examined blastema formation and tail regrowth following an amputation. The results showed that *bmp1* mutation does not affect temporal outgrowth of lost tail. Blastema formation was observed as normal and outgrowth formation timing was comparable with wild type fish to 14 days (fig 2.3 A). The

shape of newly formed tail resembled the original. Rays at the dorsal lobe were tilted towards the middle of the tail instead of being spread distally.
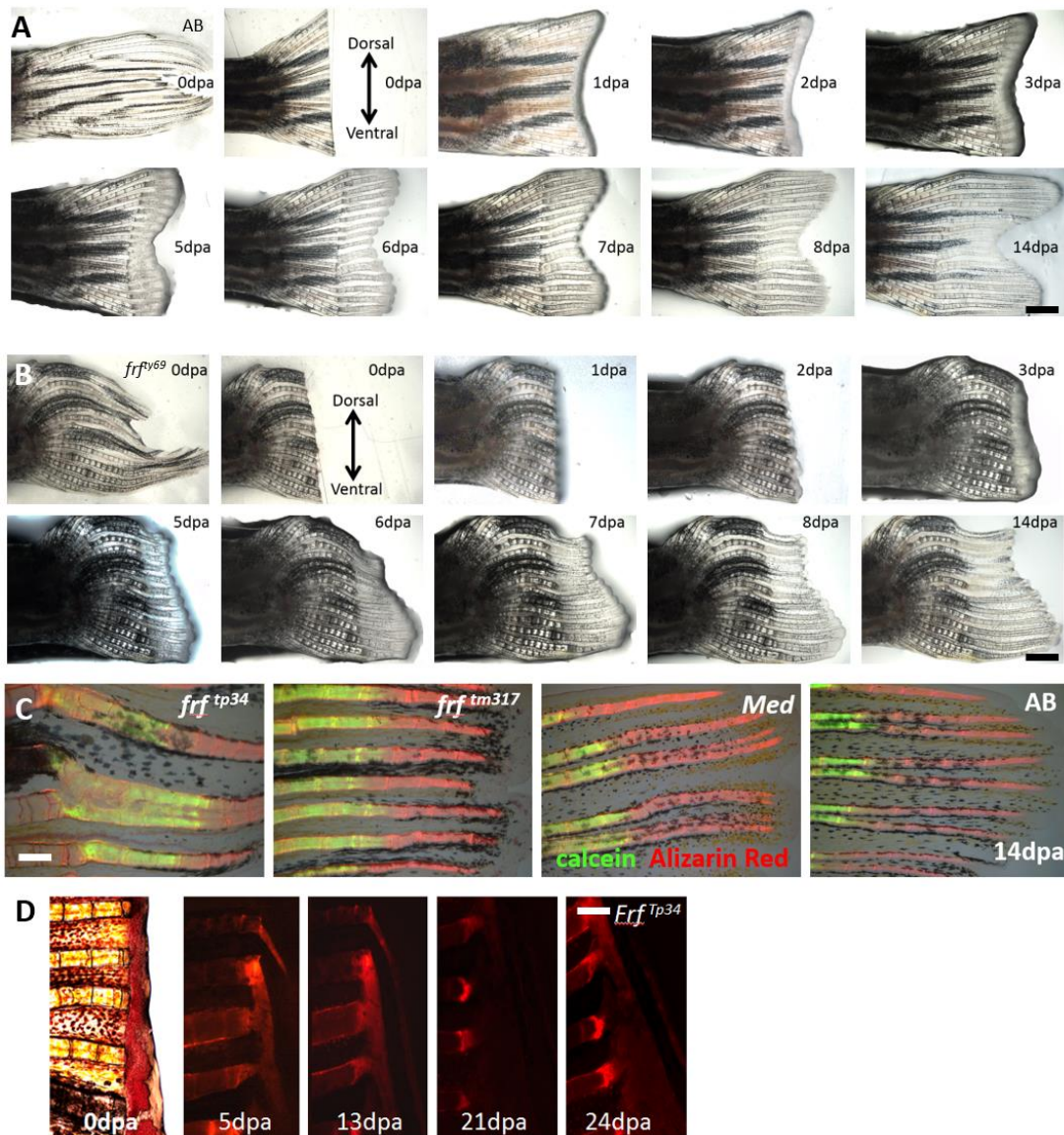


**Figure 2.3 *frf* tail regeneration after amputation**

**A)** Bright field images of blastema formation and regeneration outgrowth of amputated tail of wild type (AB) zebrafish

**B)** Bright field images of blastema formation and regeneration outgrowth of amputated tail of *frf^{ty69}* zebrafish mutant

**C)** degree of regeneration ability between different OI zebrafish models (*frilly fins – frf* and *microwaved – med*) and wild type fish (AB). Newly formed bone was consecutively stained with calcein and Alizarin Red S to assess the rate of bone deposition

**D)** extreme case of mutant fish not able to perform tail regeneration after amputation

Scale bar corresponds to 300 µm in all panels in **A** and **B**, and 100µm in all panels in **C** and **D**

To ascertain the ability of bone restoration in *frf* mutants, I assessed phenotypically more severe *frf* alleles. Interestingly, I found that the rate of overall tissue re-growth varies between alleles. While *frf*$^{ty69}$shows ability to restore the lost part of the tail as described above, in the *frf*$^{tp34}$, which contains a nonsense mutation, there was limited regeneration in some individuals. Lepidotrichia appears shortened, thickened and often joined with neighbouring rays (fig 2.3B). Some extreme cases show a complete fusion of outgrowing rays into one bone mass (fig 2.3C). Intra-allelic variability of regeneration was high, suggesting multigenic contribution.

## 2.3.2. Tail of OI zebrafish is full of randomly distributed bone calluses

Several spontaneous calluses were observed in adult *frf* zebrafish tails (green circles in fig 2.4). These tissue accumulations can be observed using bright field microscopy (fig 2.4B), however, it is Alizarin Red staining which helped me to determine that calluses are formed from mineralized tissue (fig 2.4C). Breakages occur spontaneously, with the preponderance for proximal half of the tail. No repeatable breakage pattern was observed among the mutant fish, therefore their dorsoventral distribution can be described as random.
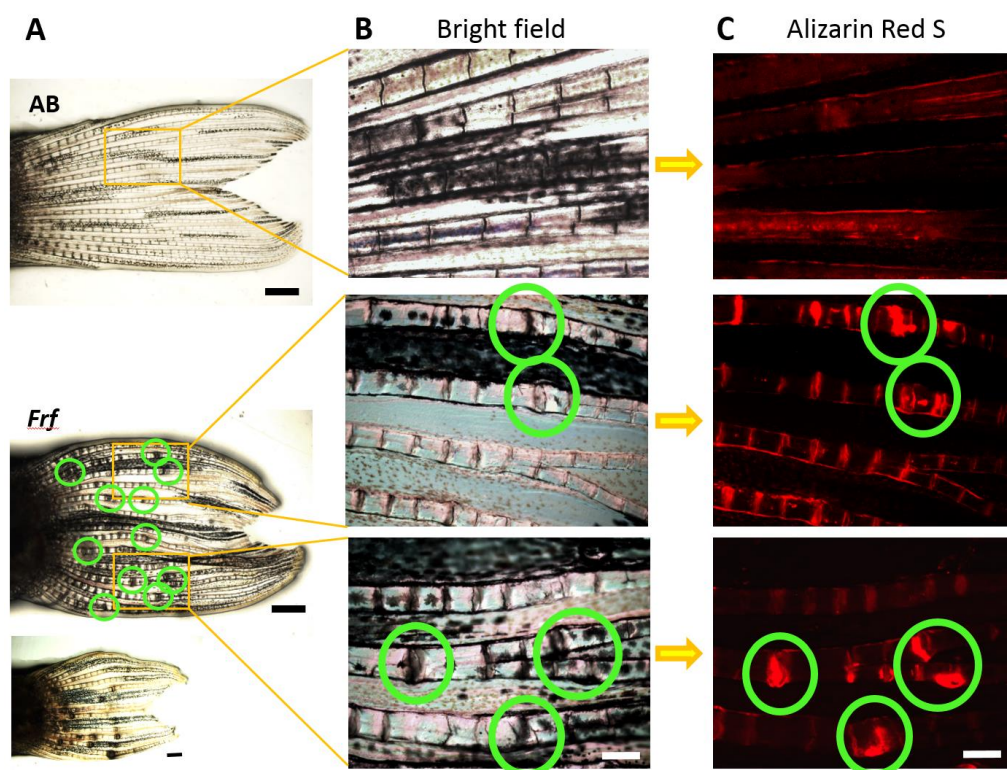


**Figure 2.4 *frf* fish tail is full of mineralized calluses**

**A)** tails of uninjured wild type and mutant fish exposing *frf* spontaneous fractures (marked by green circles)

**B)** magnifications of calluses on individual rays

**C)** Alizarin Red S stained rays showing mineralized tissue deposition at the site of spontaneous fractures

Scale bar corresponds to 300 μm in all panels in **A**, and 100μm in all panels in **B** and **C**

### 2.3.3. Fractures in OI zebrafish tail heal less efficient than wild type fish

Due to an inability to track repair of spontaneous fractures from the outset, I decided to introduce new fractures using our previously established crush model. This enabled us to track crush healing in OI model throughout all four bone healing stages.

### 2.3.4. Stage 1 – inflammation

#### 2.3.4.1. *il1* ISH reveals differences in spatial distribution

In order to estimate inflammation intensity, we performed ISH at 8hpc and 12hpc using *il1* probe described previously in chapter 1. Choice of time points was based on results from chapter 1, showing the peak of *il1* marked inflammatory response is at 8hpc and another visibly strong time point at 12hpc. 12hpc showed the slight reduction of stain intensity as compared to 8hpc in AB, but most importantly it presented different spatial distribution of marked cells, therefore I chose it as a second control time point. Both time points can be used as strong indicators of inflammation stage in crushed zebrafish rays. In both *frf* as well as AB fish, at 8hpc, inflammatory cells labelled by *il1* invaded the fracture zone and accumulated at the crush plane (fig 2.5A, 8hpc). Crush planes in fig 2.5 were indicated by yellow lines. At 12hpc in wild type fish, the majority of labelled cells appeared on the outside of the fracture plane, covering ray segments adjacent to the fracture. However, in *frf* mutants, *il1* labelled cells persist in the fracture gap until 12hpc (fig 2.5A, 12hpc). In summary, stain intensity reduction between 8hpc and 12hpc between *frf* and AB fish was comparable, however, spatial cells distribution in *frf* mutants does not remain consistent throughout temporal progression as compared to wild type fish. These results suggested that inflammation occurs with comparable rate but different cellular movement in *frf* mutant in comparison to AB fish.
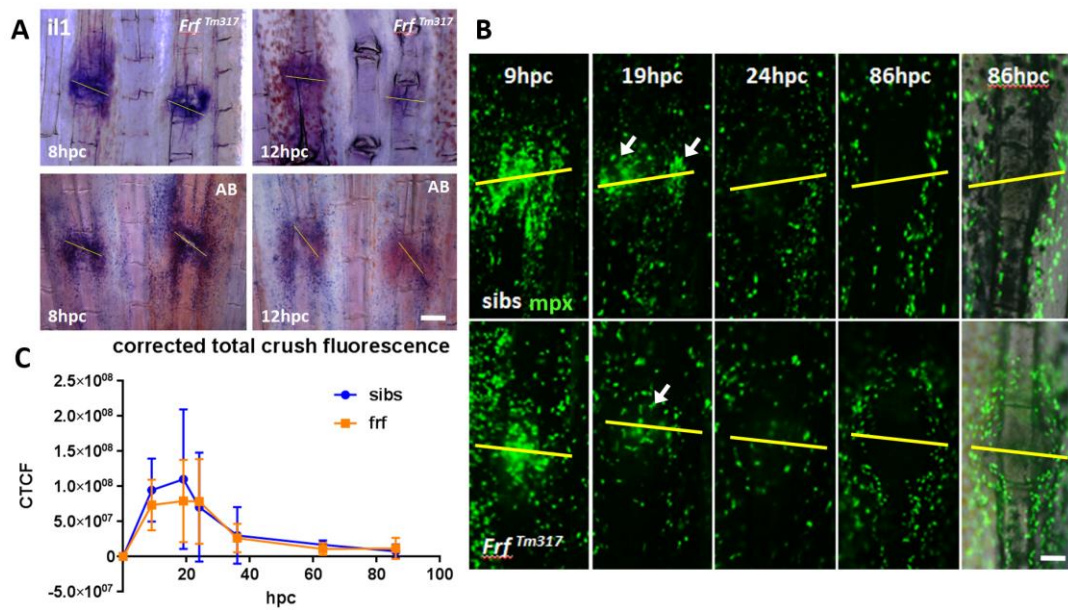
**Figure 2.5 Inflammation of crushes at *frf* fish**

**A)** Whole mount in situ hybridization comparison of *il1* expressing cells between wild type fish and *frf* mutant at two time points 8 and 12hpc, yellow lines indicate crush plane

**B)** neutrophils recruitment to the crush site and their spatio-temporal progression through 86hpc imaged in transgenic lines *Tg(mpx:GFP)* between wild type and *frf* mutant fish, yellow lines indicate crush plane. Arrows indicate difference in neutrophils distribution.

**C)** Graph representing temporal distribution of corrected total crush fluorescence for crushes of *frf* and sibs, showing no significant difference between the two, at any time point checked up to 86hpc, n=8

Scale bar corresponds to 100 μm in all panels in **A**, and 50μm in all panels in **B**

### 2.3.4.2. CTCF show no significant difference in the strength of inflammatory response

To further evaluate inflammation in OI fish I crossed *frf³¹⁷* to *Tg(mpx:GFP)* to label neutrophils with GFP, in both mutants and siblings. Crush injuries were performed and fish were imaged at 9, 19, 24 and 86hpc (Fig.2.5B). In both, *frf* and sibs, inflammation markers were upregulated and clearly visible. In both, the peak of inflammatory cells recruitment appeared at 9hpc at the centre of crush plane, indicated by the yellow line, between two parts of broken bone (Fig.2.5B, 9hpc). By 19hpc neutrophils of sibling fish accumulated at the periphery of the crush, while those of *frf* mutant persisted in the center of the crush plane (Fig.2.5B, 19hpc). This cellular spatial distribution is consistent with the in situ hybridization data (fig 2.5A). In both *frf* as well as siblings, neutrophils were completely excluded from the crush area by 86hpc (fig 2.5B, 86hpc), which was consistent with wild

type fish data reported in chapter 1. To quantify those results I performed a set of measurements and calculated Corrected Total Crush Fluorescence (CTCF). CTCF was calculated based on measurements collected through analysis, in ImageJ, of crush images taken sequentially. Microsoft Excel was then used to perform CTCF calculation, according to the following formula: CTCF = Integrated Density – (Area of selected crush X Mean fluorescence of 0hpc readings). Pooled results from 8 experimental repeats were plotted using GraphPad Prism 7 (fig 2.5C). Corrected Total Crush Fluorescence (CTCF) at each time point was comparable between *frf* and sibs (fig 2.5C). Statistical significance was checked by paired t-test at each time point.

No significant difference was found in CTCF between *frf* and sibs and the shape of the graph is comparable between *frf* and sibs. Thus, I can state that *frf* mutants show wild type immune response to the crush injury at all stages analysed.

## 2.3.5. Stage 2 – soft callus formation

### 2.3.5.1. Alcian blue stain reveals reduction in cartilage callus size in *frf* fish

To examine soft callus formation, I performed alcian blue staining on crushes of $frf^{317}$ mutant as well as wild type fish. Temporal progression of cartilage callus formation was analysed, based on images of stained crushed fins from different time points following crush injury. Callus size was determined by the ratio of callus width, measured at the widest part of formed callus, to ray width measured in the middle of the segment adjacent to the broken one (red brackets fig2.6A). Results were plotted (fig 2.6B) and statistically tested by ANOVA. On 3dpc and 5dpc, the difference between callus sizes of $frf^{317}$ and AB was statistically significant, with p values of 0.012 and 0.015 respectively. Therefore, to rigorously test obtained results, I repeated staining on other strong *frf* alleles: $frf^{tf5}$ and $frf^{tp34}$ and compared their callus sizes to results obtained from AB fish at each time point. Statistically, the significant difference was reported from $frf^{tf5}$ results at 6dpc, with p=0.0464. To determine differences in cartilage callus sizes between different mutant alleles I compared them to each other but no significant difference was observed from those comparisons.

### 2.3.5.2. Cartilage callus formation is not stopped in *frf* fish, yet callus size is significantly reduced

As per column comparison at each time point, the size of cartilage callus was reduced in all mutant alleles, however, none of them showed consistent reduction throughout all time

78

points. Instead, the significant reduction on certain days was observed as compared to AB fish (fig2.6 B). Based on those differences in callus sizes between *frf* mutants and wild type fish I concluded that stage 2, cartilage callus formation, in mutant fish was slightly impaired as compared to cartilage callus formation in wild type fish, although not totally blocked.
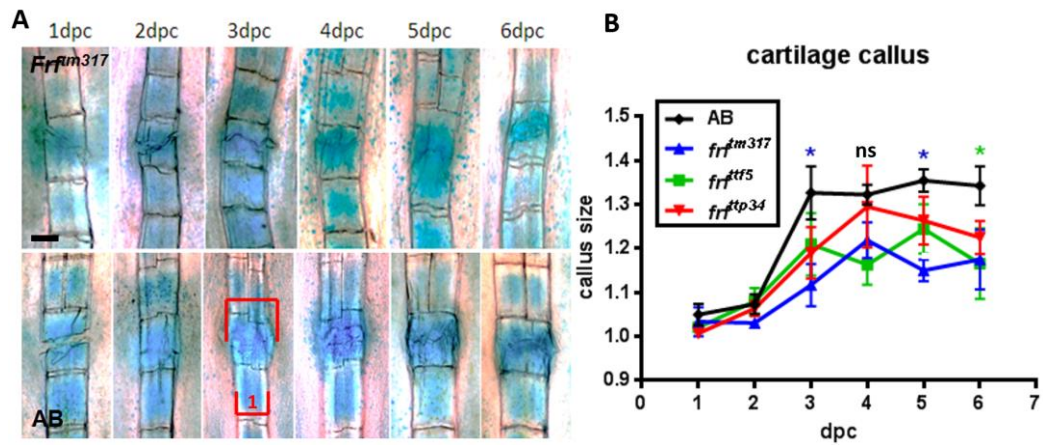


**Figure 2.6 Cartilage callus formation is reduced in *frf* fish**

**A)** Alcian Blue cartilage callus staining. Red brackets indicate how the measurements were taken. Unbroken bone's width was set as 1 and callus size was presented in proportion to this measurement. Scale bar corresponds to 50 μm in all panels

**B)** cartilage callus sizes, measured as a ratio of callus width to the width of unbroken bone, ns=non-significant, n=8

## 2.3.6. Stage 3 and 4 – callus ossification and remodelling

### 2.3.6.1. Osteogenic markers ISH helps in osteoblast distribution patterning

To ascertain the repair rate of bone, I decided to evaluate osteoblast presence in the crush site by ISH of *osteocalcin (bglap)* and *osteopontin (spp1)* on each day after crush, up to 8dpc. By observing those osteoblasts markers, I could evaluate differences and similarities in osteoblast spatial and temporal appearance in the crush site between wild type and *frf* mutant fish. *spp1* appeared in the crush site as soon as 2dpc and remained very strong until 4dpc in *frf* and 5dpc in AB. It remained present in both 8dpc. In AB, staining was directly localized at the crush site and around the forming callus, while in *frf* it appeared at the broken segments, adjacent to the breakage, in the close proximity to the fracture plane, but not in the fracture plain. *bglap,* appeared very strongly in the callus as well as segments adjacent to the fracture plane in ABs, with expression moving to adjacent ray by 8dpc (Fig 2.7A). In *frf*, expression initiated by 3dpc and its spatial focus does not change over time. It

followed the pattern of *spp1* staining and stayed on crush periphery, instead of penetrating the fracture.

### 2.3.6.2. Callus shaping process revealed by transgenetically labelled osteoblast tracing

To further evaluate osteoblast distribution as well as callus ossification, I generated *frf$^{317}$;Tg(osx:mCherry)* line with fluorescently labelled osteoblasts through the use of the *osx:mCherry* promoter (Renn and Winkler, 2009). By observing fluorescent osteoblasts encapsulating the callus (to mineralize it), the shape of the callus could be defined. While callus of wild type was nicely rounded around the fracture, encapsulating crush site and stabilizing it (fig 2.7B, AB), *frf* callus was much narrower. Fluorescence was reduced in the callus of *frf* mutants and labelled osteoblasts show different spatial distribution as demonstrated on densitometry graphs in fig 2.7C. While osteoblast fluorescence signal in crushes in AB fish came strongly at the callus periphery and as time passes fluorescence increased in the middle of the crush, osteoblast fluorescence in *frf* fish appeared overall weaker in intensity and more dispersed, giving a more even signal in the middle of the crush instead of sides of the callus. The shape of the area covered by osteoblasts in *frf* was much more challenging to define, compared to covering a rounded, mineralized callus in wild type fish (fig 2.7B, fig 2.7C).
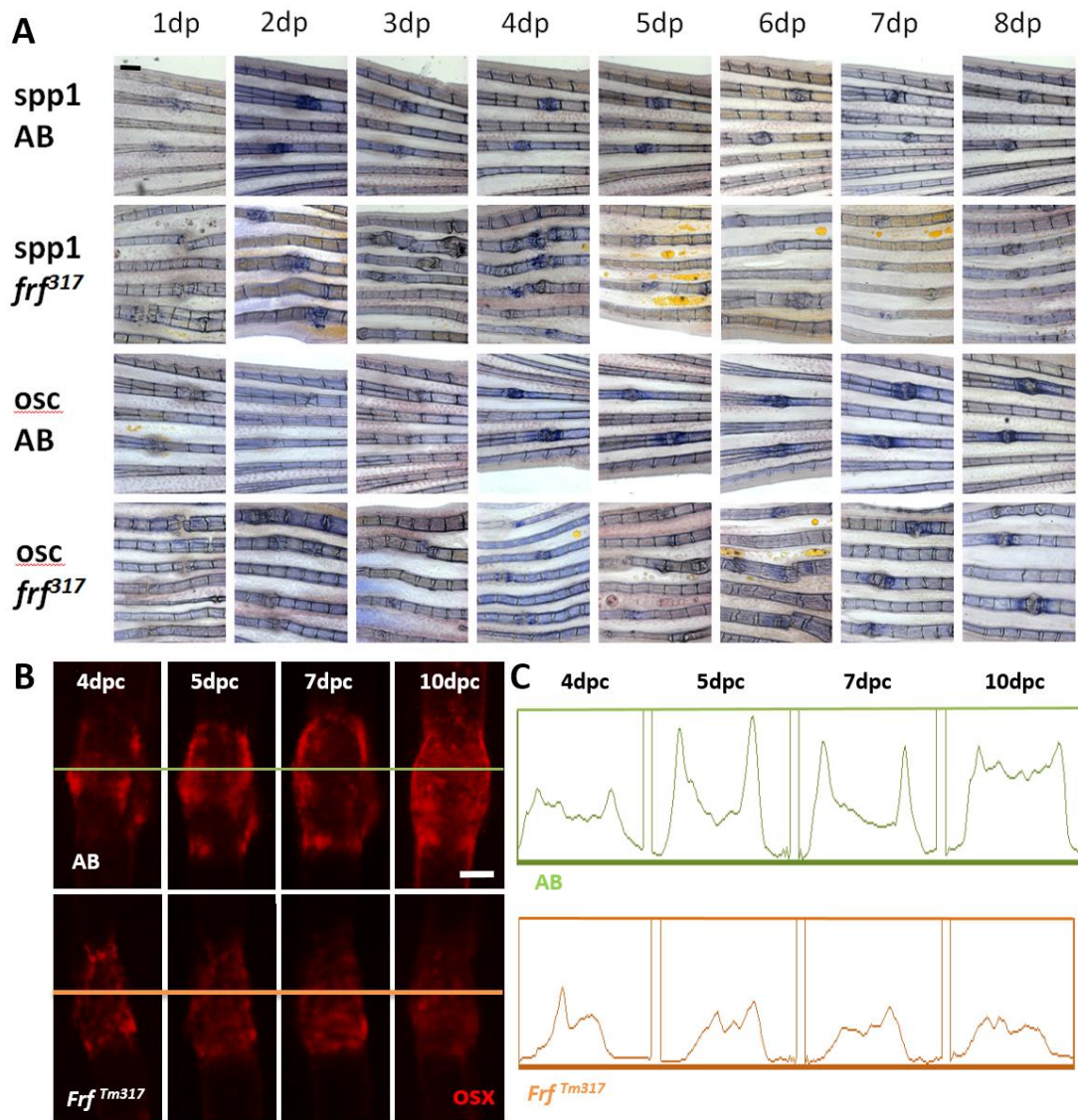
**Figure 2.7 Osteoblasts recruitment to the crush site in *frf* fish**

**A)** Whole mount in situ hybridization of osteoblast markers (spp1, osc) expression

**B)** comparison of *osx* marked osteoblast recruitment to perform callus ossification between transgenic lines of AB and *frf* mutants

**C)** densitometry of cross-section through callus images, indicating staining intensity distribution across line annotated in panel **B**

Scale bar corresponds to 100 μm in all panels in **A**, and 50μm in all panels in **B**

### 2.3.6.3. Alternate bone staining allowed tracing progressive callus ossification

Due to altered osteoblast distribution in the callus, I decided to assess bone deposition during crush repair process. To better delineate progressive bone deposition over time we stained bone through the alternate use of Alizarin Red S and calcein (fig 2.8A). This allows us to distinguish nascent bone deposition from the previously deposited bone.

### 2.3.6.4. Shape of frf mineralized callus was visibly distorted

$frf^{317}$ failed to form normal, ball-like mineralized calluses around breakage sites. Instead, chaotic bone joining was observed, in which bone matrix formed a thin connection between broken ends of the ray. Mineralization appeared delayed, while callus growth was reduced. This was quantified by measuring the width of the nascent bone at the fracture formed during repair process and normalized to adjacent, uninjured ray width (brackets in fig 2.8B).
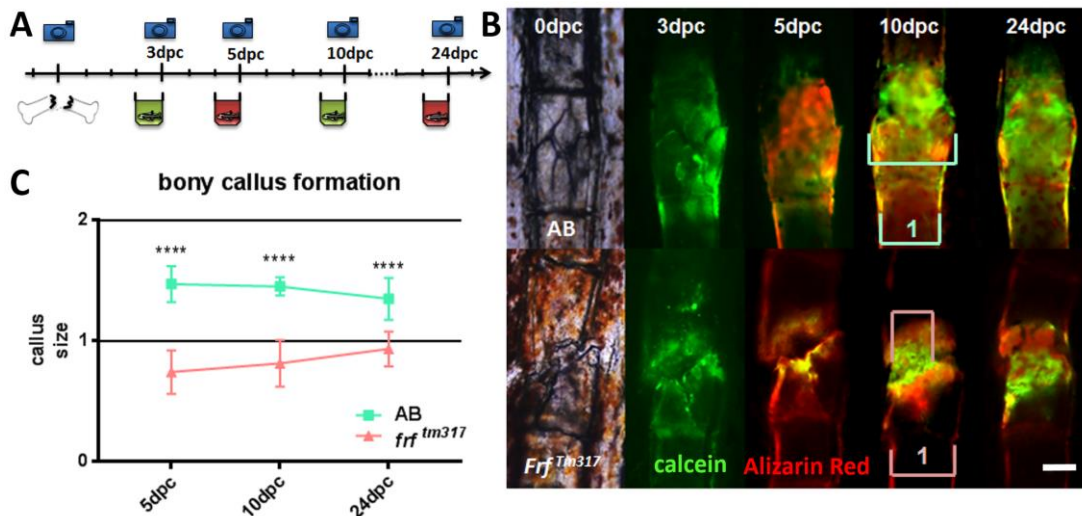


**Figure 2.8 Mineralized callus formation is reduced in *frf* fish**

**A)** experimental setup of alternate **calcein** (green) and **Alizarin Red S** (red) bone staining following crush injury

**B)** callus building progression with callus measuring method

**C)** significant differences in relative callus sizes in all measured time points between wild type and mutants, ANOVA, **** $p<0.0001$, n=16

Scale bar corresponds to 50µm in all panels in **B**

### 2.3.6.5. Size of frf bone callus was significantly reduced as compared to wild type fish

At all time points measured, there were significant differences in mineralized callus sizes. Wild type fish showed mineralised callus at the crush site by day 5. It was slowly resolved during the remodelling process indicated on the graph by callus size reduction in following time points (fig 2.8C). In contrast, callus size in *frf* mutants is much smaller. The nascent bone formation is delayed, leading to delayed callus growth. Thus whilst wild type callus is

resolving, in *frf* fish the callus remains in a growth phase to 24dpc. This relative difference in callus dynamics is presented in fig 2.8C.

### 2.3.6.6.    Osteoclasts are recruited as normal

In order to check all possible signs of remodelling, we examined osteoclasts recruitment to the crush site by *ctsK* ISH. Staining was seen at the dates corresponding to the standard *ctsK* temporal distribution of wild type fish reported in chapter 1. Staining came up as soon as 1dpc and remained at the crush site till 3dpc, then it was reduced until 10dpc when it came up again and remained till 22dpc (fig 2.9).
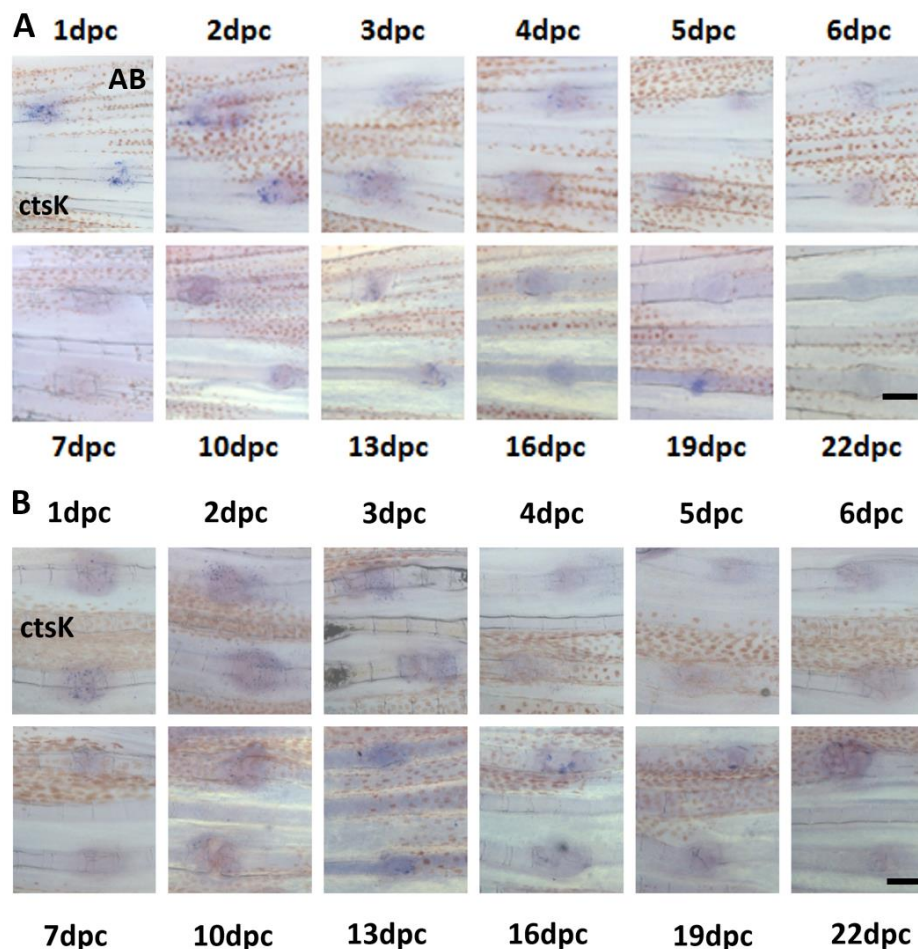


**Figure 2.9 Whole mount in situ hybridization for *ctsK* expression detection**

*ctsK* is expressed 1-3dpc and 10-22dpc in both **A** wild type fish (AB) and **B** *frf^317* mutants. Scale bar corresponds to 100 μm in all panels, n=4

### 2.3.7.    Non-union fractures

Interestingly, I observed that a number of fractures failed to connect broken parts of the ray. I separated those from the pool of crushes, calculated their amount and investigated them separately under a non-union fracture category. I found that 30% of crush injury

cases in *frf* failed to form the connection between the broken rays, whilst it always occurs in wild type fish (fig 2.10A). The gap size changes were progressively measured over time and compared to the wild type control. I saw the significant difference in the gap size throughout the whole healing process between two groups at most time points (fig 2.10B). The gap between the rays following the crush injury was reduced rapidly in wild type fish as mineral tissue was deposited in the intra-fracture space. This gap in *frf* mutants perdured for at least as long as 24days (fig 2.10B, C).
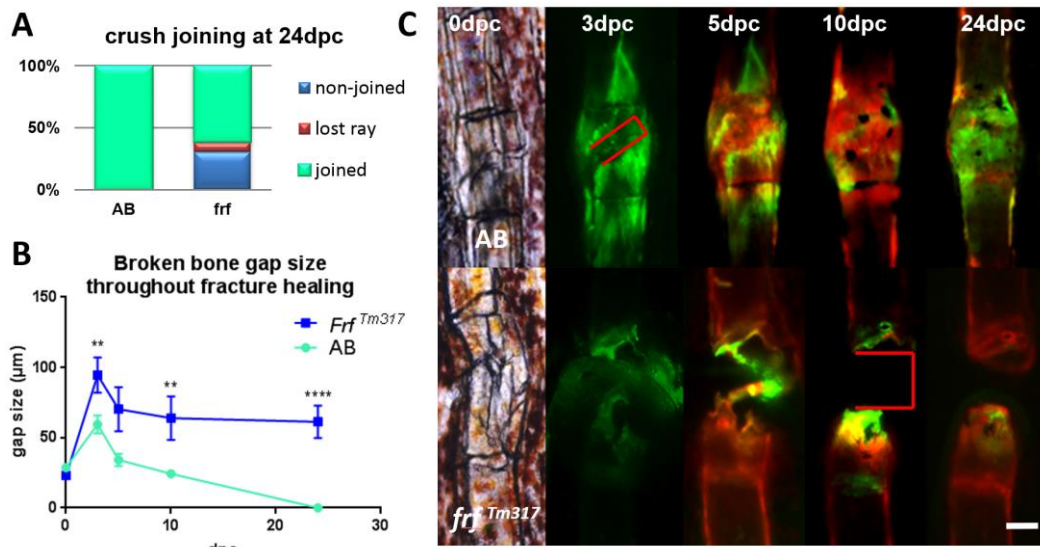


**Figure 2.10 30% of *frf* crushes led to non-union fractures**

**A)** in *frf* mutants around 30% percentage of introduced crushes were not able to re-join by 24dpc, n=24

**B)** there were significant difference in gap sizes between wild type fish and mutants ** p<0.01 **** p<0.0001, n=7, ANOVA

**C)** gap joining progression with gap measuring method indicated as red brackets, time series of the same fish

Scale bar corresponds to 50μm in all panels in **C**

## 2.4.    Discussion

In this chapter, I evaluated regeneration ability of zebrafish *frf* mutant, which represents a fish model for Osteogenesis Imperfecta (OI). I was able to show that despite their ability to regrow lost tails, *frf* bone crush healing ability was highly disrupted. Based on previously published *frf* characterization (Asharani et al., 2012), we knew that bone fragility and malformations occurred due to the mutation in *bmp1*, the procollagen C-proteinase, which caused kinked and disturbed collagen fibres formation.

### 2.4.1. frf fracture healing appeared to be strongly interrupted at the stage of hard callus formation

By use of zebrafish crush model, I examined all 4 stages of fracture healing of tail crushes in *frf* mutant fish. All four stages were slightly disturbed in *frf* mutants indicating that OI is a systemic disease influencing a range of responses, important for correct response to the injury. However, based on presented here results, I was able to pinpoint stage 3 as the phase mostly affected by the mutation, with significantly elevated difference in bony callus size and shape between wild type and mutant fish.

### 2.4.2. Stage 1 - inflammation

The strong inflammatory response was present in both mutants as well as wild type fish. Spatial differences in inflammatory cells distribution were present, which could be explained by differences in bone quality influencing bone topography between two assessed fish types. There was no significant difference in Corrected Total Crush Fluorescence (CTCF) at any time point measured. CTCF of *frf* crushes was similar to the CTCF of wild type fish crushes. The Linear trend of fluorescence temporal progression showed the same distribution pattern between the two groups. As such, there is no real difference in inflammation stage between mutant and wild type fish. Both of them upregulate inflammatory markers around 8hpc, decrease it by 24hpc with total marker exclusion form the crush site by 86hpc.

Based on these results, and lack of published correlations between *bmp1a* and inflammation, I state that stage 1 is not affected by mutation in *bmp1* gene, due to lack of differences in inflammation seen between *frf* and wild type fish.

### 2.4.3. Stage 2 – soft callus formation

We have examined soft callus formation by Alcian Blue staining. Due to lack of the clarity in the results obtained from *frf³¹⁷* staining measurements, I investigated other *frf* alleles by Alcian Blue. Results showed the general decrease in cartilage callus sizes in all assessed mutants, however, in none of these alelles callus size was significantly reduced at all time points. Therefore, I was not able to claim perturbance of stage 2 in *frf* crush recovery. I suspect that stage 2 was mildly affected. It is known that Bmp1 cleaves C-terminal of procollagen II (Moali et al., 2005) and mutations in Bmp1 lead to the lack of procollagen C-terminal cleavage. That influence kinked and distorted collagen fibers formation, yet the formation still takes place.

I believe that in *frf* fish, due to Bmp1 mutation, collagen II fibers were not formed properly influencing the structure, shape, size and overall appearance of cartilage callus, although callus formation was not blocked. This might reflect tolerance of cartilage to malformed collagen II fibers.

### 2.4.4. Stage 3 – hard callus formation

Bony callus formation was assessed by osteoblast tracking as well as evaluation of progression of mineralized tissue deposition. Mineralized callus formation was significantly impaired in *frf* mutant, and if formed, appeared as a small and thin connection between the broken bone parts instead of forming a ball-like structure encapsulating and stabilizing the crush.

I predict that lack of properly formed cartilage callus, which normally acts as a scaffold for osteoblasts to migrate onto, depositing mineralized tissue (Slowik and Bermingham-McDonogh, 2013), reduces the possibility of formation properly shaped bony callus. In addition, mutations in *bmp1* gene trigger distortion in collagen 1 fibers formation, which are the main component of osteoid, therefore mineral bone is affected. It was shown previously that in *frf* fish *bmp1* mutation led to the lack of procollagens C-terminus cleavage and bone deformations (Asharani et al., 2012). We propose that generation of mature collagen l fibers in osteoid is critical for fracture repair and callus formation.

Stage 3 of *frf* crush recovery was strongly affected in *frf* fish, due to perturbed cartilage template for osteoblasts to migrate, and to impaired collagen I fibers formation. Nevertheless, I believe that results seen in stage 3 display a collectively disruptive effect of combined disturbances in stages 2 and 3 together.

### 2.4.5. Stage 4 – remodelling

It was difficult to assess remodelling in a callus that was not even formed properly. I did not observe any reduction in callus size indicating remodelling up to 24dpc. It might be due to the fact that throughout the experiment, callus of *frf* did not reach the original width of unbroken bone, therefore remodelling was not triggered in those fractures.

Osteoclasts were recruited to the crush site as normal in the time points corresponding to the osteoclast recruitment in wild type fish, therefore we can claim that cellular cross-talk between osteoblasts and osteoclasts is unaffected in *frf* fish. Moreover, I suspect that initial osteoclasts activity on 1-3dpc, together with disrupted ability for callus formation, might

contribute to bigger gap formation in between broken parts of the bone, and leading to enlargement of injury site.

### 2.4.6. Crush in frf perfectly imitate crush healing in OI patients

Based on the result, I can clearly state that the crush zebrafish model accurately mimics mechanism of crush healing in OI patients. Data showed that around 30% of fractures in OI zebrafish model do not join, precisely imitating OI human patients, as it was reported that around 30% of fractures in human OI patients lead to non-joining fracture type (Gamble et al., 1988)

### 2.4.7. Crush model accurately assess impaired stage among 4 healing stages

In this chapter, results confirmed our predictions that usage of zebrafish crush injury model, enable to determine which fracture recovery stage might be affected in human patients. Based on data from crushes in *frf* fish, we predicted that main focus should be given to callus formation and ossification in OI patients. We found out that in *frf* inflammation is not affected, therefore focus should not be given to this stage. Callus formation was perturbed as shown through our crush model, which can be nicely explained, as *frf* mutation is known. Due to effect which mutation in *bmp1* has on collagen fibres, here presented results falls in place. However, in the case of mutation in gene of not known function, zebrafish model can be useful in helping to determine if mutation is correlated with bone problems, and determining which fracture recovery stage is affected. That knowledge could help to direct patient treatment to the specific fracture recovery stage in case of fracture occurrence. Preventative treatment could also be implemented or gene therapy directed to bones.

# 3. Chapter 3 – Bisphosphonates affect crush remodelling

## 3.1. Introduction

### 3.1.1. Bisphosphonates overview

Bisphosphonates, the analogues of pyrophosphates with a carbon instead of an oxygen bridge between two phosphates (fig 3.0A), were already known to scientists in 19th century (Rodan and Fleisch, 1996). After being used in industry as anticorrosive and antiscaling agents, researchers found a use for them in the treatment of bone diseases. Due to their calcium chelating properties they express high affinity to bone matrix and influence bone resorption by triggering osteoclast apoptosis (Hughes et al., 1995). In addition, they are shown to prevent osteoblast and osteocyte apoptosis, which was used to treat diseases characterized by low bone density (Plotkin et al., 1999).
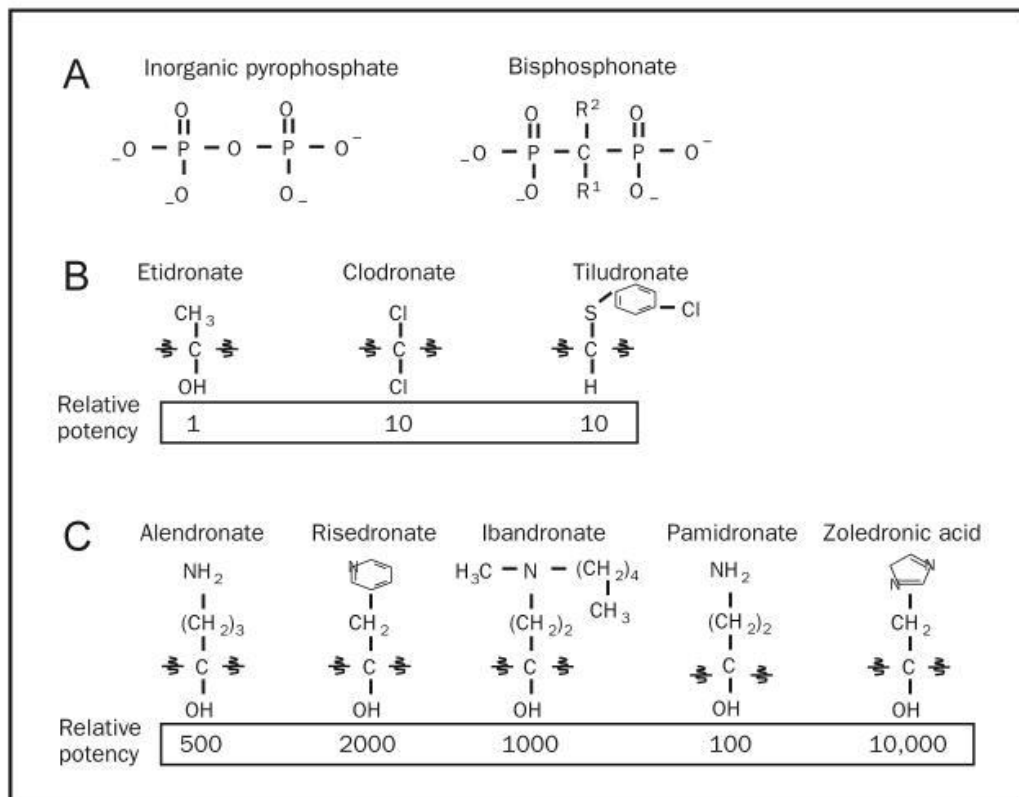


**Figure 3.0 Bisphosphonate structures and approximate relative potencies for osteoclast inhibition.**

**A** chemical structure comparison between pyrophosphate and bisphosphonate

**B** chemical structures of examples of non-nitrogenous bisphosphonates

**C** chemical structures of examples of nitrogenous bisphosphonates

(Drake et al., 2008)

### 3.1.2.     Types of bisphosphonates

There are two types of bisphosphonates, non-nitrogenous (fig 3.0B) and nitrogenous (fig 3.0C), possessing different properties and performing different mechanisms of osteoclast inactivation. Non-nitrogenous bisphosphonates, such as Etidronate or Clodronate, are metabolized in the cells to non-hydrolyzable analogs of ATP, competing with endogenous ATP and inducing osteoclast apoptosis (Frith et al., 1997). Nitrogenous bisphosphonates, such as Pamidronate, Alendronate or Zoledronate, act by blocking farnesyl diphosphate synthase (FPPS) metabolism, thus affecting mevalonate pathway. Blocking FPPS prevents the formation of farnesol and geranylgeraniol, important for sub-cellular trafficking, resulting in a disruption of osteoclasts cytoskeleton (van Beek et al., 2003). Nitrogenous bisphosphonates possess much higher bone affinity that non-nitrogenous ones, and result in the lesser side effect, thus they are more commonly used as pharmaceutics (van Beek et al., 2003).

### 3.1.3.     Bisphosphonates in clinic

Bisphosphonates became an established treatment for patients with bone disorders like osteoporosis, Paget's disease or Osteogenesis Imperfecta (OI). It was shown that daily alendronate treatment significantly improved the quality of life in children with OI, based on markers such as self-care (WeeFIM), mobility (PEDI), well-being, and use of analgesic scores (Seikaly et al., 2005). Clinical studies on OI patients report the reduction in spontaneous fractures, decreased bone pain, improved energy, and increased ambulation upon bisphosphonates treatment (Cho et al., 2014). However, negative effects such as gains in bone thickness, prolonged time to heal osteotomies, decrease in the rate of bone remodelling due to problems with callus resolving caused by inefficient osteoclast work were also reported (Anam et al., 2015).

### 3.1.4.     Bisphosphonate treatment reduce spontaneous bone fractures formation

Alendronate, a type of nitrogenous bisphosphonates, was shown to reduce the possibility of spontaneous fractures (Anam et al., 2015). In case studies, alendronate treated OI infants showed improvement of bone density and fracture reduction (Akcay et al., 2008).

Bisphosphonates were shown to increase bone density (Schindeler et al., 2008), yet decrease the healing rate of the osteotomy (Munns et al., 2004). Effect of bisphosphonates on repair of bone fractures remains unclear (Munns et al., 2004).

### 3.1.5. Long term effect of bisphosphonate treatment

Although data suggest overall positive effect of bisphosphonates on young OI patients, effects of prolonged treatment from infant stage are unclear (Anam et al., 2015). Medics express concerns including off-target effects, overall changes to bone density and bone strength, changes in OI bone matrix composition, effects on different type of bones, and effect of treatment on different OI types (Akcay et al., 2008). To address these and other questions an efficient OI models, which respond to bisphosphonate treatment, is needed.

### 3.1.6. Animal models used in assessing effect of bisphosphonate treatment on fracture healing

Influence of bisphosphonate treatment on fracture healing has been assessed in several model organisms (Savaridas et al., 2013) including dogs (Lenehan et al., 1985), mice (Burns and Corwin, 2013) and rats (Hodgkinson and Dzau, 2015). Results of animal studies show that bisphosphonates possess an inhibitory effect on fracture healing by slowing down remodelling process in wild type animals (Lenehan et al., 1985, Savaridas et al., 2013), yet showed no significant effect on Brtl/+, murine OI model (Burns and Corwin, 2013). Studies on rats showed that bisphosphonates reduce repair of bone micro damage and that there is a need of drug washout period, such as 'drug holiday', in long term bisphosphonate treatment (Hodgkinson and Dzau, 2015).

### 3.1.7. Alendronate treatment in fish

It has been previously reported that bisphosphonate treatment can reduce osteoclasts activity in teleost larvae (Yu et al., 2016). In a medaka osteoporosis model, it was shown that alendronate can reduce activity of ectopically recruited osteoclasts (Yu et al., 2016).

### 3.1.8. Aim of experiments shown in this chapter

The aim of this chapter is to assess if alendronate treatment in a zebrafish OI model reduces spontaneous fracture formation and to determine the influence of alendronate on healing of induced fractures in zebrafish tail (using previously developed model).

## 3.2.	Materials and methods

### 3.2.1.	Bisphosphonate zebrafish treatment

Alendronate sodium trihydrate (Sigma A4978) was dissolved in fish medium at concentrations from 25 to 500µg/ml. Fish were drug treated by immersion in the drug solution for 3h per treatment session.

For recovery, fish were returned to a tank of fresh water.

### 3.2.2.	Treated fish husbandry

Treated fish were kept in separate tanks, under standard husbandry conditions, with feeding and water changes performed as normal.

## 3.3.	Results

### 3.3.1.	Juvenile OI zebrafish respond to alendronate treatment

I decided to treat OI zebrafish model, *frf* mutant, with clinically relevant bisphosphonates, aiming to reduce the amount of spontaneous fracture occurrence through late stages of metamorphosis. I followed a 'drug holiday' treatment regime (Diab and Watts, 2013), where patients were treated for a certain period of time allowing drug accumulation in the body followed by a break in treatment. Due to strong drug affinity to the bone, alendronate was shown to persist in human bone for up to 10 years after treatment (Diab and Watts, 2013).

Two groups of *frf^{tm317}* zebrafish, 7 individuals in each, were checked for spontaneous fractures at 6wpf. At that stage no spontaneous fractures were observed (fig 3.1C), therefore any observed fracture reported at later time points occurred after the start of the treatment. To ensure a fair comparison between the two groups, similarly sized fish were paired and distributed one into each group. In order to mimic clinical practice, juvenile OI zebrafish *frf^{tm317}* were subjected to repetitive, pulsed alendronate treatment, mimicking 'drug holiday' treatment style. Treatment started at 6wpf and lasted for 3 weeks. Twice a week (on Tuesdays and Fridays) fish were moved to drug or mock solution for 3h each day (3pm to 6pm) (fig 3.1A). One group was subjected to 50 µg/ml alendronate treatment, second to mock treatment. The mock treatment included moving fish between tanks, but there was no drug addition to their water. After treatment, fish were returned into fresh tank water. Fish were imaged at 6wpf, 11wpf and 13wpf (fig 3.1C, D).

Reduction in the number of spontaneous fractures in alendronate treated fish was observed (fig 3.1B). The difference in spontaneous fracture occurrence between treated and mock treated fish groups was significant at 11wpf (2weeks post treatment), where treated fish showed significant reduction of fractures as compared to mock treated fish. Significance was calculated using Mann-Whitney statistical test. By 13wpf both groups presented with spontaneous fractures in the fins, however, there appeared to be a lower number of fractures in treated fish. This difference in fractures between the groups at 13wpc was not significant (fig 3.1B). There was a large variation in fracture numbers indicating a stochastic process. While imaging drug and mock treated fish, I also imaged *frf* fish from the same batch which were not moved to treatment tanks. This was to control for fractures caused by repeated handling. These *frf* fish showed a similar rate of tail fractures, indicating they occur due to the genetic lesion (fig 3.1D). Thus, the significantly lowered amount of fractures in treated fish is an effect of drug treatment. Therefore, I concluded that there is a trend in fracture reduction in OI fish model following alendronate treatment, however, better treatment dose or higher n-number would be needed to further substantiate long term alendronate effect on spontaneous fracture reduction in juvenile OI zebrafish.
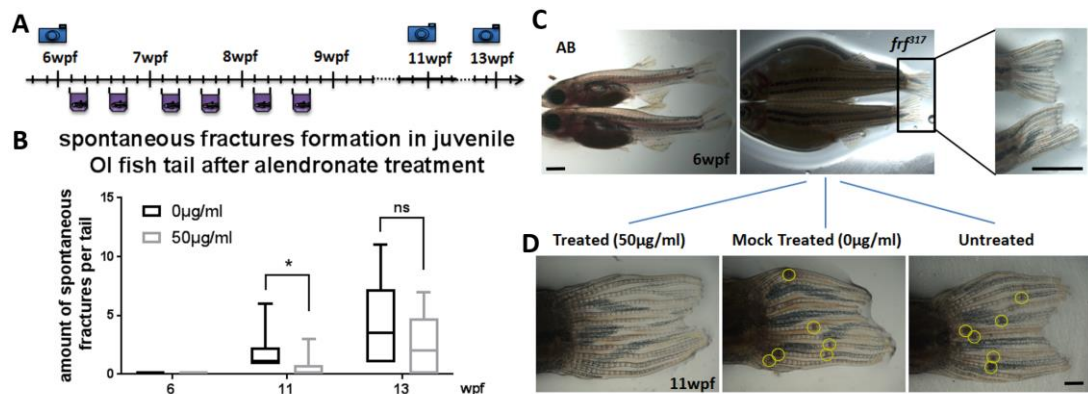


**Figure 3.1 Alendronate treatment reduces amount of spontaneous fractures in juvenile OI zebrafish**

**A)** graphical representation of alendronate 'holiday treatment' on juvenile fish. Fish were treated for 3 weeks (6dpf to 9dpf), twice a week (Tuesday and Friday), 3h each day (3-6pm) and imaged on 6, 11 and 13 weeks post fertilization (wpf)

**B)** counts of numbers of crushes per tail between two treatment groups (0 and 50µg/ml). The Difference between those 2 groups was tested by Mann-Whitney statistical test and showed a significant difference at 11wpf but not at 13wpf, n=7

**C)** difference in overall appearance of *frf* mutant and wild type fish at 6wpf. Enlarged panel

emphasises abnormal physiology of *frf* tails showing shortened length, no bifurcations, and lack of spontaneous fractures at this stage

**D)** spontaneous fractures formation by 11wpf and reduction in their amount at Alendronate treatment. Yellow circles indicate spontaneous fractures.

Scale bars corresponds to 1mm in panels in **C**, and 300μm in all panels in **B**

### 3.3.2.    Alendronate affects bone fracture healing in wild type fish

Different effects of alendronate treatment for fracture healing have been reported in several model animals (Savaridas et al., 2013, Xue et al., 2014, Lenehan et al., 1985). As I have shown that alendronate reduces spontaneous fracture rate in juvenile *frf*[tm317] fish, I decided to determine alendronate ability to influence bone fracture recovery. A number of treatment regimes and range of concentrations (0, 25, 50, 75, 100, 250, 500μg/ml) were tested on wild type fish to optimise the conditions. In the first scenario, fish were treated with a range of concentrations (0 - 500μg/ml) for 24 hours before the crush (hbc), then, crush injury was introduced, followed by returning fish into treatment solution for another 24h, (48h continued treatment) (fig 3.2A). 1dpc fish were examined for abnormalities. At 4dpc fish were stained with calcein and imaged in order to assess if initiation of callus mineralisation was taking place in alendronate treated fish (fig 3.2E).
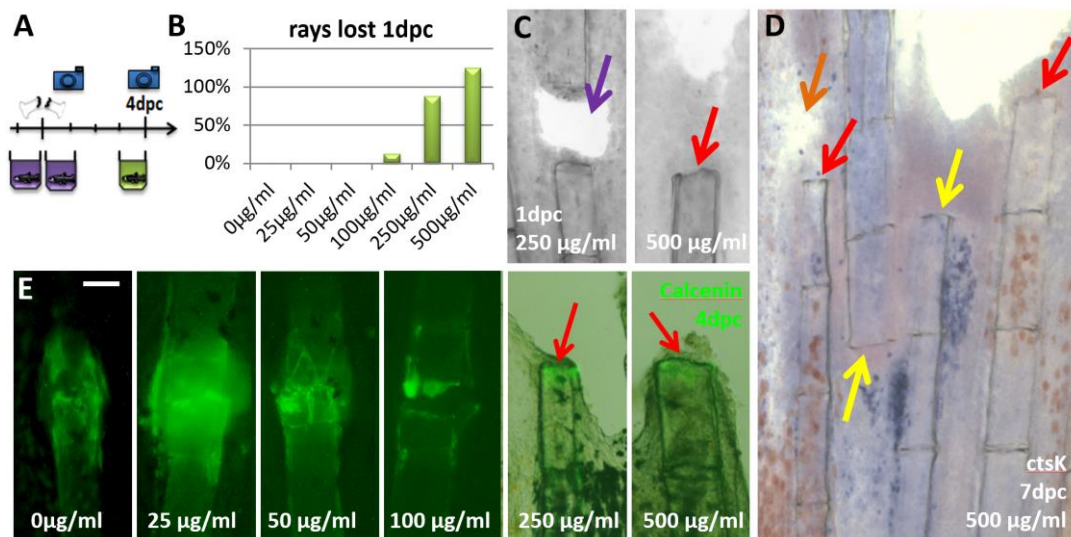


**Figure 3.2 Negative effects of continuous alendronate treatment on fracture healing**

**A)** graphical representation of the experimental set up for determining the optimal alendronate concentration for treatment of adult fish: 1 day of drug treatment, followed by crush injury and returning fish to drug solution for another day. Fish were imaged on 1dpc

and on 4dpc following calcein staining. Colour solutions indicate fish submersion in a **drug** or **calcein**.

**B)** percentage of rays which have lost distal part of fractured ray evaluated 1dpc

**C, D)** defects observed in rays of fish treated with high alendronate concentration 1dpc **(C)** and 7dpc **(D)**. **Red arrows** indicate loss of ray distal to the crush, **purple arrow** indicates single ray segment loss, **yellow arrows** indicate misplacement of broken ray placed in between two fractured rays, **brown arrow** indicates non-healing skin wound

**E)** 4dpc calcining stained fractured rays at the range of fish treated with alendronate, showing initiation of callus ossification at 0, 25 , 50 and 100µg/ml and a lack of regeneration in 250 and 500µg/ml

Scale bar corresponds to 50µm in all panels

### 3.3.2.1. Prolonged exposure to high levels of alendronate leads to a loss of distal ray following fracture

At the highest concentrations (250 and 500µg/ml), ray segments distal to the fracture site were lost, including the segments that were crushed (red arrows, fig3.2). 12.5% of fractured rays lost their distal part at 100µg/ml, almost 90% at 250µg/ml, while at 500µg/ml all fractured rays were lost, sometimes (20% of them) together with adjacent, unfractured rays (fig 3.2B, images not shown). There were also cases where only the fractured segment was lost, creating a hole in the tail (purple arrow, fig 3.2C). In other cases, rays adjacent to the fractured ones were affected, showing breakages and misplacements (yellow arrows fig 3.2D). Moreover, regeneration of lost rays was never observed, even at 21dpc. Loss of adjacent rays at the highest concentrations, as well as non-healing skin wounds (brown arrow fig 3.2D) suggested the broader effect of treatment beyond the reduction of osteoclast activity. Hence the range was limited to only 25-100µg/ml alendronate for subsequent experiments.

### 3.3.3. Alendronate treatment does not block callus formation but affects callus resorption

I performed a new set of experiments with alendronate range restricted to a maximum of 100µg/ml (fig 3.3). I varied not only the drug concentration, but also the length of treatment. I tested continuous 48h treatment with crush introduced in the middle of the treatment (fig 3.3B), in addition to two types of pulse treatments: short pulse treatment (4hbc) and long pulse treatment (14hbc) (fig 3.3D). In order to assess temporal changes in

callus formation, we alternated bone staining with calcining and Alizarin Red S (fig 3.3B and D), which allowed me to assess progressively deposited nascent bone (fig 3.3A and E).

### 3.3.3.1.   Continuous alendronate treatment affects callus formation and resorption

In continuous treatment, callus formation in fish treated with 25µg/ml alendronate appears normal and follows the rates observed in mock treated fish callus formation rate (fig 3.3A, C). In contrast, the 100µg/ml treated group shows significant reduction in the hard callus formation stage (5dpc to 11dpc). However, both treated groups show continuous increase in callus size up to 56dpc, while the non-treated fish data shows reduction in callus size indicating remodelling stage consistent with previous observations (fig 3.3A, C). This data suggests that continuous alendronate treatment affects mineralised callus formation at higher drug doses and also disrupts bone remodelling at both high as well as low drug dose.

### 3.3.3.2.   Pulse alendronate treatment affects callus resorption

In both short and long pulse treatments, whilst callus formation appeared unaffected, significant differences in a callus size were observed between mock and drug treated fish from 21dpc onwards (fig 3.3F and G), hence in the time frame normally allocated for callus remodelling (based on the results presented in chapter 1). I observed continuous increase in callus size in the treated fish and the normal decrease in callus size was not observed at all up to at least 56dpc. We observed no qualitative difference in response to treatment with a short or long pulse at a given concertation.
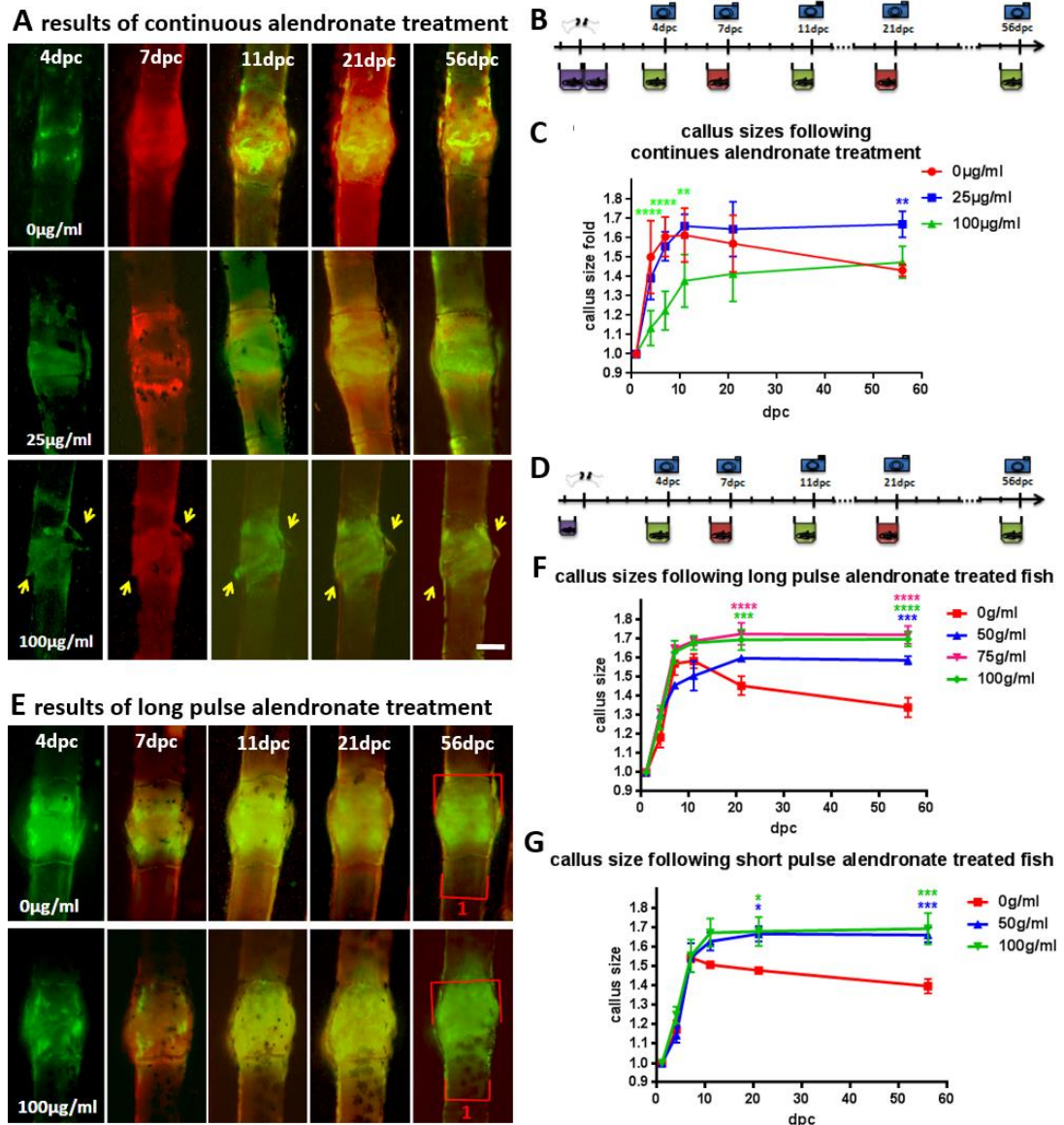
**Figure 3.3 Temporal formation of mineralised callus after crush injury in alendronate treated adult, wild type zebrafish**

**A)** temporal progression of mineralised callus formation in continuously treated fish, yellow arrow indicates bone debris

**B)** graphical representation of continuous treatment experimental set up. Colour of solutions indicate either **drug**, **calcein** or **Alizarin Red S**

**C)** callus size measurements from fish continuously alendronate treated, showing significantly smaller callus in the callus formation stages in high alendronate concentration and lack of callus size reduction in both drug treated groups. ** $p < 0.01$, **** $p < 0.0001$, ANOVA, Tukey's multiple comparisons test, n=8

**D)** graphical representation of pulse treatment experimental set up. Colour of solutions indicate either **drug**, **calcein** or **Alizarin Red S**

**E)** temporal progression of mineralised callus formation in pulse treated fish

**F)** callus size measurements from fish treated with the **long** pulse of alendronate prior to the crush showing significant difference in callus size through remodelling stage between alendronate treated and mock treated fish. * p<0.05, ** p<0.01, *** p<0.001, **** p<0.0001, ANOVA, Tukey's multiple comparisons test, n=8

**G)** callus size measurements from fish treated with **short** pulse of alendronate prior to the crush showing the significant difference in callus size through remodelling stage between alendronate treated and mock treated fish * p<0.05, ** p<0.01, *** p<0.001

Scale bar corresponds to 50μm in all panels in **A** and **E**

### 3.3.4. Alendronate treatment reduces initial osteoclast activity

I observed that upon continuous alendronate treatment, bony callus was formed normally, however unlike the mock treated fish, drug treated fish tails retained bony debris and sharp edges of bone (yellow arrows in fig 3.3A and 3.4A), suggesting reduced osteoclast activity. I examined clearance of bone debris and sharp edges following continuous alendronate treatment in 0, 25, 100μg/ml. Results showed the prolonged persistence of bony debris and sharp bone edges in drug treated animals (fig 3.4C).
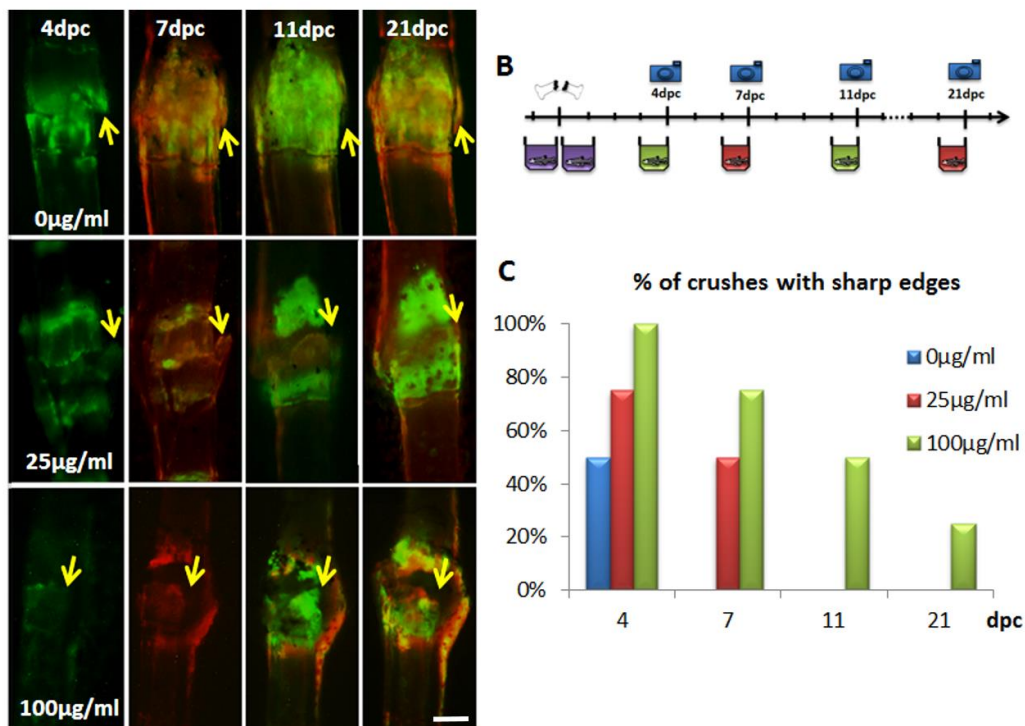


**Figure 3.4 Temporal clearance of bone debris and sharp edges indicating osteoclast activity**

**A)** temporal progression of clearance of bone debris and sharp edges, yellow arrow indicates sharp edges/ bone debris. Scale bar corresponds to 50μm in all panels

**B)** graphical representation of continuous treatment experimental set up. Colour of solutions indicate either **drug**, **calcein** or **Alizarin Red S**

**C)** temporal progression in sharp edges removal, n=8

### 3.3.4.1. Alendronate treatment does not block osteoclast recruitment

Results reported in fig 3.3 and fig 3.4, showed no reduction in callus size, yet impaired debris clearing in individuals exposed to continuous alendronate treatment. This suggested a lack of or reduced osteoclast activity, therefore I decided to examine osteoclast recruitment to the crush site. I performed continuous treatment in the initial range between 25μg/ml and 500μg/ml, as well as short and long pulse experiments in drug concentration range 25μg/ml and 100μg/ml. Tails were collected 1dpc and the whole mount in situ hybridization of *ctsK* was performed on them in order to check osteoclasts presence. Osteoclasts were detected at all concentrations in all types of treatment (fig 3.5), indicating that alendronate does not affect osteoclasts recruitment to crush site. Therefore, I concluded that alendronate might have an effect on osteoclast performance (fig 3.3), but do not influence their recruitment to the crush site.
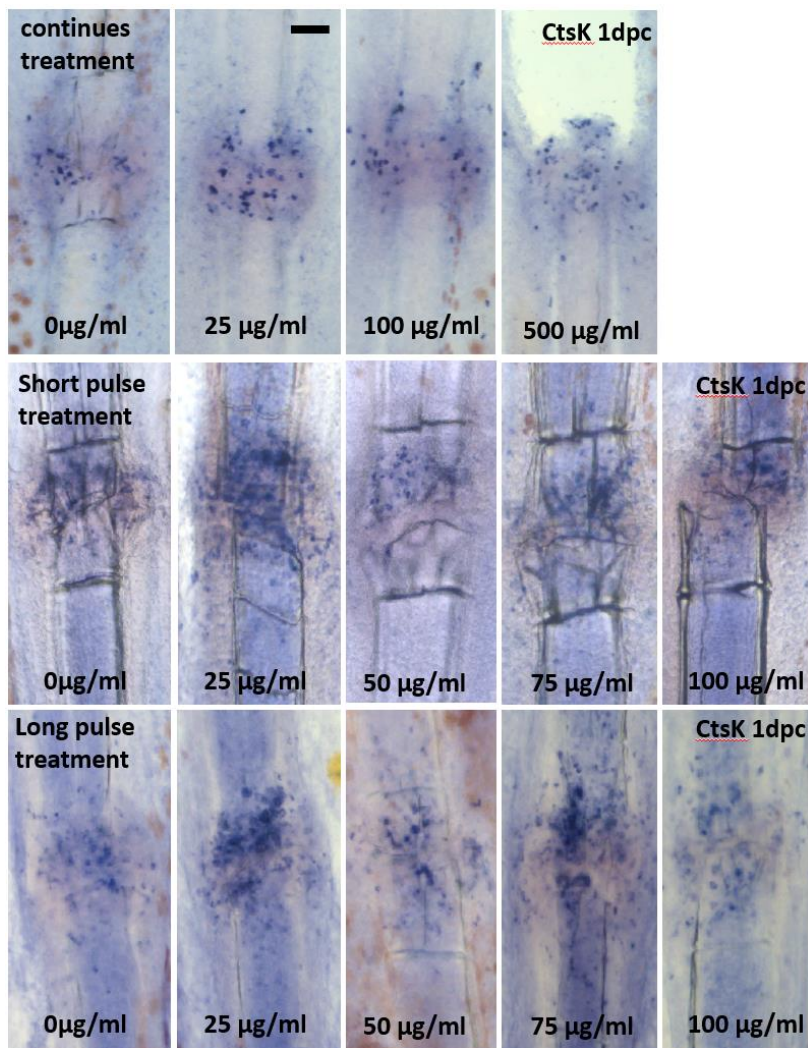
**Figure 3.5 Alendronate treatment does not affect osteoclast recruitment to the crush site**

Whole mount in situ hybridization for *ctsK* has been performed on zebrafish tails after continues, short pulse and long pulse treatment. Osteoclast were recruited to all crush sites despite the drug treatment.

Scale bar corresponds to 50µm in all panels

### 3.3.5. Alendronate does not have significant effect on callus size in OI fish

After optimising treatment conditions on wild type fish, I performed crushes on alendronate treated *frf* fish in order to model what effect alendronate treatment might have on fractures of alendronate treated OI patients. I introduced crushes to 3 months old (3mpf) *frf* fish, which were 'drug holiday' treated at 6wpf (fig 3.6A, B) and their untreated peers which were treated with long pulse of alendronate prior to the crush (fig 3.6 D, E). Callus size was measured at 7, 11 and 21dpc for 'drug holiday' treated and 5, 10 and 24dpc

for long pulse treated fish. Consecutive staining with Calcein and Alizarin Red S were applied as per previous experiments in order to track bone deposition at the crush site. The results show no significant difference in callus size between drug treated and mock treated *frf* fish (fig 3.6). Neither 'drug holiday' nor long pulse treatment had a strong effect on callus size in *frf* fish. However, in alendronate treated fish, I observed persistent bone debris on which new bone matrix was deposited (yellow arrows in fig 3.6), indicating inefficient osteoclast activity, but efficient deposition by osteoblasts.
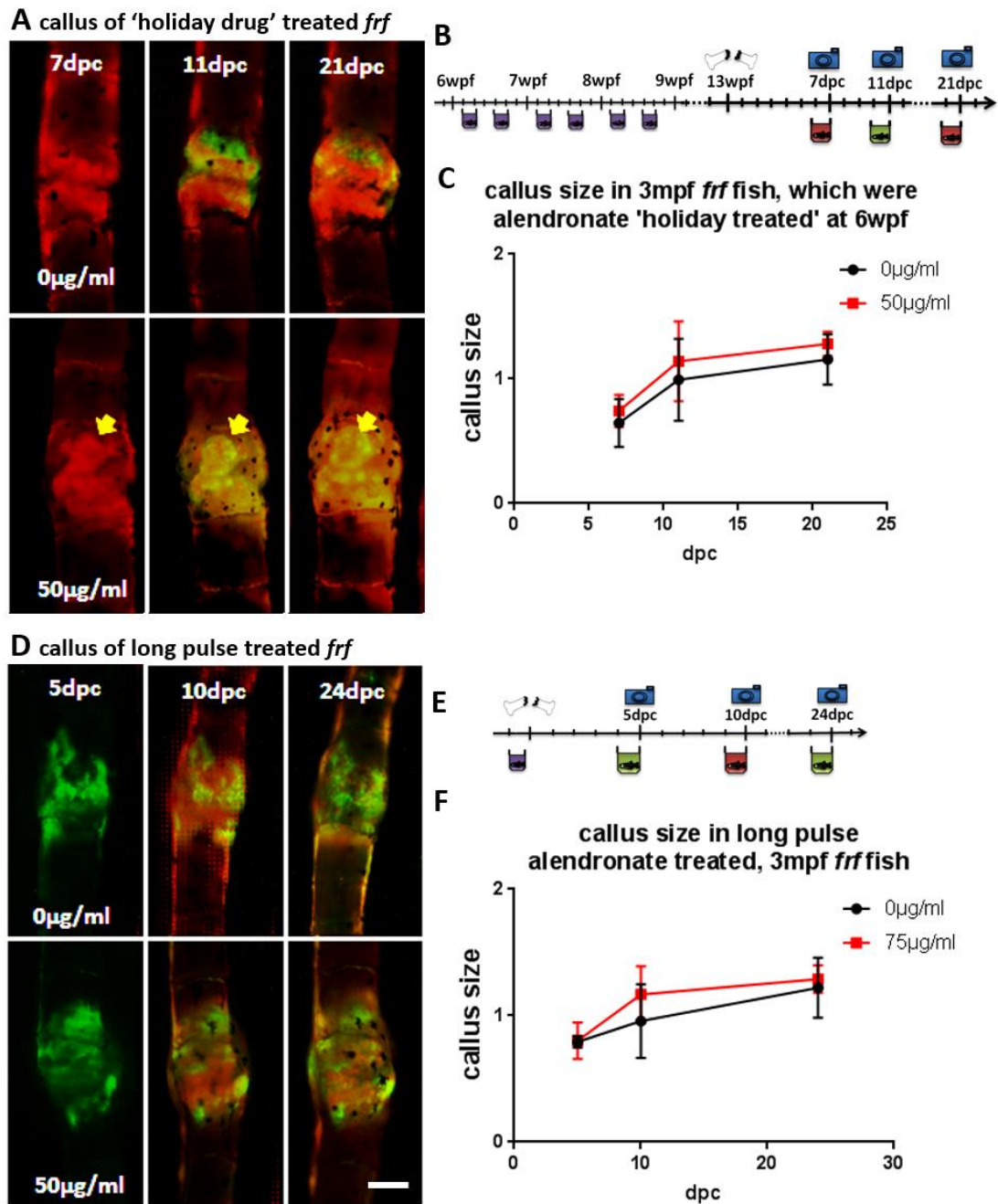


**Figure 3.6 Alendronate treatment has no significant effect on mineralized callus in *frf* fish**

**A)** temporal progression of mineralised callus formation in *frf* fish after 'drug holiday'

alendronate treatment, yellow arrows indicate unremoved bony debris on which mineralisation get deposited

**B)** graphical representation of experimental set up where colour of solutions indicate **drug**, **calcein** or **Alizarin Red S**

**C)** callus size measurements from 3mpf *frf* fish, which were 'alendronate holiday' treated prior to the crush. No significant difference in callus size between alendronate treated and mock treated fish can be detected, n=8

**D)** temporal progression of mineralised callus formation in *frf* fish after long pulse alendronate treatment

**E)** graphical representation of experimental set up where colour of solutions indicate **drug**, **calcein** or **Alizarin Red S**

**F)** callus size measurements from 3mpf *frf* fish, which were treated with long pulse of alendronate prior to the crush showing no significant difference in callus size between alendronate treated and mock treated fish

Scale bar corresponds to 50μm in all panels in **A** and **D**


## 3.4. Discussion

### 3.4.1. Spontaneous fracture formation in juvenile zebrafish as a model for OI drug testing

OI zebrafish model*, frf* mutant, treated with alendronate at late stages of metamorphosis, showed to be responsive to bisphosphonate treatment. These results were comparable to results obtained from rodent models (McCarthy et al., 2002). The data presented in here show that alendronate treatment in zebrafish OI model reduces spontaneous fractures in juvenile fish following 'drug holiday' alendronate treatment. Reduction in spontaneous fractures formation resembles human patients' responses to alendronate treatment (Seikaly et al., 2005), therefore we propose OI zebrafish as an accurate model for potential OI drug testing.

### 3.4.2. High alendronate concentration is strongly disruptive for fracture healing

Disruptive effects of high dosage of prolonged bisphosphonate treatment in orthopaedics patients were raised as problems by clinicians and were researched on by scientists working on animal models (Hodgkinson and Dzau, 2015). In here, I showed that alendronate had a strong, disruptive effect on zebrafish crush healing. Prolonged exposure of high alendronate concentration treatments led to ray loss and spontaneous loss of

uncrushed rays. Bisphosphonates are known for potent calcium chelating properties, which targets them to bone efficiently (Hughes et al., 1995), but upon over exposure bisphosphonates may reduce available calcium in the tissue. I predict that in my experiment, high alendronate concentration caused a major shift in ion balance in the tissue. Thus off target effects on wound healing and tissue integrity may have resulted. These results bring to the focus optimization of bisphosphonate doses and treatment times, as well as a need for developing a technique allowing bisphosphonate removal from the bone upon overexposure. Chemical trials are already performed in rodents (Hodgkinson and Dzau, 2015), therefore we propose zebrafish crush model as an appropriate and cheaper alternative animal model.

### 3.4.3. Efficient drug to bone binding occurs after as little as 4h of treatment

Due to variability of experimental regimes presented in this chapter, with altered length of alendronate treatments due to drug dosage optimizations, I was able to assess the speed of drug to bone affinity. Results from the short pulse treatment followed closely the results seen after long pulse treatment, indicating that fish drug absorption from the water is fast, and that the drug affinity to fish bones is high. It appeared that 4h of pre-crush alendronate treatment was sufficient to give as strong results as long pulse treatment. Moreover, following previous results from continuous treatment, where I saw destructive results on induced fractures at high drug doses (250 and 500µg/ml) as soon as 1dpc, suggest that absorption and accumulation happen fast and very efficient.

### 3.4.4. Alendronate treatment blocks remodelling in wild type fish

According to the data presented in this chapter, alendronate had a negative effect on mineralized callus remodelling. No sign of remodelling in crush healing of alendronate treated fish was observed. Mineralised calluses were formed as normal, however, no reduction was observed in their size in time, as it was the case for untreated fish. This serves as a strong indicator that in alendronate treated fish osteoclasts do not perform their role correctly and they do not reduce the size of the callus. These results are comparable to results obtained from rodent bone fracture experiment, where lack of callus remodelling was also noted (Savaridas et al., 2013)

### 3.4.5. Reduced initial osteoclast activity results in decreased bone debris clearance

I have observed that in drug treated crushes bony debris and sharp bone edges formed at the crush initiation were not cleared away at the normal rate. Clearance took longer that in untreated controls and was dose dependent. Lack of bone debris resorption can be explained, as above, by reduced osteoclast activity. It could also contribute to the overall increase in callus size in treated fish, as nascent bone would be laid around the sharp edges encapsulating scattered bone debris.

### 3.4.6. Alendronate does not block osteoclast recruitment to the crush site

On the other hand, my data showed that osteoclasts were normally recruited to the crush site, despite the strength or timing of alendronate treatment. Based on these results, I conclude that alendronate treatment affects osteoclasts activity, but does not interfere with the mechanism which recruits osteoclasts to the crush site. This data is consistent with medaka research data (Yu et al., 2016). Moreover, based on ISH results, osteoclasts' clumping was suspected, similar to previously described (Yu et al., 2016). However, to confirm this statement more investigation is needed, for example measurements of osteoclast size would be required.

### 3.4.7. Alendronate treatment does not seem to affect fracture healing of OI fish

Data presented in this chapter showed that alendronate had no effect on fracture healing in *frf* fish, in neither 'holiday treated nor long pulse treated experimental regimes. These results were comparable to results obtained from mice OI model, Brtl/+ mice (Burns and Corwin, 2013), reporting that upon alendronate treated wild type mice showed alterations in the healing dynamics and lack of callus remodelling, while Brtl/+ showed no significant differences in fracture healing upon treatment (Burns and Corwin, 2013).

I predict that lack of strong evidence of reduction of osteoclast activity in alendronate treated *frf* arises from initial low osteoclast activity in callus remodelling in those mutants. As described in the previous chapter, osteoclast driven remodelling stage in *frf* fish is hardly distinguishable. Fish struggle to re-build the connection between broken bone parts, therefore the importance of restoration of bone structure in the fracture plane, which is a main role of remodelling, in these fish loses its priority. Previously, I have shown that in *frf* fish bone anabolic processes overwhelmed fracture healing in *frf* fish, therefore reducing osteoclast activity in them would not give as significant results as in wild type fish.

# 4. Chapter 4 – *Staphylococcus aureus* infection of crush injury

## 4.1. Introduction

### 4.1.1. *Staphylococcus aureus* as an infection cause

*Staphylococcus aureus* (*S. aureus*) is a gram positive bacterium commonly found on human skin and within the respiratory system, with almost 50% of human population being colonized (Frank et al., 2010). This normally non-pathogenic commensal bacterium can be a cause of serious infections when invading open wounds or entering the blood stream causing bacteraemia (Tong et al., 2015). Many of the *S. aureus* cases were reported in strongly industrialized countries and they are highly associated with the use of surgical implants (Tong et al., 2015). Historically, *S. aureus* infections were successfully treated with penicillin, however, the incident rise of antibiotic resistant strains, such us Methicillin-resistant *Staphylococcus aureus* (MRSA) and vancomycin-intermediate *S. aureus* (VRSA), caused emerging problems in clinics (Chambers and Deleo, 2009). Bacteria are usually passed from human to human (Yang et al., 2012). *S. aureus* is known as being highly resistant to environmental factors so it can non-pathogenically colonize human skin and reside there before infecting the host. It can also be transmitted on objects, such as medical tools or implants, and through the air, bringing an issue of cross-infection in the hospitals (Yang et al., 2012). The broad range of diseases caused by *S. aureus*, and difficulty in killing this infectious bacterium brought *S. aureus* to the focus of epidemiologists and resulted in it being classified as a serious, complex clinical problem (Tong et al., 2015). The range of infections caused by *S. aureus* include bacteraemia, infective endocarditis, pleuropulmonary infections, skin and soft tissue infections, prosthetic devices infections and osteoarticular infections (Tong et al., 2015), but for the purpose of this study I focus here mainly on the latter.

### 4.1.2. Bone related *S. aureus* infections

*S. aureus* is the major pathogen of bone fractures. *S. aureus* osteoarticular infections can be divided into three main classes: osteomyelitis (bone infection), prosthetic joint infection, and native joint septic arthritis (Tong et al., 2015). Osteomyelitis is characterized by bone infection, destruction, and re-formation, and is divided into haematogenous (caused by

infected blood) and contiguous (caused by contact with an infected object e.g. tissue or implant) (Waldvogel et al., 1970). Based on experiments performed on animal models, it is known that osteomyelitis rarely forms in healthy bones, its occurrence requires bone infection, trauma or presence of foreign bodies (Lew and Waldvogel, 1997). *S. aureus* can cause bone infection by adhering to bone matrix components such as collagen or laminin through adhesion receptors (Elasri et al., 2002). Adhesion helps *S. aureus* to form biofilms, where bacteria hidden from antimicrobial agents can divide, maintaining a constant supply of new pathogenic agent, leading to chronic infections (Clauss et al., 2013). Moreover*, S. aureus* can survive internalization in osteoblasts as well as macrophages and upon release from dying cells, they can re-infect surrounding tissues (Hamza and Li, 2014).

### 4.1.3.    Influence of *S. aureus* infections on bone healing

Negative effects of *S. aureus* infections on bone fractures healing, such as delayed consolidation, fracture non-union, failed osteosynthesis, the interposition of soft tissue and re-fractures are common clinical problems (Kierdorf and Kierdorf, 2011). Bacterial infection is one of the most common causes of tibia fracture non-unions (Ciciliot and Schiaffino, 2010). Several methods were proposed for the early diagnosis of bone fracture infection (Bando et al., 2011, Del Debbio et al., 2010). Case studies reported that the posttraumatic infection time and the time of infection detection are crucial in determining infection strength and effect that infection has on healing process (Arthur and Heber-Katz, 2011), therefore clinicians report the need for further research this matter. Due to lack of possibility to research on patients, animal models are needed.

### 4.1.4.    Animals used in *S. aureus* related bone infections

*S*cientists introduced controlled bone infections in animals in order to understand the mechanisms driving infection and its subsequent impact on bone repair. Several animal models, such as rabbits (Henriksson and Brisby, 2013), rats (Murray et al., 2012) or mice (Koriyama et al., 2012) were used in the research on fracture infection. Diverse ways of introducing pathogen to the host bone were developed, including direct *S. aureus* injections to the bone, either through holes drilled in bones (Henriksson and Brisby, 2013) or through introduced bone fractures (Murray et al., 2012). Another infection techniques involved usage of *S. aureus* colonialized medical devices and implants, such as joint replacements (Koriyama et al., 2012). The diversity of surgical procedures and ways of bacteria inoculation was developed in order to model as many clinical scenarios observed in patients as possible.

### 4.1.5. Zebrafish in *S. aureus* studies

*Danio rerio* (embryo and larvae stage) was used in studies on host-pathogen interactions, virulence, and pathogenicity during *S. aureus* infections, showing possibility of zebrafish infection with non-host specialized pathogen (Prajsnar et al., 2008), however publications about *S. aureus* skeleton infections in adult zebrafish nor any adult teleost fish were not found.

### 4.1.6. Aim of experiments presented in this chapter

Up to date, model of bone infection in zebrafish has not been produced. The aim of this chapter is to show the possibility of localized infection in the tail of adult zebrafish, and the establishment of the method of *S.aureus* infection into zebrafish ray crush. Upon obtaining successful infection, the second aim is to characterize *S.aureus* pathogenic behaviour, as well as examine the influence of infection on the crush healing.

## 4.2. Material and methods

### 4.2.1. *S. aureus* strains used

*Staphylococcus aureus* SH1000 derived strains, mCherry-expressing and GFP-expressing (Prajsnar et al., 2008), were kindly provided by Josie Gibson from the Steve Renshaw laboratory.

### 4.2.2. *S. aureus* preparation

The overnight culture was set up from single colony spread on an agar LB plate with 10µl/ml tetracycline. 25ml of LB with antibiotic was inoculated and incubated at 37˚C with shaking overnight. After 16-18h of incubation, 500µl of the culture was transferred to a fresh 50ml tetracycline LB and grown at 37˚C in a shaker for 2h. OD of culture was measured and bacteria were spun down (13 min, 21 000rpm, 4˚C), and re-suspended in PBS, which amount was calculated by C1*V1 = C2*V2 equation (where C1 – measured concentration, V1 - volume spun down, C2 - required concentration, V2 – volume of PBS to re-suspend bacteria). Re-suspended bacteria were kept on ice, ready for immediate use for injections.

### 4.2.3. *S. aureus* injections

Bacteria were injected into the crush site at a range of time points after the crush (immediately post crush (0hpc), 0.5dpc, 1dpc, 2dpc). Glass needles used for injections were pulled with Sutter Instruments P-97 Flaming/Brown Micropipette Puller using Standard Wall Borosilicate Tubing without Filament (Sutter Instruments B100-50-10). Fish were

anaesthetised in 0.13% tricaine, rays in the tail were crushed (method described in chapter 1), and bacteria were injected into the tail through the crush in the bone using Narishige IM-300 Microinjector. The needle was inserted through the crush inside the ray into the intra-ray space proximal to the breakage. Bacteria were injected while retrieving the needle from the crush. After infection, fish were returned to separate tanks filled with standard tank water.

### 4.2.4.    Control injections
0.005% calcein was injected as a control.

### 4.2.5.    Infected fish husbandry
Infected fish were kept separately in a designated rack. They were fed as normally, while water in the tanks was changed daily to avoid the bacterial outbreak in the water.

## 4.3.    Results

Diverse methods of controlled, *S. aureus* open fracture infections, such as direct bacterial injection into the fracture site or injection cutaneous injection in the fracture proximity, were performed on rodent research animals models (Reizner et al., 2014), however, examples of localized bone infections in adult zebrafish were not found. Adapting and optimizing the method was a challenge. I have decided to perform direct bacterial injections into the crush site. This technique gives control over the infection source, directs the outbreak, allows tracking the bacterial movement and limits initial randomness of infection opportunity, in contrast to immersing wounded fish into fish water infected with bacteria.

### 4.3.1.    Zebrafish clear small localized infection in 3 days.
Bacterial injection method was adapted from (Prajsnar et al., 2008). Bacteria were injected into the crush at a concentration of 2500 cfu/nl which, based on (Prajsnar et al., 2008) is optimal for injections of *S. aureus* into zebrafish embryo cardiovascular system. Alternatively, 0.005% calcein was injected as a fluorescent control (Fig 4.1 A).
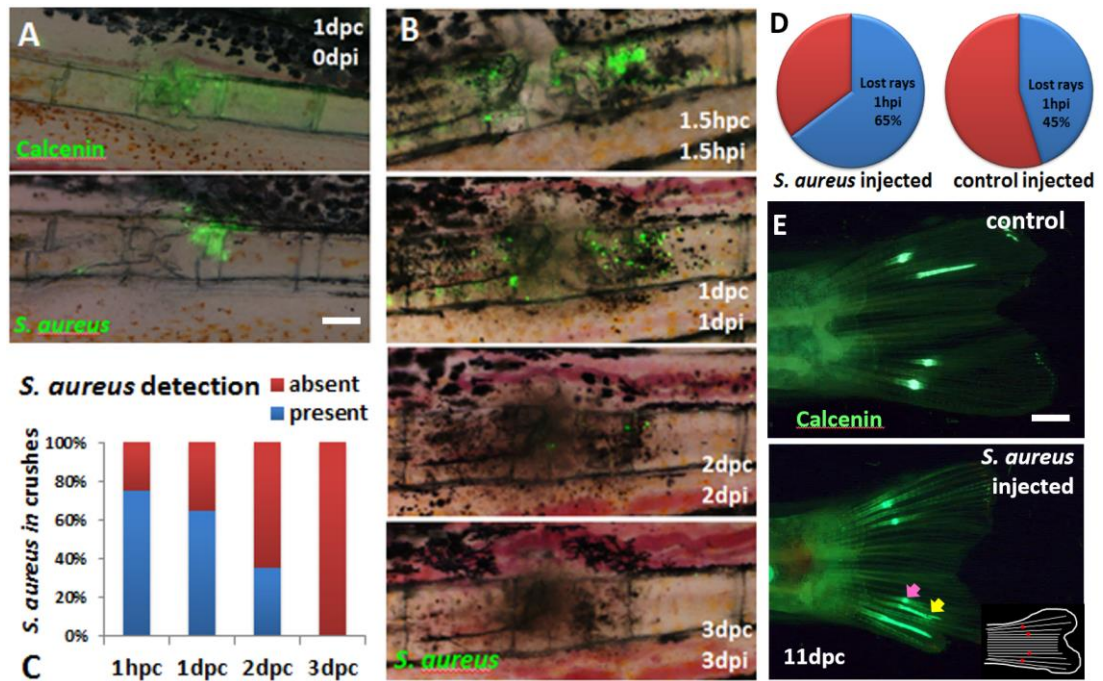
**Figure 4.1 Small, localized to crush *S. aureus* infection are cleared in 3 days**

**A)** injection efficiency and accuracy was tested with fluorescent calcein and green fluorescent *S. aureus*

**B)** time course of infected crush, which allowed tracking the clearance of bacteria from the crush site. Both spatial and temporal distribution of bacteria can be assessed, as well as progression in the crush healing

**C)** graph representation of pooled results of bacteria clearance from 20 infected crushes, showing progressive bacteria clearance up for to 3 days, when all crushes were cleared from infection. Initial efficiency of injections can be examined based on readouts form 1hpc

**D)** graph representation of ray loss influenced by injections in *S. aureus* infected crushes as well as calcein injected controls, showing that crush injections cause high disturbance to the broken rays

**E)** images representing recovery after the injury, showing the difference in the rate as well as the quality of regrown rays, between infected and control fish. Nascent bone was stained with calcein. Yellow arrow indicates kinked ray forming following *S. aureus* infection, pink arrow indicates spontaneous fracture

Scale bars corresponds to 50µm in all panels in **A** and **B**, and 300µm in panels in **E**

While fluorescent calcein was gone from the crush 2 days post infection (dpi), bacteria clearance took zebrafish up to 3 days to clear (Fig 4.1B). Injected bacteria (0.5nl) initially resided within the hemiray cavities of proximal and distal parts of broken ray, with slight spillage into intradermal space, and at this point bacteria appeared as a strongly fluorescent mass, where individual bacteria were not distinguishable. By 1dpi colonies were observed. Excess injection fluid was slowly reduced over 24hr, improving image clarity. By 2dpi, a reduction in the number of bacterial colonies was noticed and by 3dpi all had been cleared away (Fig 4.1B). At 1hpc, 75% of injected crushes had visible bacteria (Fig 4.1C), I imaged injected crushes over 3days (Fig 4.1B, C). Despite relatively fast bacterial clearance, the injection process into the crush appeared to be a generally disruptive procedure as almost half of calcein (control) injected crushes, and 65% of *S. aureus* injected crushes lost distal part of the ray (Fig 4.1D). For calcein injections, lost rays are restored by little blastema formation and regeneration (control, Fig 4.1E). However, in infected crushes, infection visibly influenced regrowth of lost rays making them kinked and distorted (yellow arrow in Fig 4.1E). It also led to the formation of spontaneous crushes in the rays adjacent to the ones possessing infected crushes (pink arrow in Fig 4.1E) and occasionally to loss of whole adjacent rays.

### 4.3.2. Large volume injections into crush site lead to the further loss of the distal part of a broken ray

An initial experiment showed that small localized infections were cleared by 3dpi (fig 4.1 C). Since the aim was to achieve a prolonged *S. aureus* bone infection, I have decided to increase the volume of injected bacteria, keeping concentration at the same level of 2500 cfu/nl. The volume of bacteria was increased from 0.5nl to 4nl.
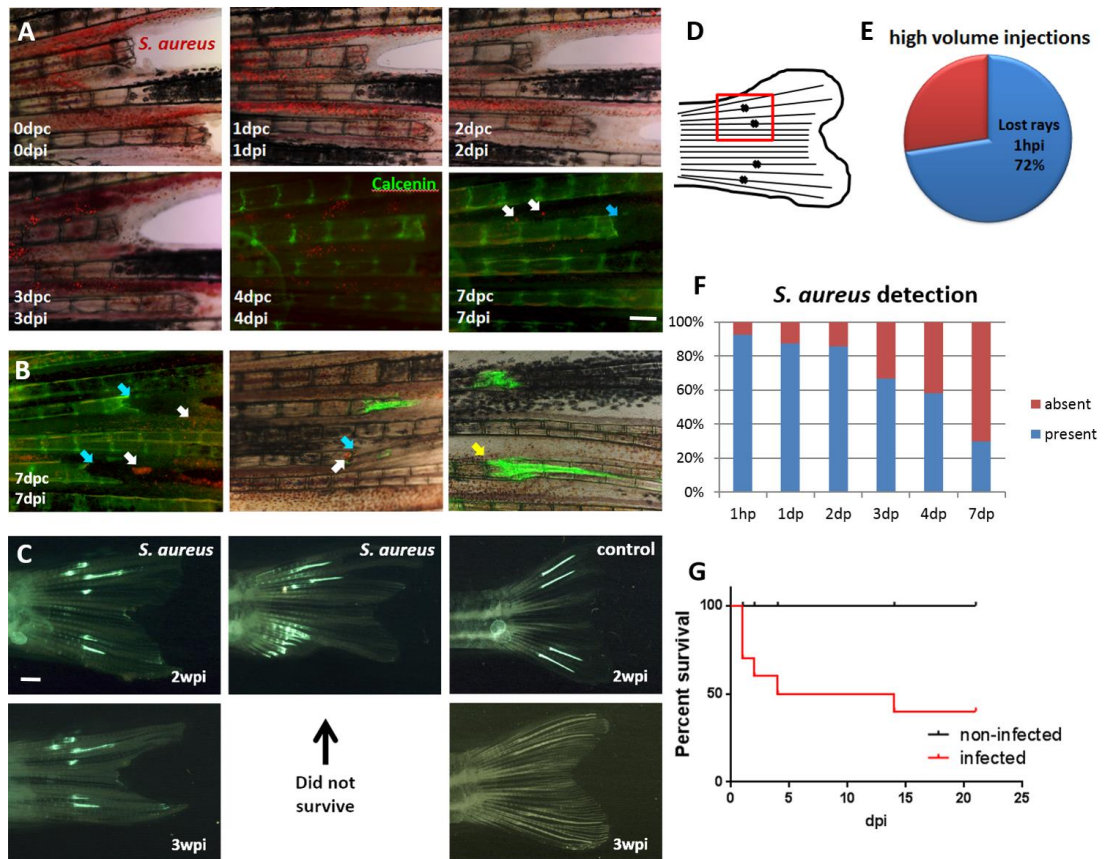
**Figure 4.2 Large volume *S. aureus* injections into the crush site lead to the loss of the distal part of a fractured ray, prolonged time of bacterial infection, and increased fish mortality**

**A)** spatial and temporal distribution of fluorescent red *S. aureus* in the zebrafish tail after high volume bacterial injections into crushed rays. High volume injections lead to a loss of all parts of the crushed rays and persistent bacteria presence blocked regeneration of lost rays. White arrows indicate persistent bacteria at 7dpi, blue arrow indicates the lack of regrowth.

**B)** re-growing rays showed impaired formation due to bacteria presence when checked 7 days after injury. White arrows indicate persistent bacteria, blue arrows indicate lack of regrowth, yellow arrow indicates newly formed outgrowing ray, invading a present non-lost ray

**C)** 2 and 3 weeks post injury recovery impairment was clearly visible due to previous bacteria presence. While control fish fully restored their lost ray fragments, previously infected fish showed strong malformations of re-growing rays as well as loss of adjacent to crushed rays and inability to regrow them

**D)** graphical representation of tail, where red rectangular shows area imaged in panel **A**

**E)** graph representation of ray loss influenced by high volume injections showing increased

111

to 72% ray loss in crushes injected with a high volume of bacteria solution

**F)** graph representation of bacteria clearance rate from crushes infected with high volume of *S. aureus* showing that even 7dpi around 30% of crushes still showed presence of bacteria

**G)** Kaplan-Meier curve of infected fish along days post infection (dpi) showing that half of infected fish died as soon as 4dpi

Scale bars corresponds to 100µm in all panels in **A** and **B**, and 300µm in panels in **C**

Following experiments were performed with *S. aureus* expressing mCherry, in order to distinguish it from green fluorescence of calcein staining. Increased injection volume induced more ray loss than previously described, increasing ray loss rate up to 72% (fig 4.2E) from 65% reported after small volume bacterial injections (fig 4.1D). The loss was observed as soon as 1hpi indicating that rays were lost due to the mechanical disturbance by injected volume rather than a result of bacterial infection. I observed that injected fluid spilled into the inter-ray spaces filling intradermal space with *S. aureus* injection fluid (fig 4.2A). The high amount of mCherry positive bacteria can be observed in the infected crushed tails (fig 4.2A). As soon as 1dpi bacteria form bigger clumps, indicating bacterial growth and colonies formation. Bacteria were slowly cleared, but even 7 days post infection I were able to detect bacteria in the tail (white arrows, fig 4.2A, B). Regeneration of lost rays was blocked (blue arrow, fig 4.2A). By 7dpi *S. aureus* was still present in 30% of infected crushes (fig 4.2F). Interestingly, for lost rays, regrowth did not initiate until bacteria were cleared. Normally regrowth can be observed as soon as 3dpc (data presented in chapter 1), however, in infected rays regrowth was delayed while the bacteria were present. As late as 7dpc no regrowth was observed if bacteria were not cleared (white arrows indicates bacteria, blue arrows indicate the lack of regrowth fig 4.2B). In fact, even if bacteria where cleared, regrowth was impeded, re-growing rays were kinked and deformed or were formed ectopically (yellow arrow fig 4.2B). Abnormal regrowth of lost rays could even be seen weeks post infection, with bacteria injected fish being unable to properly restore lost rays (fig 4.2C), as compared to control injected rays, which reformed fully. Rays adjacent to the infected crushes often showed spontaneous fractures and loss of ray fragments. None of the infected crushes fully restored lost rays by 3wpi. In addition, injection of large doses of bacteria caused high mortality among infected fish (fig 4.2G), although the exact cause of death was not investigated further. It is possible that fish died from septic shock caused by bacteraemia. I have visually checked the spread of bacteria to

other parts of the fish body, such as gills or mouth, but I did not find any bacterial trace on those organs. Necropsy would be required to ascertain the cause of death and systemic injection load.

### 4.3.3. Crush healing was affected by the concentration of injected bacteria, as well as the time of infection.

Due to the previously observed ray loss, I decided to decrease the volume of bacteria back to of 0.5nl (reported in fig. 4.1), and in order to increase the amount of injected bacteria, I doubled the concentration of bacteria from 2500 cfu/nl to 5000 cfu/nl. Moreover, based on suggestions from orthopaedists who were interested in differences in fracture repair progression based on different infection times throughout fracture recovery, I decided to infect at 0.5, 1 and 2 days following crushing, checking injection possibilities as well as infection progression.

### 4.3.4. 1dpc was the most effective while 2dpc the most accurate, time points for intra-crush bacterial infections.

Crush injuries were introduced to fish tails 2, 1 and 0.5 days before *S. aureus* infection. Bacteria were injected, providing a range of infections in several stages of early crush recovery.

0.5dpc crush remained as an open tissue. Bacteria injected into this space either dispersed or attached to crush periphery only, usually adjacent skin and intra-ray tissue. To circumvent this, I inserted the needle into the intra-ray cavity of the adjacent segment and injected bacterial liquid there. This led to bacterial accumulation in soft tissue adjacent to the crush and not the crushed bone (fig 4.3 A1). When wound closure occurred, bacteria infected the crush site by 2dpi (fig 4.3 A2).

In 1 day old crushes I was able to inject bacteria directly at the crush site, with mild spillage to surrounding tissues (fig 4.3 A7). The high number of bacteria was accumulated at the crush site showing much higher crush infection efficiency than the 0.5dpc time point described above.

Injections into 2dpc crushes were more challenging. 2dpc crush site was hardened and the breakage connection was forming, and there was no free movement between broken ray parts. These characteristics made it challenging to penetrate the crush site with a thin glass needle. At 2dpi, there was limited free diffusion of injected bacterial solution, therefore

bacteria stay tightly packed at the crush plane (fig 4.3 A13). The frequent overflow was observed, reducing the amount of bacteria remaining at the crush site.

### 4.3.5. Bacteria were excluded from the crush site over time

In all three scenarios, where bacterial injections were performed at different stages of crush recovery, bacteria did not remain at the crush site over time. By 3dpi bacteria displaced distally for all injection timings (fig 4.3A, C). In order to check if there is a trend of bacteria exclusion from the crush site, I examined the temporal and spatial distribution of bacteria in reference to the position of the crush (fig 4.3B). The crush images were divided according to the scale: 0 indicates crush plane, 1 - end of crushed segment, 2 - middle of adjacent segment, 3 – end of adjacent segment. Negative numbers indicated positions proximal from the crush, positive numbers indicated positions distal from the crush (fig 4.3B). I counted the lines which were crossed by a group of bacteria at each time point (red lines fig 4.3 B). Results were plotted on the graph, indicating bacterial spatial distribution across 5dpi (fig 4.3C). 1dpi data showed that proximity of injection location to the crush site was dependent on the stage of crush recovery at the point of injection. By 2dpi, despite the initial bacteria position, all bacteria were found approximately the same place, slightly beyond the crush plane. At 3dpi almost all of them were seen around the distal edge of crushed segment. 0.5dpc and 1dpc injected crushes showed further distal bacterial displacement. 2dpc showed the spatial bacterial arrest. The smallest overall displacement was seen in the crushes infected 2dpc, while the biggest in the crushes infected 0.5dpc (fig 4.3C).
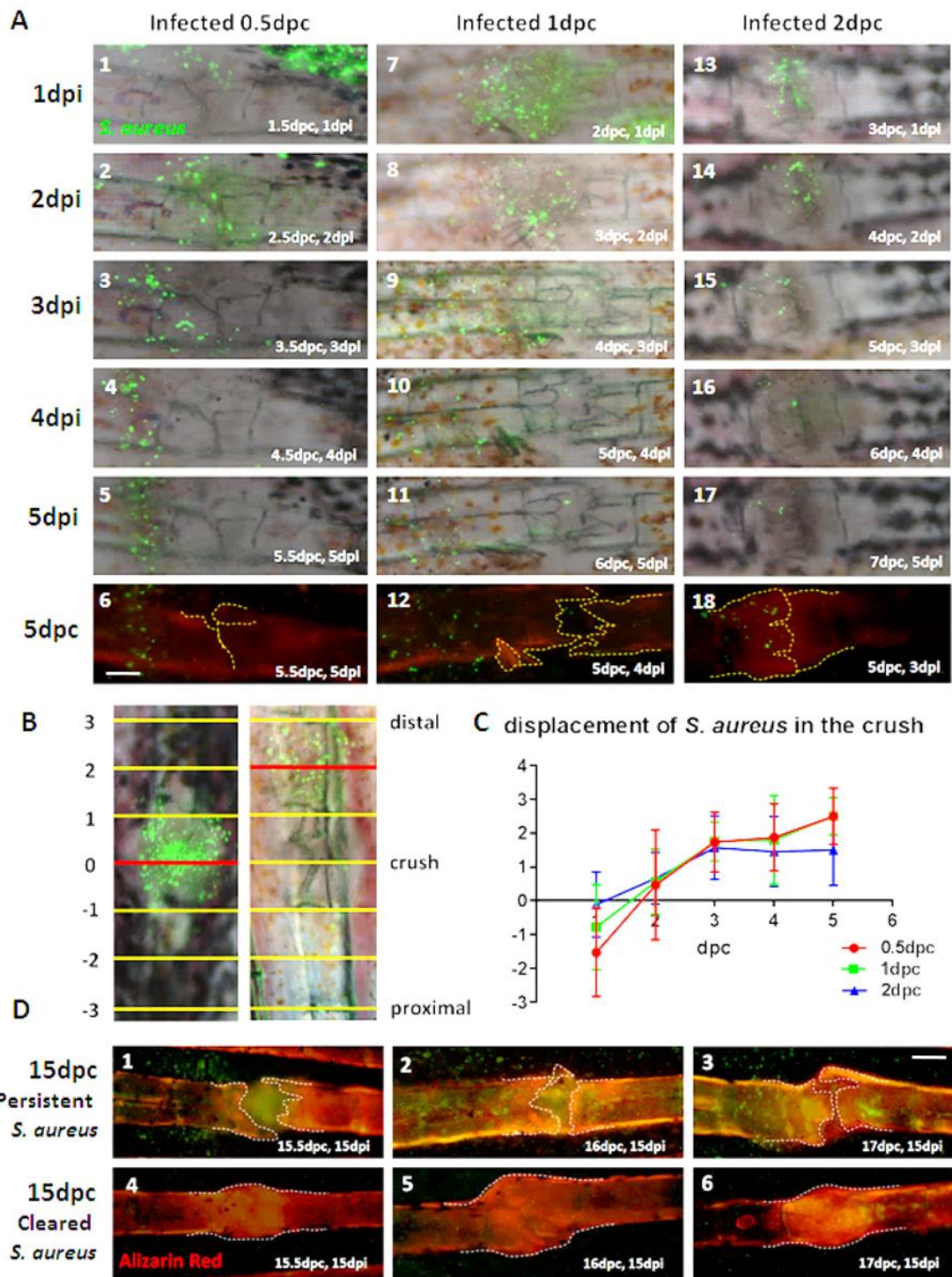
**Figure 4.3 Time course of bacteria clearance and crush healing in the fractures infected at different time points with low volume but high concentration of *S. aureus* solution**

**A 1-6)** time course of crush infected with *S. aureus* 0.5dpc. This panel set up allowed tracking spatial and temporal distribution of the green fluorescent bacteria around the crush. Results showed that the bacteria were fully displaced from the crush site over time

**A 7-12)** time course of crush infected with *S. aureus* 1dpc, showing that bacteria were also displaced from the crush site, however, spread of bacteria was higher than in crushes

infected 0.5dpc

**A 13-18)** time course of crush infected with *S. aureus* 2dpc

**B)** Example images showing how each image was divided order to spatially determine the position of bacteria with respect to the position of the crush. Vertical lines divide pictures according to the scale: 0 indicates crush plane, 1 - end of crushed segment, 2 - middle of adjacent segment, 3 – end of adjacent segment. Negative numbers indicate positions proximal from the crush, positive numbers indicate positions distal from the crush. Red lines indicate the position of bacteria and the classification selected for that particular images.

**C)** graph representing spatial and temporal distribution of bacteria in reference to the crush plane, showing initial accuracy of injections and bacterial displacement over time

**D 1-3)** examples of crushes which did not remove bacteria by 15dpc showing a lack of crush repair

**D 1-3)** examples of crushes which remove bacteria by 15dpc showing mineralized callus formation

Scale bars correspond to 50µm in all panels

### 4.3.6.    *S. aureus* infection blocks crush healing process

5dpc all infected crushes were stained with Alizarin Red S in order to examine mineralized callus formation. In injections performed 0.5 and 1dpc, no bony callus was observed at 5dpc (fig 4.3 A6, 12), the time point when normally mineralized callus was present (previous chapters). Sharp crush edges were still clearly visible (fig 4.3 A6, 12) indicating that the crush repair process was not even started. In the group injected 2dpc, slight bonny calluses were observed at 5dpc, however, they appeared unchanged from infection date indicating arrest of callus growth (fig 4.3 A18). In addition, loose bone debris was noticed as along the sharp edges at the crush plane, indicating that crush repair had not occurred.

### 4.3.7.    Prolonged crush infection blocks crush healing

All crushes were also checked at 15dpc for callus formation by repeated Alizarin Red S in vivo staining (fig 4.3D). At this time point, clear division in the crush healing and bony callus formation was observed between crushes which had persistent bacteria present, in comparison to those in which bacteria was already cleared away. I was able to observe, that in the presence of green fluorescent *S. aureus* near the crush site, there was no evidence of crush healing process in term of mineralized callus formation (fig 4.3 D1, 2, 3). Edges still appeared sharp (fig 4.3 D1), loose bony debris were present (fig 4.3 D2) and bones were not aligned (fig 4.3 D3). In comparison, crushes from which bacteria were

cleared away appeared joined by mineralized calluses on 15dpc (fig 4.3 D4-6). All results observed at 15dpc were independent of the timing of the infection in relation to the crush. All described outcomes were found in all groups injected either 0.5dpc (fig 4.3 D1,4)., 1dpc (fig 4.3 D2,5) and 2dpc (fig 4.3 D3,6).

### 4.3.8.  *S. aureus* infection is responsible for prolonged crush inflammation

Prolonged infection appeared to block crush healing. As I saw no signs of hard callus formation nor remodelling, I decided to examine the inflammation in infected crushes, by infecting crushes in *Tg(mpx:GFP)* fish. *Tg(mpx:GFP)* fish possess fluorescently labelled neutrophils, therefore I used it as an indicator of inflammation (following the method described in chapter 1). *S. aureus* was injected into the crush site at the peak of crush inflammatory response, at 12hpc (based on the results we accumulated and described in previous chapters). I took images of GFP positive neutrophils prior to infection (fig 4.4A, 0.5dpc, ni). Images were taken daily for 5 dpi. At 1dpc I was able to observe bacteria mixed with inflammatory cells at the crush sites. By 2dpi bacterial colonies were much more distinguishable and accumulation of inflammatory cells at the crush site was clear. Prolonged accumulation of both was seen at 3dpi and was slowly fading away on following days. Dates of complete bacterial clearance varied between crushes, even between different crushes within same individual (fig 4.4A) but all of them followed the trend described above. To quantify inflammatory response, I decided to use CTCF calculation method (as presented in chapter 2). I calculated total crush fluorescence based on crush areas identified by white circles (fig 4.4A). I plotted results of 4.5dpc time course graphically and statistically tested differences in CTCF between infected and uninfected crushes (fig 4.4B). Data showed the significant increase in total crush fluorescence of infected fish at 1.5 and 2.5dpc (1 and 2dpi). Enhanced and prolonged inflammation was detected in the *S. aureus* infected crushes. Big error bars at the graph showing CTCF of infected crushes, indicated differences in the rates of progressive bacterial clearance and the different strength of inflammatory response at the crush site depending on the spatial distribution of the bacteria in the infected tails.
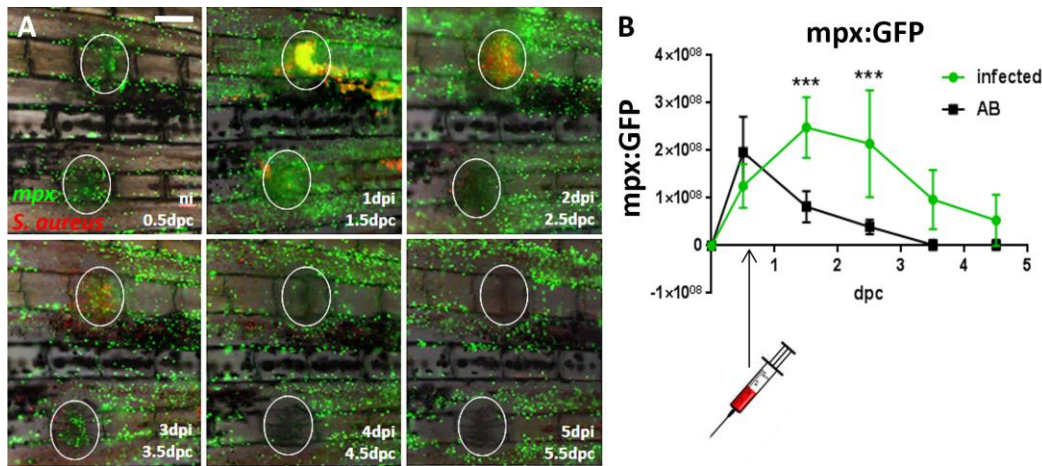
**Figure 4.4 *S. aureus* infection caused enhanced and prolonged crush inflammation**

**A)** time series of *Tg(mpx:GFP)* fish crushes infected with fluorescent red *S. aureus* 0.5dpc, showing the recruitment of fluorescent neutrophils marked by *mpx*:GFP into the crush site. White circles indicate areas which were captures for CTCF measurements; ni – not infected; Scale bar corresponds to 100μm in all panels

**B)** CTCF results presented on the graph showing significant upregulation in CTCF of infected fish on 1.5 and 2.5dpc. Syringe indicates moment of bacterial infection into the crush, *** $p<0.001$, ANOVA, n=8

## 4.4. Discussion

### 4.4.1. Adult zebrafish are sensitive to *S. aureus* infection

In this chapter, I provided an evidence that adult zebrafish, similarly to the zebrafish embryos (Prajsnar et al., 2008), are sensitive to *S. aureus* infections. I showed that bacterial infection can be localized at the injury site and can be directly introduced into the crush through precise bacterial injections. This accurately mimics human open fracture infection conditions (Kierdorf and Kierdorf, 2011), which were also modelled in other model animals (Reizner et al., 2014).

### 4.4.2. Technique of accurate infection of zebrafish tail crush

I developed a technique for accurate and effective zebrafish crush infections by direct injections of *S. aureus* to the crush site. I assessed results of several regimes of infections to find differences in bacteria clearance between them and to find the most efficient time point, which would be the most useful in biomedical research for mimicking human conditions. I altered volume, concentration, and timing of bacterial infection.

### 4.4.2.1.  High volume of bacterial injections triggered ray loss

In this chapter, I observed that high volume injections into the crushed ray in zebrafish tail resulted in the loss of rays distal to the crush. This occurred for both calcein and *S. aureus* injections, indicating that volume of injection was the critical factor. However, whilst calcein injected fish always regenerated these lost rays, bacterial injections reduced or blocked regeneration. These results indicate that infection, even if cleared from the crush site, have a negative effect for tail healing.

### 4.4.2.2.  Injection at 1dpc was optimal because of mechanical properties of tissues at this recovery stage

I was able to determine that 1dpc was the most effective time point for intra-crush bacterial infections. Due to tissue disruption, early infection resulted in bacterial spillage inside and around crushed ray reducing the accuracy of injection to the crush, as well as bacterial retention. Bacteria injected 1dpc were able to directly reside at the crush site, possibly due to the partial wound closure, affording tissue stability. Soft wound closure seemed to form the substrate for injected pathogen.

Injections into 2dpc crushes were much more difficult to perform. I suspect that at 2dpc crush site was already partially stabilized and cartilage callus was maturing, making crush penetration and infection troublesome. On top of that, I suspect that dense environment did not allow for free diffusion of injected bacterial solution, therefore bacteria were tightly packed in the crush site. There appeared to be fewer bacteria present in the crush after the infection than in the group infected 1dpc, which could explain their lowered effectiveness. However, since no bacteria counts were taken to compare the different injected groups, this statement is not backed by data.

### 4.4.2.3.  Injection time influence infection size

I conclude that time of infection following the fracture is crucial for initial bacteria distribution, which subsequently can affect bacterial load and biofilm spreading area in the injury site. These results confirm clinicians' predictions that infection time can alter infection strength, due to tissue accessibility (Arthur and Heber-Katz, 2011).

## 4.4.3.  Fish possess the ability to fight *S. aureus* infection

In this chapter, I showed that adult zebrafish, similar to humans (Nauseef, 2007), and to the zebrafish embryos (Renshaw et al., 2006), possesses the ability to fight *S. aureus* infections. I observed that *mpx* marked inflammatory cells' recruitment to the crush site was correlated with progressive reduction of bacterial colony numbers over time. After bone

injury in humans, inflammatory cells are also recruited to the infected fracture site to clear the bacteria residing there (Nauseef, 2007). Rodent data showed that *mpx* positive neutrophils possess anti-microbial properties and ability to communicate and recruit other cell types such as mesenchymal cells, osteoclasts or osteoblasts (Pape et al., 2010). Inflammation was shown to be a result of cumulative, simultaneous work of numerous anti-microbial elements, which collaborate to create an environment, optimized to kill microbes (Nauseef, 2007). I showed that adult zebrafish had the ability to clear *S. aureus* infection from the crush site in a similar way and simultaneously to possibly arrest following fracture healing stages. In addition, I reported bacterial spatial distribution changes, which are challenging to track in higher animals.

### 4.4.4. Migration / pushing away of bacteria from the crush site

In all performed crush infections, bacteria were gradually excluded from the crush site. Based on previous crush healing observations, as well as observations of *S. aureus* infected *Tg(mpx:GFP)* line, I predict that this displacement occurred due to work of the inflammatory cells. I observed a clearance of inflammatory cells from uninfected crushes by 3dpc. However, in infected crushes, total clearance of neutrophils was concomitant with the exclusion of bacteria. Such a clearance of neutrophils was delayed in the infected crushes.

### 4.4.5. Infection causes inflammation separate to crush inflammatory wave, which prolongs overall inflammation

I measured the relative strength of inflammation by measuring the intensity of fluorescence emitted by neutrophils in *Tg(mpx:GFP)* line. I saw highly enhanced and prolonged inflammation response in the crushes infected with *S. aureus.* I predict that inflammation delay crush healing response. It is interesting to see that in infected crushes showing the lack of callus formation, inflammation is significantly stronger and prolonged. That gives reasons to believe that inflammation is inhibiting the callus deposition. It was shown in murine models that inflammation drives fracture recovery through cell recruitment and inducing cell differentiation (Pape et al., 2010). There is a full network of factors enabling crosstalk between inflammatory and osteogenic cells (fig 4.5) (Kansara et al., 2014) through which inflammatory cells might have an ability to control fracture recovery progress.
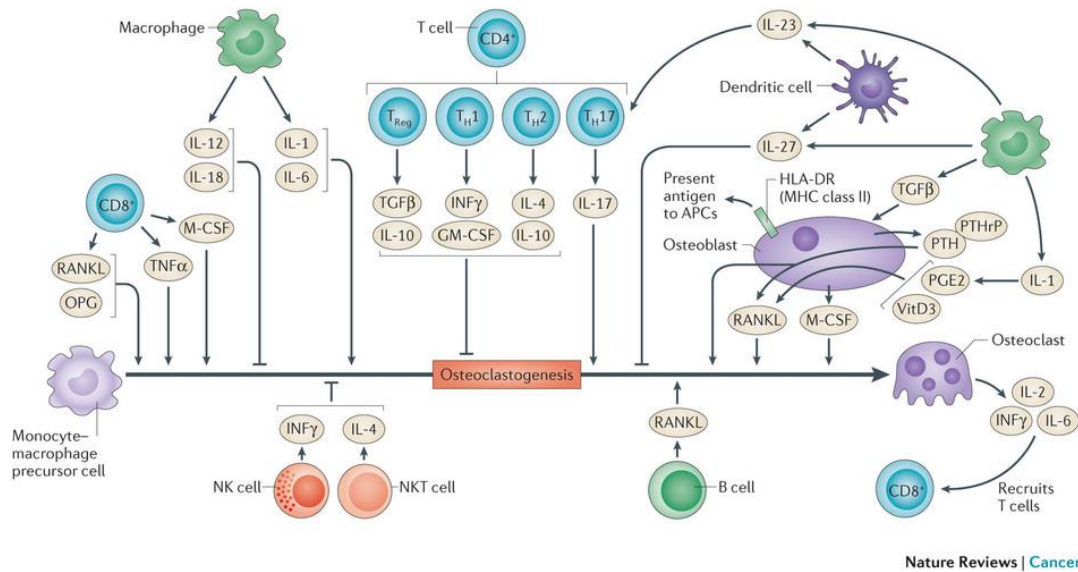
**Figure 4.5 Osteoclast, osteoblast and inflammatory cell crosstalk.**

Communication between bone related cells and inflammatory cells is common. Osteoclast differentiation requires receptor activator of nuclear factor-κB ligand (RANKL) and macrophage colony-stimulating factor (M-CSF). RANKL is produced by osteoblasts in response to prostaglandin E2 (PGE2) and 1,25 dihydroxy vitamin D3 (VitD3) and by activated T cells. Osteoblasts express the parathyroid hormone (PTH) receptor which can induce osteoclast activity by increasing RANKL expression. Immune cells produce M-CSF which stimulates RANK expression in monocyte–macrophage osteoclast precursor cells. Immune cells secrete factors which can promote or suppress osteoclast formation. Cytokines can be secreted by osteoclasts to facilitate T cell recruitment as well as activation. Macrophages produce transforming growth factor-β (TGFβ) which can induce osteoblast proliferation, recruit osteoblast precursors and block apoptosis. Major histocompatibility complex II (MHC class II) is expressed by osteoblasts in order to present antigen.

GM-CSF granulocyte–macrophage colony stimulating factor; APCs antigen-presenting cells; HLA-DR human leukocyte antigen d-related; IFNγ interferon-γ; NK natural killer; NKT natural killer T; $T_H$ T-helper; OPG osteoprogerin; TNFα tumour necrosis factor-α; $T_{Reg}$ regulatory T; IL interleukin

(Kansara et al., 2014)


Possible use of immune modulators to determine the role of neutrophils in this infection induced inhibition would be required. I performed initial experiments using hydrocortisone to suppress immune-response. Preliminary data showed the successful reduction in

inflammatory response at the crush site after hydrocortisone use. This model could be used in bacterial infection studies as well as the basic determination if lack of inflammation arrest fracture healing. It has been shown previously, that inflammatory cell ablation affect tail recovery after amputation (Petrie et al., 2014), therefore it would be interesting to use genetic ablation of inflammatory cells in the crush healing model.

### 4.4.6.    Bacterial presence blocks crush healing

According to our data, healing of the crushed ray was arrested at the point at which bacterial infection occur and was kept on hold until bacteria were cleared away from the crush site and its surroundings. These results were consistent with the fracture healing arrest seen in infected human fractures (Arthur and Heber-Katz, 2011), indicating that infected zebrafish crush injury serves as an accurate human bone open fracture infection model.

# 5. Conclusions and future project ideas

## 5.1. Crush injury is a precise animal model for human bone fracture studies

I have developed and validated an in vivo bone fracture model in the zebrafish tail, showing that crush injury recovery followed the stages documented for human bone fracture healing. Stages were marked by genetic and histological markers conserved across from human, through mice to fish, and zebrafish crush healing appeared outwardly to mimic both human and murine fracture responses. I showed the usefulness of zebrafish model in understanding basic processes underlining human fracture healing as well as fracture healing under perturbed conditions, testing the crush model in animals with genetic disorders equivalent to human patients, showing results which follow trends seen in humans. I showed zebrafish crush injury as a potential model for human bone related drug testing and simulated bacterial infection of fractures using zebrafish. I also showed that zebrafish bone fracture model holds several advantages over existing fracture models in other research animals.

Firstly, zebrafish offer a number of advantages as a model system, including ease of imaging and genome modifications allows fast generation of bone specific transgenic lines and mutants. The ability to recapitulate precise genetic lesions offers the ability to provide personalised models for genetic bone disorders of human patients in the near future. Use of the crush procedure developed here adds to the methods for characterising the ensuing bone phenotype, allowing direct evaluation of the outcome of the genetic lesion on fracture repair. Furthermore, the fecundity of zebrafish provides high sample numbers for experimental replicates, whilst compounds are easy to administer through immersion.

The fin lepidotrichia offers an elegant and simple system for fracture analysis; both readily accessible for fracture, manipulation and imaging, as well as simplified with only a limited number of cell types in the tissue. I have demonstrated that it is possible to alter the fracture response through genetic, pharmacological and infection administration readily.

## 5.2.    Advantages of zebrafish crush model over other animals

### 5.2.1.    Zebrafish crush model shortens experimental time

The bone fracture healing process progresses faster than for any known animal model, with the peak of each phase reached in half of the time as compared to mice fracture model (Marsell and Einhorn, 2011), and thus shortens the experimental time. In sum, the system offers the ability to interrogate the cellular and molecular processes of fracture repair under normal and physiologically perturbed scenarios and will complement clinical and mammalian model studies.

### 5.2.2.    Zebrafish tail mechanical simplicity is another advantage of our model

I believe that developed here zebrafish tail crush model brings an innovative view to the biomedical field of regenerative medicine. I developed, validated, proved and tested in the range of condition model, which serve as a great example for human bone fracture studies. The simplicity of mechanical structure of zebrafish tail work here for an advantage, serving with only this, what is absolutely necessary for bone fracture studies. That is exactly what an animal model is supposed to be. The ideal model should be a simplified and idealized version of complicated system, which helps in understanding it. I believe that zebrafish crush model is exactly what is needed to answer basic as well as more complex fracture healing related questions, which are too difficult to reveal from higher organisms.

## 5.3.    All 4 stages of healing are required for correct recovery

I showed correlations between the stages and their dependency on each other and accumulative effects of distortion in one stage reflecting on the efficiency of others. I observed that presence of each stage was important and individual stages progression influenced the other stages.

For example, I showed that prolonged inflammatory response led to the temporal arrest in healing progression. It was consistent with rodent data which showed that inflammation can compromise rate of healing progression by stimulating recruitment and differentiation of osteogenesis related cell types (Pape et al., 2010). In zebrafish, Petrie et al. (2014)

showed that genetic ablation of macrophages negatively influence tail formation after amputation. It would be of interest to determine the effect of macrophages ablation on fracture healing through genetic ablation or use of glucocorticoids, and to perform infection analysis on those fish with regards to fracture healing.

## 5.4.        Zebrafish respond to human drugs

In chapter 3, I presented results which showed that zebrafish was able to respond to treatment with bisphosphonates, which are used heavily on the orthopaedic clinical setting to treat certain bone diseases. Extended exposure to very high doses of alendronate was deleterious to bone regrowth after fracture induction. This may have been due to the $Ca^{++}$ chelating properties of the drug which possibly abrogated normal wound healing responses, although other tissue responses may be sensitive. Indeed I noted a large increase in spontaneous distal lepidotrichia loss and failure to regenerate. However at more moderate concentrations with shorter exposure durations, led to reduced callus remodelling, as well as a measurable reduction in spontaneous fractures in *bmp1a* mutant zebrafish. Results indicating the reduction in osteoclast activity, were consistent with previously published data (Yu et al., 2016).

## 5.5.        Fish respond to human pathogens

I developed and validated the method of bacterial injections into the adult zebrafish tail crush injury. I showed the local response to the infection. Changes in standard parameters such as prolonged inflammation indicated that zebrafish crush is prone to infections with human pathogens. I believe that this technique can bring big advantages in unrevealing human bone infection related issues.

## 5.6.        Mechanism of sensing severity of injury

Throughout the thesis, I demonstrated that a standardised zebrafish fracture is sensitive to external factors like drugs, genetic mutations, mechanical crush distortions and infection. Based strength of the influencing factor, crush healing reacted differently. Healing either performed normally; was temporarily arrested, was completely blocked, or redirected from crush healing to epimorphic regeneration by losing distal part of broken ray and introducing mini blastema formation.

Based on those observations I propose that there is an inflammatory cells driven, injury severity sensing mechanism, allowing zebrafish to undertake actions adequate to the situation. I believe that this mechanism is highly regulated on a molecular level via cellular cross-talk mentioned above. Unrevealing details of this mechanism would be the aim of my future work.

## 5.7.  Zebrafish tail crush injury model open doors to answers of many not resolved queries connected to human fracture healing

I believe that the zebrafish crush model possesses the potential to help scientists in many diverse fields within the biomedical research of human fracture healing. Genetic predisposition, drug treatment and bacterial infections of the crush were presented in here, however, I believe that possibilities of this model usage are endless. The Zebrafish crush model has certain limitations, such as bone structure or aquatic life style, however I believe that they could be outweighed by possible advantages, which the use of the model can bring. I think that the crush method is simple in execution, therefore easy to reproduce, which certainly helps in comparing results between studies. I trust that this method and this model will be wildly accepted and utilised by the scientific community.

# Acknowledgments

Firstly, I would like to thank Department of Biomedical Science at the University of Sheffield, UK and Agency for Science, Technology and Research (A*STAR), Singapore, for funding my research and giving me the opportunity to carry out my PhD project.

I would like to truly thank my supervisors. Dr Henry Roehl for help in developing and shaping initial zebrafish crush model idea and for great advises throughout the time of my postgraduate studies. Dr Tom Carney for ideas and opportunities of testing zebrafish crush model as a useful tool in translational research. I would like to express my gratitude for all advices, great continuous support, numerous brainstorming meetings and corrections of my PhD thesis

My lab colleagues, past and present, in both Roehl Lab and Carney Lab, thank you all for sharing your knowledge and expertise, for great advises regarding my project and for constructive criticism improving the quality of my work. Also for stimulating and comforting work atmosphere. Special thanks to Josie Gibson for help with infection experiments.

Huge thanks to great friend Maja and amazing fiancé Andy for mental support, motivation and encouragement throughout thesis writing period. Also for priceless help in correcting the English language in my thesis. This work would not be in this shape without amazing help of two of you.

I would like to acknowledge my parents Renata and Wieslaw for being inspiring examples of personal growth and of determination in achieving personal goals. Thank you both, and thank to my sister Ola and for giving me strength in time of doubts. Without your love and support, this work would not be possible.

Last but not least, I would love to thank all my wonderful friends who accompany me throughout the journey of my postgraduate studies. Thank you all for your support, help and understanding.

# Bibliography

ABEL, E. J., BAUMAN, T. M., WEIKER, M., SHI, F., DOWNS, T. M., JARRARD, D. F. & HUANG, W. 2014. Analysis and validation of tissue biomarkers for renal cell carcinoma using automated high-throughput evaluation of protein expression. *Human pathology,* 45**,** 1092-9.

ADAMSKI, M. G., GUMANN, P. & BAIRD, A. E. 2014. A method for quantitative analysis of standard and high-throughput qPCR expression data based on input sample quantity. *PloS one,* 9**,** e103917.

AKCAY, T., TURAN, S., GURAN, T. & BEREKET, A. 2008. Alendronate treatment in children with osteogenesis imperfecta. *Indian pediatrics,* 45**,** 105-9.

AKIBA, E., YONEI-TAMURA, S., YAJIMA, H., OMI, M., TANAKA, M., SATO-MAEDA, M., TAMURA, K. & IDE, H. 2001. Fibroblast growth factor-induced gene expression and cartilage pattern formation in chick limb bud recombinants. *Development, growth & differentiation,* 43**,** 165-75.

AKIMENKO, M. A., JOHNSON, S. L., WESTERFIELD, M. & EKKER, M. 1995. Differential induction of four msx homeobox genes during fin development and regeneration in zebrafish. *Development,* 121**,** 347-57.

ANAM, E. A., RAUCH, F., GLORIEUX, F. H., FASSIER, F. & HAMDY, R. 2015. Osteotomy Healing in Children With Osteogenesis Imperfecta Receiving Bisphosphonate Treatment. *Journal of bone and mineral research : the official journal of the American Society for Bone and Mineral Research,* 30**,** 1362-8.

APSCHNER, A., SCHULTE-MERKER, S. & WITTEN, P. E. 2011. Not all bones are created equal - using zebrafish and other teleost species in osteogenesis research. *Methods in cell biology,* 105**,** 239-55.

ARTHUR, L. M. & HEBER-KATZ, E. 2011. The role of p21 in regulating mammalian regeneration. *Stem Cell Res Ther,* 2**,** 30.

ASHARANI, P. V., KEUPP, K., SEMLER, O., WANG, W., LI, Y., THIELE, H., YIGIT, G., POHL, E., BECKER, J., FROMMOLT, P., SONNTAG, C., ALTMULLER, J., ZIMMERMANN, K., GREENSPAN, D. S., AKARSU, N. A., NETZER, C., SCHONAU, E., WIRTH, R., HAMMERSCHMIDT, M., NURNBERG, P., WOLLNIK, B. & CARNEY, T. J. 2012. Attenuated BMP1 function compromises osteogenesis, leading to bone fragility in humans and zebrafish. *American journal of human genetics,* 90**,** 661-74.

BAKER, R., ORTON, E., TATA, L. J. & KENDRICK, D. 2016. Epidemiology of poisonings, fractures and burns among 0-24 year olds in England using linked health and mortality data. *European journal of public health*.

BANDO, T., HAMADA, Y., KURITA, K., NAKAMURA, T., MITO, T., OHUCHI, H. & NOJI, S. 2011. Lowfat, a mammalian Lix1 homologue, regulates leg size and growth under the Dachsous/Fat signaling pathway during tissue regeneration. *Dev Dyn,* 240**,** 1440-53.

BARRETT, R., CHAPPELL, C., QUICK, M. & FLEMING, A. 2006. A rapid, high content, in vivo model of glucocorticoid-induced osteoporosis. *Biotechnology journal,* 1**,** 651-5.

BARUAH, R. K. 2007. Ilizarov methodology for infected non union of the Tibia: Classic circular transfixion wire assembly vs. hybrid assembly. *Indian J Orthop,* 41**,** 198-203.

BELY, A. E. & NYBERG, K. G. 2010. Evolution of animal regeneration: re-emergence of a field. *Trends Ecol Evol,* 25**,** 161-70.

BHAKTA, S., HONG, P. & KOC, O. 2006. The surface adhesion molecule CXCR4 stimulates mesenchymal stem cell migration to stromal cell-derived factor-1 in vitro but does

not decrease apoptosis under serum deprivation. *Cardiovascular revascularization medicine : including molecular interventions,* 7**,** 19-24.

BIANCO, P. & ROBEY, P. G. 2000. Marrow stromal stem cells. *Journal of Clinical Investigation,* 105**,** 1663-1668.

BIELBY, R., JONES, E. & MCGONAGLE, D. 2007. The role of mesenchymal stem cells in maintenance and repair of bone. *Injury-International Journal of the Care of the Injured,* 38**,** S26-S32.

BLUM, N. & BEGEMANN, G. 2012. Retinoic acid signaling controls the formation, proliferation and survival of the blastema during adult zebrafish fin regeneration. *Development,* 139**,** 107-16.

BOLANDER, M. E. 1992. REGULATION OF FRACTURE REPAIR BY GROWTH-FACTORS. *Proceedings of the Society for Experimental Biology and Medicine,* 200**,** 165-170.

BOSTROM, M. P., LANE, J. M., BERBERIAN, W. S., MISSRI, A. A., TOMIN, E., WEILAND, A., DOTY, S. B., GLASER, D. & ROSEN, V. M. 1995. Immunolocalization and expression of bone morphogenetic proteins 2 and 4 in fracture healing. *Journal of orthopaedic research : official publication of the Orthopaedic Research Society,* 13**,** 357-67.

BOYLE, W. J., SIMONET, W. S. & LACEY, D. L. 2003. Osteoclast differentiation and activation. *Nature,* 423**,** 337-42.

BRIDGMAN, S. & WILSON, R. 2004. Epidemiology of femoral fractures in children in the West Midlands region of England 1991 to 2001. *The Journal of bone and joint surgery. British volume,* 86**,** 1152-7.

BROCKES, J. P., KUMAR, A. & VELLOSO, C. P. 2001. Regeneration as an evolutionary variable. *J Anat,* 199**,** 3-11.

BURNS, J. C. & CORWIN, J. T. 2013. A historical to present-day account of efforts to answer the question: "what puts the brakes on mammalian hair cell regeneration?". *Hear Res,* 297**,** 52-67.

CAMPBELL, B. G., WOOTTON, J. A., MACLEOD, J. N. & MINOR, R. R. 2001. Canine COL1A2 mutation resulting in C-terminal truncation of pro-alpha2(I) and severe osteogenesis imperfecta. *Journal of bone and mineral research : the official journal of the American Society for Bone and Mineral Research,* 16**,** 1147-53.

CARLSON, B. M. 2005. Some principles of regeneration in mammalian systems. *Anat Rec B New Anat,* 287**,** 4-13.

CASAR-BOROTA, O., OYSTESE, K. A., SUNDSTROM, M., MELCHIOR, L. & POPOVIC, V. 2016. A high-throughput analysis of the IDH1(R132H) protein expression in pituitary adenomas. *Pituitary,* 19**,** 407-14.

CASTILLO, R. C., BOSSE, M. J., MACKENZIE, E. J., PATTERSON, B. M. & GROUP, L. S. 2005. Impact of smoking on fracture healing and risk of complications in limb-threatening open tibia fractures. *J Orthop Trauma,* 19**,** 151-7.

CHAMBERS, H. F. & DELEO, F. R. 2009. Waves of resistance: Staphylococcus aureus in the antibiotic era. *Nature reviews. Microbiology,* 7**,** 629-41.

CHEN, G. Y. & NUNEZ, G. 2010. Sterile inflammation: sensing and reacting to damage. *Nat Rev Immunol,* 10**,** 826-37.

CHIPMAN, S. D., SWEET, H. O., MCBRIDE, D. J., JR., DAVISSON, M. T., MARKS, S. C., JR., SHULDINER, A. R., WENSTRUP, R. J., ROWE, D. W. & SHAPIRO, J. R. 1993. Defective pro alpha 2(I) collagen synthesis in a recessive mutation in mice: a model of human osteogenesis imperfecta. *Proceedings of the National Academy of Sciences of the United States of America,* 90**,** 1701-5.

CHO, Y., DI LIBERTO, V., CARLIN, D., ABE, N., LI, K. H., BURLINGAME, A. L., GUAN, S., MICHAELEVSKI, I. & CAVALLI, V. 2014. Syntaxin13 expression is regulated by mammalian target of rapamycin (mTOR) in injured neurons to promote axon regeneration. *J Biol Chem,* 289**,** 15820-32.

CICILIOT, S. & SCHIAFFINO, S. 2010. Regeneration of mammalian skeletal muscle. Basic mechanisms and clinical implications. *Curr Pharm Des,* 16**,** 906-14.

CLAES, L., RECKNAGEL, S. & IGNATIUS, A. 2012. Fracture healing under healthy and inflammatory conditions. *Nat Rev Rheumatol,* 8**,** 133-43.

CLARKE, B. 2008. Normal bone anatomy and physiology. *Clin J Am Soc Nephrol,* 3 Suppl 3**,** S131-9.

CLAUSS, M., TAFIN, U. F., BIZZINI, A., TRAMPUZ, A. & ILCHMANN, T. 2013. Biofilm formation by staphylococci on fresh, fresh-frozen and processed human and bovine bone grafts. *European cells & materials,* 25**,** 159-66.

DEDEOGLU, B. G. 2014. High-throughput approaches for microRNA expression analysis. *Methods in molecular biology,* 1107**,** 91-103.

DEL DEBBIO, C. B., BALASUBRAMANIAN, S., PARAMESWARAN, S., CHAUDHURI, A., QIU, F. & AHMAD, I. 2010. Notch and Wnt signaling mediated rod photoreceptor regeneration by Muller cells in adult mammalian retina. *PLoS One,* 5**,** e12425.

DIAB, D. L. & WATTS, N. B. 2013. Bisphosphonate drug holiday: who, when and how long. *Therapeutic advances in musculoskeletal disease,* 5**,** 107-11.

DONALDSON, L. J., RECKLESS, I. P., SCHOLES, S., MINDELL, J. S. & SHELTON, N. J. 2008. The epidemiology of fractures in England. *Journal of epidemiology and community health,* 62**,** 174-80.

DRAKE, M. T., CLARKE, B. L. & KHOSLA, S. 2008. Bisphosphonates: mechanism of action and role in clinical practice. *Mayo Clin Proc,* 83**,** 1032-45.

DRIEVER, W., SOLNICA-KREZEL, L., SCHIER, A. F., NEUHAUSS, S. C., MALICKI, J., STEMPLE, D. L., STAINIER, D. Y., ZWARTKRUIS, F., ABDELILAH, S., RANGINI, Z., BELAK, J. & BOGGS, C. 1996. A genetic screen for mutations affecting embryogenesis in zebrafish. *Development,* 123**,** 37-46.

DURAN, I., CSUKASI, F., TAYLOR, S. P., KRAKOW, D., BECERRA, J., BOMBARELY, A. & MARI-BEFFA, M. 2015. Collagen duplicate genes of bone and cartilage participate during regeneration of zebrafish fin skeleton. *Gene expression patterns : GEP,* 19**,** 60-9.

EAMES, B. F., YAN, Y. L., SWARTZ, M. E., LEVIC, D. S., KNAPIK, E. W., POSTLETHWAIT, J. H. & KIMMEL, C. B. 2011. Mutations in fam20b and xylt1 reveal that cartilage matrix controls timing of endochondral ossification by inhibiting chondrocyte maturation. *Plos Genetics,* 7**,** e1002246.

EGERMANN, M., GOLDHAHN, J., HOLZ, R., SCHNEIDER, E. & LILL, C. A. 2008. A sheep model for fracture treatment in osteoporosis: benefits of the model versus animal welfare. *Laboratory animals,* 42**,** 453-64.

EINHORN, T. A. 1995. Enhancement of fracture-healing. *The Journal of bone and joint surgery. American volume,* 77**,** 940-56.

EINHORN, T. A. 1998. The cell and molecular biology of fracture healing. *Clinical orthopaedics and related research***,** S7-21.

ELASRI, M. O., THOMAS, J. R., SKINNER, R. A., BLEVINS, J. S., BEENKEN, K. E., NELSON, C. L. & SMELTZER, M. S. 2002. Staphylococcus aureus collagen adhesin contributes to the pathogenesis of osteomyelitis. *Bone,* 30**,** 275-80.

EPARI, D. R., DUDA, G. N. & THOMPSON, M. S. 2010. Mechanobiology of bone healing and regeneration: in vivo models. *Proceedings of the Institution of Mechanical Engineers. Part H, Journal of engineering in medicine,* 224**,** 1543-53.

EVASON, M. D., TAYLOR, S. M. & BEBCHUK, T. N. 2007. Suspect osteogenesis imperfecta in a male kitten. *The Canadian veterinary journal. La revue veterinaire canadienne,* 48**,** 296-8.

FANG, Y. N., ZHENG, B. B., WANG, L., YANG, W., WU, X. M., XU, Q. & GUO, W. W. 2016. High-throughput sequencing and degradome analysis reveal altered expression of

miRNAs and their targets in a male-sterile cybrid pummelo (Citrus grandis). *BMC genomics,* 17**,** 591.

FISHER, S., JAGADEESWARAN, P. & HALPERN, M. E. 2003. Radiographic analysis of zebrafish skeletal defects. *Developmental Biology,* 264**,** 64-76.

FORLINO, A., CABRAL, W. A., BARNES, A. M. & MARINI, J. C. 2011. New perspectives on osteogenesis imperfecta. *Nature reviews. Endocrinology,* 7**,** 540-57.

FORLINO, A., PORTER, F. D., LEE, E. J., WESTPHAL, H. & MARINI, J. C. 1999. Use of the Cre/lox recombination system to develop a non-lethal knock-in murine model for osteogenesis imperfecta with an alpha1(I) G349C substitution. Variability in phenotype in BrtlIV mice. *The Journal of biological chemistry,* 274**,** 37923-31.

FRANK, D. N., FEAZEL, L. M., BESSESEN, M. T., PRICE, C. S., JANOFF, E. N. & PACE, N. R. 2010. The human nasal microbiota and Staphylococcus aureus carriage. *PloS one,* 5**,** e10598.

FRITH, J. C., MONKKONEN, J., BLACKBURN, G. M., RUSSELL, R. G. & ROGERS, M. J. 1997. Clodronate and liposome-encapsulated clodronate are metabolized to a toxic ATP analog, adenosine 5'-(beta, gamma-dichloromethylene) triphosphate, by mammalian cells in vitro. *J Bone Miner Res,* 12**,** 1358-67.

GALICKA, A. 2012. [Mutations of noncollagen genes in osteogenesis imperfecta-- implications of the gene products in collagen biosynthesis and pathogenesis of disease]. *Postepy higieny i medycyny doswiadczalnej,* 66**,** 359-71.

GAMBLE, J. G., RINSKY, L. A., STRUDWICK, J. & BLECK, E. E. 1988. Non-union of fractures in children who have osteogenesis imperfecta. *The Journal of bone and joint surgery. American volume,* 70**,** 439-43.

GARCIA, P., HISTING, T., HOLSTEIN, J. H., KLEIN, M., LASCHKE, M. W., MATTHYS, R., IGNATIUS, A., WILDEMANN, B., LIENAU, J., PETERS, A., WILLIE, B., DUDA, G., CLAES, L., POHLEMANN, T. & MENGER, M. D. 2013. Rodent animal models of delayed bone healing and non-union formation: a comprehensive review. *European cells & materials,* 26**,** 1-12; discussion 12-4.

GERAUDIE, J., MONNOT, M. J. & FERRETTI, P. 1995. CAUDAL FIN REGENERATION IN WILD-TYPE AND LONG-FIN MUTANT ZEBRAFISH IS AFFECTED BY RETINOIC ACID. *International Journal of Developmental Biology,* 39**,** 373-381.

GEURTZEN, K., KNOPF, F., WEHNER, D., HUITEMA, L. F., SCHULTE-MERKER, S. & WEIDINGER, G. 2014. Mature osteoblasts dedifferentiate in response to traumatic bone injury in the zebrafish fin and skull. *Development,* 141**,** 2225-34.

HAMMOND, C. L. & MORO, E. 2012. Using transgenic reporters to visualize bone and cartilage signaling during development in vivo. *Frontiers in endocrinology,* 3**,** 91.

HAMZA, T. & LI, B. 2014. Differential responses of osteoblasts and macrophages upon Staphylococcus aureus infection. *BMC microbiology,* 14**,** 207.

HENRIKSSON, H. B. & BRISBY, H. 2013. Development and regeneration potential of the mammalian intervertebral disc. *Cells Tissues Organs,* 197**,** 1-13.

HODGKINSON, C. P. & DZAU, V. J. 2015. Conserved microRNA program as key to mammalian cardiac regeneration: insights from zebrafish. *Circ Res,* 116**,** 1109-11.

HOWE, K., CLARK, M. D., TORROJA, C. F., TORRANCE, J., BERTHELOT, C., MUFFATO, M., COLLINS, J. E., HUMPHRAY, S., MCLAREN, K., MATTHEWS, L., MCLAREN, S., SEALY, I., CACCAMO, M., CHURCHER, C., SCOTT, C., BARRETT, J. C., KOCH, R., RAUCH, G. J., WHITE, S., CHOW, W., KILIAN, B., QUINTAIS, L. T., GUERRA-ASSUNCAO, J. A., ZHOU, Y., GU, Y., YEN, J., VOGEL, J. H., EYRE, T., REDMOND, S., BANERJEE, R., CHI, J., FU, B., LANGLEY, E., MAGUIRE, S. F., LAIRD, G. K., LLOYD, D., KENYON, E., DONALDSON, S., SEHRA, H., ALMEIDA-KING, J., LOVELAND, J., TREVANION, S., JONES, M., QUAIL, M., WILLEY, D., HUNT, A., BURTON, J., SIMS, S., MCLAY, K., PLUMB, B., DAVIS, J., CLEE, C., OLIVER, K., CLARK, R., RIDDLE, C., ELLIOT, D., THREADGOLD, G., HARDEN, G.,

WARE, D., BEGUM, S., MORTIMORE, B., KERRY, G., HEATH, P., PHILLIMORE, B., TRACEY, A., CORBY, N., DUNN, M., JOHNSON, C., WOOD, J., CLARK, S., PELAN, S., GRIFFITHS, G., SMITH, M., GLITHERO, R., HOWDEN, P., BARKER, N., LLOYD, C., STEVENS, C., HARLEY, J., HOLT, K., PANAGIOTIDIS, G., LOVELL, J., BEASLEY, H., HENDERSON, C., GORDON, D., AUGER, K., WRIGHT, D., COLLINS, J., RAISEN, C., DYER, L., LEUNG, K., ROBERTSON, L., AMBRIDGE, K., LEONGAMORNLERT, D., MCGUIRE, S., GILDERTHORP, R., GRIFFITHS, C., MANTHRAVADI, D., NICHOL, S., BARKER, G., et al. 2013. The zebrafish reference genome sequence and its relationship to the human genome. *Nature,* 496**,** 498-503.

HUGHES, D. E., WRIGHT, K. R., UY, H. L., SASAKI, A., YONEDA, T., ROODMAN, G. D., MUNDY, G. R. & BOYCE, B. F. 1995. Bisphosphonates promote apoptosis in murine osteoclasts in vitro and in vivo. *Journal of bone and mineral research : the official journal of the American Society for Bone and Mineral Research,* 10**,** 1478-87.

IMAI, Y., YOUN, M. Y., INOUE, K., TAKADA, I., KOUZMENKO, A. & KATO, S. 2013. Nuclear receptors in bone physiology and diseases. *Physiol Rev,* 93**,** 481-523.

IRION, U., KRAUSS, J. & NUSSLEIN-VOLHARD, C. 2014. Precise and efficient genome editing in zebrafish using the CRISPR/Cas9 system. *Development,* 141**,** 4827-30.

KANSARA, M., TENG, M. W., SMYTH, M. J. & THOMAS, D. M. 2014. Translational biology of osteosarcoma. *Nat Rev Cancer,* 14**,** 722-35.

KARIMI, M., DEPICKER, A. & HILSON, P. 2007. Recombinational cloning with plant gateway vectors. *Plant physiology,* 145**,** 1144-54.

KHILLAN, J. S., OLSEN, A. S., KONTUSAARI, S., SOKOLOV, B. & PROCKOP, D. J. 1991. Transgenic mice that express a mini-gene version of the human gene for type I procollagen (COL1A1) develop a phenotype resembling a lethal form of osteogenesis imperfecta. *The Journal of biological chemistry,* 266**,** 23373-9.

KIERDORF, U. & KIERDORF, H. 2011. Deer antlers - a model of mammalian appendage regeneration: an extensive review. *Gerontology,* 57**,** 53-65.

KNOPF, F., HAMMOND, C., CHEKURU, A., KURTH, T., HANS, S., WEBER, C. W., MAHATMA, G., FISHER, S., BRAND, M., SCHULTE-MERKER, S. & WEIDINGER, G. 2011. Bone regenerates via dedifferentiation of osteoblasts in the zebrafish fin. *Developmental Cell,* 20**,** 713-24.

KORIYAMA, Y., SUGITANI, K., MATSUKAWA, T. & KATO, S. 2012. An application for mammalian optic nerve repair by fish regeneration-associated genes. *Adv Exp Med Biol,* 723**,** 161-6.

LAIZE, V., GAVAIA, P. J. & CANCELA, M. L. 2014. Fish: a suitable system to model human bone disorders and discover drugs with osteogenic or osteotoxic activities. *Drug Discovery Today: Disease Models,* 13, 2014**,** 29-37.

LAWSON, N. D. & WEINSTEIN, B. M. 2002. In vivo imaging of embryonic vascular development using transgenic zebrafish. *Developmental Biology,* 248**,** 307-18.

LEE, R. T., THIERY, J. P. & CARNEY, T. J. 2013. Dermal fin rays and scales derive from mesoderm, not neural crest. *Current biology : CB,* 23**,** R336-7.

LEE, Y., HAMI, D., DE VAL, S., KAGERMEIER-SCHENK, B., WILLS, A. A., BLACK, B. L., WEIDINGER, G. & POSS, K. D. 2009. Maintenance of blastemal proliferation by functionally diverse epidermis in regenerating zebrafish fins. *Dev Biol,* 331**,** 270-80.

LENEHAN, T. M., BALLIGAND, M., NUNAMAKER, D. M. & WOOD, F. E., JR. 1985. Effect of EHDP on fracture healing in dogs. *Journal of orthopaedic research : official publication of the Orthopaedic Research Society,* 3**,** 499-507.

LEW, D. P. & WALDVOGEL, F. A. 1997. Osteomyelitis. *The New England journal of medicine,* 336**,** 999-1007.

LI, X., CHUNG, L. W., MIZUNO, H., MIYAWAKI, A. & MOROKUMA, K. 2010. Competitive mechanistic pathways for green-to-red photoconversion in the fluorescent protein Kaede: a computational study. *The journal of physical chemistry. B,* 114**,** 16666-75.

LIETMAN, C. D., MAROM, R., MUNIVEZ, E., BERTIN, T. K., JIANG, M. M., CHEN, Y., DAWSON, B., WEIS, M. A., EYRE, D. & LEE, B. 2015. A transgenic mouse model of OI type V supports a neomorphic mechanism of the IFITM5 mutation. *Journal of bone and mineral research : the official journal of the American Society for Bone and Mineral Research,* 30**,** 489-98.

LODER, R. T. 1988. The influence of diabetes mellitus on the healing of closed fractures. *Clin Orthop Relat Res***,** 210-6.

MACKAY, E. W., APSCHNER, A. & SCHULTE-MERKER, S. 2013. A bone to pick with zebrafish. *BoneKEy reports,* 2**,** 445.

MARINI, J. C., REICH, A. & SMITH, S. M. 2014. Osteogenesis imperfecta due to mutations in non-collagenous genes: lessons in the biology of bone formation. *Current opinion in pediatrics,* 26**,** 500-7.

MARIOTTI, M., CARNOVALI, M. & BANFI, G. 2015. Danio rerio: the Janus of the bone from embryo to scale. *Clinical cases in mineral and bone metabolism : the official journal of the Italian Society of Osteoporosis, Mineral Metabolism, and Skeletal Diseases,* 12**,** 188-94.

MARSELL, R. & EINHORN, T. A. 2011. The biology of fracture healing. *Injury,* 42**,** 551-5.

MCCARTHY, E. A., RAGGIO, C. L., HOSSACK, M. D., MILLER, E. A., JAIN, S., BOSKEY, A. L. & CAMACHO, N. P. 2002. Alendronate treatment for infants with osteogenesis imperfecta: demonstration of efficacy in a mouse model. *Pediatric research,* 52**,** 660-70.

MCCLOY, R. A., ROGERS, S., CALDON, C. E., LORCA, T., CASTRO, A. & BURGESS, A. 2014. Partial inhibition of Cdk1 in G 2 phase overrides the SAC and decouples mitotic events. *Cell cycle,* 13**,** 1400-12.

MCCUSKER, C., BRYANT, S. V. & GARDINER, D. M. 2015. The axolotl limb blastema: cellular and molecular mechanisms driving blastema formation and limb regeneration in tetrapods. *Regeneration (Oxf),* 2**,** 54-71.

MCKIBBIN, B. 1978. The biology of fracture healing in long bones. *The Journal of bone and joint surgery. British volume,* 60-B**,** 150-62.

MOALI, C., FONT, B., RUGGIERO, F., EICHENBERGER, D., ROUSSELLE, P., FRANCOIS, V., OLDBERG, A., BRUCKNER-TUDERMAN, L. & HULMES, D. J. 2005. Substrate-specific modulation of a multisubstrate proteinase. C-terminal processing of fibrillar procollagens is the only BMP-1-dependent activity to be enhanced by PCPE-1. *The Journal of biological chemistry,* 280**,** 24188-94.

MORIYAMA, Y. & TAKEDA, H. 2013. Evolution and development of the homocercal caudal fin in teleosts. *Dev Growth Differ,* 55**,** 687-98.

MORSHED, S. 2014. Current Options for Determining Fracture Union. *Advances in medicine,* 2014**,** 708574.

MUIR, A. M., REN, Y., BUTZ, D. H., DAVIS, N. A., BLANK, R. D., BIRK, D. E., LEE, S. J., ROWE, D., FENG, J. Q. & GREENSPAN, D. S. 2014. Induced ablation of Bmp1 and Tll1 produces osteogenesis imperfecta in mice. *Human molecular genetics,* 23**,** 3085-101.

MUNNS, C. F., RAUCH, F., ZEITLIN, L., FASSIER, F. & GLORIEUX, F. H. 2004. Delayed osteotomy but not fracture healing in pediatric osteogenesis imperfecta patients receiving pamidronate. *Journal of bone and mineral research : the official journal of the American Society for Bone and Mineral Research,* 19**,** 1779-86.

MURRAY, A. J., PEACE, A. G., TUCKER, S. J. & SHEWAN, D. A. 2012. Mammalian growth cone turning assays identify distinct cell signalling mechanisms that underlie axon growth, guidance and regeneration. *Methods Mol Biol,* 846**,** 167-78.

NAUSEEF, W. M. 2007. How human neutrophils kill and degrade microbes: an integrated view. *Immunological reviews,* 219**,** 88-102.

NECHIPORUK, A. & KEATING, M. T. 2002. A proliferation gradient between proximal and msxb-expressing distal blastema directs zebrafish fin regeneration. *Development,* 129**,** 2607-17.

NEFF, M. M., NEFF, J. D., CHORY, J. & PEPPER, A. E. 1998. dCAPS, a simple technique for the genetic analysis of single nucleotide polymorphisms: experimental applications in Arabidopsis thaliana genetics. *The Plant journal : for cell and molecular biology,* 14**,** 387-92.

NG, D. W., SHI, X., NAH, G. & CHEN, Z. J. 2014. High-throughput RNA-seq for allelic or locus-specific expression analysis in Arabidopsis-related species, hybrids, and allotetraploids. *Methods in molecular biology,* 1112**,** 33-48.

OGRYZKO, N. V., HOGGETT, E. E., SOLAYMANI-KOHAL, S., TAZZYMAN, S., CHICO, T. J., RENSHAW, S. A. & WILSON, H. L. 2014. Zebrafish tissue injury causes upregulation of interleukin-1 and caspase-dependent amplification of the inflammatory response. *Disease Models & Mechanisms,* 7**,** 259-64.

PAN, Y. A., FREUNDLICH, T., WEISSMAN, T. A., SCHOPPIK, D., WANG, X. C., ZIMMERMAN, S., CIRUNA, B., SANES, J. R., LICHTMAN, J. W. & SCHIER, A. F. 2013. Zebrabow: multispectral cell labeling for cell tracing and lineage analysis in zebrafish. *Development,* 140**,** 2835-46.

PAPE, H. C., MARCUCIO, R., HUMPHREY, C., COLNOT, C., KNOBE, M. & HARVEY, E. J. 2010. Trauma-induced inflammation and fracture healing. *Journal of orthopaedic trauma,* 24**,** 522-5.

PEREIRA, R., KHILLAN, J. S., HELMINEN, H. J., HUME, E. L. & PROCKOP, D. J. 1993. Transgenic mice expressing a partially deleted gene for type I procollagen (COL1A1). A breeding line with a phenotype of spontaneous fractures and decreased bone collagen and mineral. *The Journal of clinical investigation,* 91**,** 709-16.

PERREN, S. M., RAHN, B. & CORDEY, J. 1975. [Mechanics and biology of fracture healing]. *Fortschritte der Kiefer- und Gesichts-Chirurgie,* 19**,** 33-7.

PETRIE, T. A., STRAND, N. S., YANG, C. T., RABINOWITZ, J. S. & MOON, R. T. 2014. Macrophages modulate adult zebrafish tail fin regeneration. *Development,* 141**,** 2581-91.

PLOTKIN, L. I., WEINSTEIN, R. S., PARFITT, A. M., ROBERSON, P. K., MANOLAGAS, S. C. & BELLIDO, T. 1999. Prevention of osteocyte and osteoblast apoptosis by bisphosphonates and calcitonin. *The Journal of clinical investigation,* 104**,** 1363-74.

POSS, K. D., SHEN, J., NECHIPORUK, A., MCMAHON, G., THISSE, B., THISSE, C. & KEATING, M. T. 2000. Roles for Fgf signaling during zebrafish fin regeneration. *Dev Biol,* 222**,** 347-58.

PRAJSNAR, T. K., CUNLIFFE, V. T., FOSTER, S. J. & RENSHAW, S. A. 2008. A novel vertebrate model of Staphylococcus aureus infection reveals phagocyte-dependent resistance of zebrafish to non-host specialized pathogens. *Cellular microbiology,* 10**,** 2312-25.

REIZNER, W., HUNTER, J. G., O'MALLEY, N. T., SOUTHGATE, R. D., SCHWARZ, E. M. & KATES, S. L. 2014. A systematic review of animal models for Staphylococcus aureus osteomyelitis. *European cells & materials,* 27**,** 196-212.

RENN, J. & WINKLER, C. 2009. Osterix-mCherry transgenic medaka for in vivo imaging of bone formation. *Developmental dynamics : an official publication of the American Association of Anatomists,* 238**,** 241-8.

RENSHAW, S. A., LOYNES, C. A., TRUSHELL, D. M., ELWORTHY, S., INGHAM, P. W. & WHYTE, M. K. 2006. A transgenic zebrafish model of neutrophilic inflammation. *Blood,* 108**,** 3976-8.

RODAN, G. A. & FLEISCH, H. A. 1996. Bisphosphonates: mechanisms of action. *The Journal of clinical investigation,* 97**,** 2692-6.

ROLLAND-LAGAN, A. G., PAQUETTE, M., TWEEDLE, V. & AKIMENKO, M. A. 2012. Morphogen-based simulation model of ray growth and joint patterning during fin development and regeneration. *Development,* 139**,** 1188-97.

SANTAMARIA, J. A., MARI-BEFFA, M. & BECERRA, J. 1992. Interactions of the lepidotrichial matrix components during tail fin regeneration in teleosts. *Differentiation,* 49**,** 143-50.

SAVARIDAS, T., WALLACE, R. J., SALTER, D. M. & SIMPSON, A. H. 2013. Do bisphosphonates inhibit direct fracture healing?: A laboratory investigation using an animal model. *The bone & joint journal,* 95-B**,** 1263-8.

SCHILCHER, J., KOEPPEN, V., RANSTAM, J., SKRIPITZ, R., MICHAELSSON, K. & ASPENBERG, P. 2013. Atypical femoral fractures are a separate entity, characterized by highly specific radiographic features. A comparison of 59 cases and 218 controls. *Bone,* 52**,** 389-92.

SCHILLING, T. F. & KIMMEL, C. B. 1994. Segment and cell type lineage restrictions during pharyngeal arch development in the zebrafish embryo. *Development,* 120**,** 483-94.

SCHINDELER, A., MCDONALD, M. M., BOKKO, P. & LITTLE, D. G. 2008. Bone remodeling during fracture repair: The cellular picture. *Seminars in Cell & Developmental Biology,* 19**,** 459-66.

SCHNEIDMULLER, D., RODER, C., KRAUS, R., MARZI, I., KAISER, M., DIETRICH, D. & VON LAER, L. 2011. Development and validation of a paediatric long-bone fracture classification. A prospective multicentre study in 13 European paediatric trauma centres. *BMC musculoskeletal disorders,* 12**,** 89.

SEIKALY, M. G., KOPANATI, S., SALHAB, N., WABER, P., PATTERSON, D., BROWNE, R. & HERRING, J. A. 2005. Impact of alendronate on quality of life in children with osteogenesis imperfecta. *Journal of pediatric orthopedics,* 25**,** 786-91.

SHAHAR, R. & DEAN, M. N. 2013. The enigmas of bone without osteocytes. *BoneKEy reports,* 2**,** 343.

SHARIF, F., DE BAKKER, M. A. & RICHARDSON, M. K. 2014. Osteoclast-like Cells in Early Zebrafish Embryos. *Cell journal,* 16**,** 211-24.

SHEN, Q., LITTLE, S. C., XU, M., HAUPT, J., AST, C., KATAGIRI, T., MUNDLOS, S., SEEMANN, P., KAPLAN, F. S., MULLINS, M. C. & SHORE, E. M. 2009. The fibrodysplasia ossificans progressiva R206H ACVR1 mutation activates BMP-independent chondrogenesis and zebrafish embryo ventralization. *The Journal of clinical investigation,* 119**,** 3462-72.

SILLENCE, D. O., SENN, A. & DANKS, D. M. 1979. Genetic heterogeneity in osteogenesis imperfecta. *Journal of medical genetics,* 16**,** 101-16.

SLOWIK, A. D. & BERMINGHAM-MCDONOGH, O. 2013. Notch signaling in mammalian hair cell regeneration. *Trends Dev Biol,* 7**,** 73-89.

SMITH, A., AVARON, F., GUAY, D., PADHI, B. K. & AKIMENKO, M. A. 2006. Inhibition of BMP signaling during zebrafish fin regeneration disrupts fin growth and scleroblasts differentiation and function. *Developmental Biology,* 299**,** 438-54.

SMITH, A., ZHANG, J., GUAY, D., QUINT, E., JOHNSON, A. & AKIMENKO, M. A. 2008. Gene expression analysis on sections of zebrafish regenerating fins reveals limitations in the whole-mount in situ hybridization method. *Developmental dynamics : an official publication of the American Association of Anatomists,* 237**,** 417-25.

SOUSA, S., VALERIO, F. & JACINTO, A. 2012. A new zebrafish bone crush injury model. *Biology open,* 1**,** 915-21.

SPOORENDONK, K. M., PETERSON-MADURO, J., RENN, J., TROWE, T., KRANENBARG, S., WINKLER, C. & SCHULTE-MERKER, S. 2008. Retinoic acid and Cyp26b1 are critical regulators of osteogenesis in the axial skeleton. *Development,* 135**,** 3765-74.

STEWART, S., GOMEZ, A. W., ARMSTRONG, B. E., HENNER, A. & STANKUNAS, K. 2014. Sequential and opposing activities of Wnt and BMP coordinate zebrafish bone regeneration. *Cell Rep,* 6**,** 482-98.

SUZUKI, N., LABOSKY, P. A., FURUTA, Y., HARGETT, L., DUNN, R., FOGO, A. B., TAKAHARA, K., PETERS, D. M., GREENSPAN, D. S. & HOGAN, B. L. 1996. Failure of ventral body wall closure in mouse embryos lacking a procollagen C-proteinase encoded by Bmp1, a mammalian gene related to Drosophila tolloid. *Development,* 122**,** 3587-95.

TAKEYAMA, K., CHATANI, M., TAKANO, Y. & KUDO, A. 2014. In-vivo imaging of the fracture healing in medaka revealed two types of osteoclasts before and after the callus formation by osteoblasts. *Developmental Biology,* 394**,** 292-304.

TANAKA, E. M. & REDDIEN, P. W. 2011. The cellular basis for animal regeneration. *Dev Cell,* 21**,** 172-85.

THISSE, C., AND THISSE, B. 2005. High Throughput Expression Analysis of ZF-Models Consortium Clones. *ZFIN Direct Data Submission*.

THISSE, C. & THISSE, B. 2008. High-resolution in situ hybridization to whole-mount zebrafish embryos. *Nature Protocols,* 3**,** 59-69.

TONG, S. Y., DAVIS, J. S., EICHENBERGER, E., HOLLAND, T. L. & FOWLER, V. G., JR. 2015. Staphylococcus aureus infections: epidemiology, pathophysiology, clinical manifestations, and management. *Clinical microbiology reviews,* 28**,** 603-61.

TU, S. & JOHNSON, S. L. 2011. Fate Restriction in the Growing and Regenerating Zebrafish Fin. *Developmental Cell,* 20**,** 725-732.

VALADARES, E. R., CARNEIRO, T. B., SANTOS, P. M., OLIVEIRA, A. C. & ZABEL, B. 2014. What is new in genetics and osteogenesis imperfecta classification? *Jornal de pediatria,* 90**,** 536-41.

VAN BEEK, E. R., COHEN, L. H., LEROY, I. M., EBETINO, F. H., LOWIK, C. W. & PAPAPOULOS, S. E. 2003. Differentiating the mechanisms of antiresorptive action of nitrogen containing bisphosphonates. *Bone,* 33**,** 805-11.

VAN EEDEN, F. J., GRANATO, M., SCHACH, U., BRAND, M., FURUTANI-SEIKI, M., HAFFTER, P., HAMMERSCHMIDT, M., HEISENBERG, C. P., JIANG, Y. J., KANE, D. A., KELSH, R. N., MULLINS, M. C., ODENTHAL, J., WARGA, R. M. & NUSSLEIN-VOLHARD, C. 1996. Genetic analysis of fin formation in the zebrafish, Danio rerio. *Development,* 123**,** 255-62.

WALDVOGEL, F. A., MEDOFF, G. & SWARTZ, M. N. 1970. Osteomyelitis: a review of clinical features, therapeutic considerations and unusual aspects. *The New England journal of medicine,* 282**,** 198-206.

WALKER, M. B. & KIMMEL, C. B. 2007. A two-color acid-free cartilage and bone stain for zebrafish larvae. *Biotechnic & histochemistry : official publication of the Biological Stain Commission,* 82**,** 23-8.

WATSON, C. J. & KWON, R. Y. 2015. Osteogenic programs during zebrafish fin regeneration. *BoneKEy reports,* 4**,** 745.

WEHNER, D. & WEIDINGER, G. 2015. Signaling networks organizing regenerative growth of the zebrafish fin. *Trends Genet,* 31**,** 336-43.

WEIGELE, J. & FRANZ-ODENDAAL, T. A. 2016. Functional bone histology of zebrafish reveals two types of endochondral ossification, different types of osteoblast clusters and a new bone type. *Journal of anatomy,* 229**,** 92-103.

WHITEHEAD, G. G., MAKINO, S., LIEN, C. L. & KEATING, M. T. 2005. fgf20 is essential for initiating zebrafish fin regeneration. *Science,* 310**,** 1957-60.

WITTEN, P. E. & HUYSSEUNE, A. 2009. A comparative view on mechanisms and functions of skeletal remodelling in teleost fish, with special emphasis on osteoclasts and their function. *Biological reviews of the Cambridge Philosophical Society,* 84**,** 315-46.

XUE, D., LI, F., CHEN, G., YAN, S. & PAN, Z. 2014. Do bisphosphonates affect bone healing? A meta-analysis of randomized controlled trials. *Journal of orthopaedic surgery and research,* 9**,** 45.

YANG, S. M., CHEN, W., GUO, W. W., JIA, S., SUN, J. H., LIU, H. Z., YOUNG, W. Y. & HE, D. Z. 2012. Regeneration of stereocilia of hair cells by forced Atoh1 expression in the adult mammalian cochlea. *PLoS One,* 7**,** e46355.

YOSHINARI, N. & KAWAKAMI, A. 2011. Mature and juvenile tissue models of regeneration in small fish species. *Biol Bull,* 221**,** 62-78.

YU, T., WITTEN, P. E., HUYSSEUNE, A., BUETTNER, A., TO, T. T. & WINKLER, C. 2016. Live imaging of osteoclast inhibition by bisphosphonates in a medaka osteoporosis model. *Disease Models & Mechanisms,* 9**,** 155-63.

YUE, L., HAN, C., LI, Z., LI, X., LIU, D., LIU, S. & YU, H. 2016. Fucosyltransferase 8 expression in breast cancer patients: A high throughput tissue microarray analysis. *Histology and histopathology,* 31**,** 547-55.